Preparation and Characterization of High Density Polyethylene/Graphene Nanocomposites by In-situ Polymerization

BY

Farrukh Shehzad

A Thesis Presented to the

DEANSHIP OF GRADUATE STUDIES

KING FAHD UNIVERSITY OF PETROLEUM & MINERALS

DHAHRAN, SAUDI ARABIA

In Partial Fulfillment of the
Requirements for the Degree of

MASTER OF SCIENCE

In

CHEMICAL ENGINEERING

APRIL 2014

KING FAHD UNIVERSITY OF PETROLEUM & MINERALS

DHAHRAN- 31261, SAUDI ARABIA

DEANSHIP OF GRADUATE STUDIES

This thesis, written by **FARRUKH SHEHZAD** under the direction his thesis advisor and approved by his thesis committee, has been presented and accepted by the Dean of Graduate Studies, in partial fulfillment of the requirements for the degree of **MASTER OF SCIENCE IN CHEMICAL ENGINEERING.**

Dr. Mamdouh Ahmad Al Harthi
(Advisor)

For Dr. Usamah A. Al-Mubaiyedh
Department Chairman

Dr. Abdulhadi A.R. Al-Juhani
(Member)

Dr. Salam A. Zummo
Dean of Graduate Studies

Dr. Mohammed Saleh
Ba-Shammakh
(Member)

24/6/14
Date

Dr. Abdallah A. Al-Shammari
(Member)

Dr. Zuhair Omar Malaibari
(Member)

DEDICATION

Dedicated to my family and friends

ACKNOWLEDGMENTS

First of all thanks to Almighty Allah for blessing me with the spirit and sound health to pursue higher education. I am gratefully thankful to my advisor Dr. Mamdouh A. Al-Harthi for his kind supervision, guidance and encouragement throughout this research work. I am thankful to my committee members, Dr. Abulhadi-al-Juhani, Dr. Muhammad Saleh Ba-Shammakh, Dr. Abdallah Al-Shammri and Dr. Zuhair Omar Malyabari for their sugggestions and recommendations for this work.

I appreciate Mr. Sarath P. Unikrri for his help and support in synthesis and characterization. I am also thankful to Mr. Abdul Lateef, Department of Mechanical Engineering for his help in SEM analysis.

Conclusively, I acknowledge my deep appreciation to KFUPM and Department of Chemical Engineering for their cooperation and facilitation of my study as well as the research work. Last but not the least, my sincere gratitude to all my friends. This period of time would not have been so interesting and exciting without you people.

TABLE OF CONTENTS

LIST OF SCHEMES

LIST OF TABLES

LIST OF FIGURES

LIST OF ABBREVIATIONS

MAO	Methylaluminoxane
CNTs	Carbon nanotubes
TRG	Thermally reduced graphene
CMG	Chemically modified graphene
GO	Graphene oxide
ATRP	Atom transfer radical polymerization
DSC	Differential scanning calorimetry
CRYSTAF	Crystallization analysis fractionation
GPC	Gel permeation chromatography
FTIR	Fourier transform infrared spectroscopy
PCFC	Pyrolysis flow combustion calorimetry
DMA	Dynamic mechanical analysis
MWD	Moelcular weight distribution

ABSTRACT

Full Name : Farrukh Shehzad

Thesis Title : Preparation and Characterization of High Density Polyethylene /Graphene Nano-Composites By In-Situ Polymerization

Major Field : Chemical Engineering

Date of Degree : April 2014

High density Polyethylene (HDPE) is widely in use thermoplastic. It possess some distinctive properties such as high strength, non-corrosive nature and affordable cost. HDPE is generally used outdoors. Therefore, its lifetime depends on various factors for instance solar radiation, pollutants, humidity and most importantly ultra-violet (UV) radiation. Improvement in the intrinsic characteristics of HDPE such as mechanical and thermal stability as well as improvement in degradation resistance has attracted enormous scientific interest. One route to achieve this improvement is by the incorporation of nanofillers in the polymer matrix.

In this research HDPE/graphene nanocomposites were synthesized by in-situ polymerization. Zriconocene was used as a catalyst and methylaluminoxane (MAO) as a co-catalyst. The effect of graphene on the activity of the catalyst, mechanical and thermal characteristics of HDPE was investigated. Both the thermal and mechanical properties of HDPE were enhanced with a slight reduction in the activity of the catalyst. A significant increase in weight average molecular weight (M_W) occurred in the presence of graphene. Through microcalorimetric analysis a major decrease in the peak decomposition temperature as well the total heat released for the HDPE/graphene nanocomposites was noticed. Differential scanning calorimetry was used in study of non-isothermal melt

crystallization. Mo-method was applied to the analysis of crystallization process. Vyazovkin non-linear iso-conversional method was used to determine the effective activation energy (E_A). The nucleating effect of graphene was observed during the crystallization process, corroborated by, a decrease in E_A, an increase in the T_{on}, and the nucleation efficiency. The natural weathering of the nanocomposites was also studied. Thin films of the nanocomposites were exposed outdoor in a natural environment for varying time spans. Through FTIR analysis it was observed that the carbonyl index of the degraded samples is significantly less as compared to that of the pristine HDPE. Furthermore, the changes in molecular weight as well as the storage modulus were also less significant for HDPE/graphene nanocomposites. The improvement in weathering resistance for graphene reinforced HDPE nanocomposites was also corroborated by Scanning Electron Microscopy (SEM) of the degraded surfaces.

So far as the product development is concerned, this work shows how to synthesize HDPE nanocomposites which have a high molecular weight, better processibility (High PDI), improved flame retardency and more degradation resistance.

ملخص الرسالة

الاسم الكامل: فرّخ شهزاد

عنوان الرسالة: تحضير وتشخيص الحشوة النانوية للبولي ايثيلين عالي الكثافة و للجرافين باستخدام تقنية المكانيرا

التخصص: الهندسة الكيميائية

العلمية الدرجة تاريخ: ١٤ جمادى الثاني ١٤٣٥هـ

بولي ايثالين عالي الكثافة (HDPE) هو أحد أهم أنواع البلاستيك الحراري وذلك لخواصه المميزة مثل شدته الميكانيكية العالية, وطبيعته غير التآكلية وثمنه المناسب لذلك فإن (HDPE) يستخدم في الأغلب خارجيا في الهواء الطلق. ان عمره الإفتراضي يعتمد على عوامل متعددة مثل الإشعاع الشمسي، الرطوبة ، الملوثات وبالأخص الأشعة فوق البنفسجية. ان دارسة تطوير الخواص الجوهرية لـ (HDPE) مثل الميكانيكية والإستقرار الحراري بالإضافة إلى مقاومة التحلل تعد من اهم اهتمامات العلماء. ان أحد هذه الخيارات لتطوير خواصه الجوهرية هي إدماج المالئات متناهية الصغر (nano-fillers) في البنية التركيبة للبوليمر.

في هذا المشروع سوف يتم يتم تصنيع المركبات النانومتريه (nanocomposites) للجرافين/ بولي ايثالين بواسطة البلمرة الموضعية في تواجد الحفاز الزيركوسين (zirconocene) والمساعد المحفز (methylaluminoxane).

لقد تم دراسة تأثير الجرافين على نشاط الحفاز، الخواص الميكانيكية ، والحرارية لـ (HDPE). ان كلا من الخواص الميكانيكية والحرارية تحسنت ولكن على حساب انخفاض طفيف لنشاط الحفاز. ادت اضافة الجرافين الى زيادة ملحوظة في الوزن الجزيئي. ان تحليل الحرق (combustion analysis) للمركبات النانومتريه (nanocomposites) أوضح تحسن في تاخير عملية الاحتراق للمركبات النانومتريه (nanocomposites). لقد تم دراسة التبلور غير متماثل حراريا للمركبات النانومتريه (nanocomposites) بواسطة مسعر المسح التباينى

differential scanning calorimetry (DSC) . ان طاقة النشاط المؤثرة (E_A) تم حسابها بواسطة طريقة (Vyazovkin) الاعتيادية غير الخطية. تم ملاحظة تأثير الجرافين على عملية التبلور من خلال من زيادة حرارة البلمرة (T_{on}) ، نقصان في طاقة النشاط المؤثرة (E_A) وزيادة كفاءة النواة. ايضا لقد تم دراسة تأثير الجرافين على التعرية الطبيعية natural weathering. لقد تم تعريض شريحة نحيفة من المركبات النانومتريه (nanocomposites) للتعرية الطبيعية في الهواء الطلق خلال ازمان مختلفة. ان تحليل العينات بواسطة تحويل فوريه الطيفي بالأشعة تحت الحمراء Fourier Transform Infrared Spectroscopy (FTIR) أوضح مجموعة الكاربونيل carbonyl للمركبات النانومتريه (nanocomposites) للجرافين/ بولي ايثاليين أقل بكثير من (HDPE) الأصلي. بالإضافة ان التغير في الوزن الجزيئي و storage modulus أقل للمركبات النانومتريه (nanocomposites) للجرافين/ بولي ايثاليين. لقد تم تاكيد المقاومة اتجاه التعرية الجوية للسطح المعرضة بواسطة المجهر الالكتروني الماسح Scanning Electron Microscopy (SEM).

على العموم ان هذه العمل اظهر كيفية صناعة منتج البولي ايثاليين(HDPE) ذو وزن جزيئي عالي، تصنيع أفضل (High PDI) ، وتحسن في عملية تاخير الاحتراق ومقاومة أفضل للتحلل.

CHAPTER 1

INTRODUCTION AND OBJECTIVES

1.1 Introduction

Polyethylene (PE) is extensively in use commercial polymer due to its intrinsic characteristics such as good mechanical strength, resistance to chemical attack and easy processing. Incorporation of micro and nano-fillers into polyethylene is an active area of research on account of improving specific properties. A nano-filler is defined as the material which have at least one dimension in the range of nano meters [1,2]. The incorporation of nanofiller affects the structural as well as physical properties of polymers and suitable application of the products could be designed based on the results.

Recently, carbon based nano-particles, in particular carbon nanotubes (CNTs) have proved to improve several properties of polymers like mechanical characteristics, thermal and electrical conductivity and thermal stability.

Like other carbon based nano-fillers, graphene has also attracted enormous scientific interest, due to its exceptional characteristics like ultra-high mechanical strength, thermal and electrical conductivity and chemical functionalization capability [3]. Graphene is 2D carbon nano-filler. It is an atomically thin hexagonal structure of sp^2 hybridized carbon atoms. As stated by H. Kim et al. graphene is considered to be, “the thinnest material in universe” [4].

Apart from indoor uses, Polyethylene (PE) is extensively used outdoor. Therefore, its lifetime depends on various factors like solar radiation, pollutants, humidity and particularly the ultra-violet (UV) radiation. High density polyethylene (HDPE) is a semi crystalline polymer. HDPE has the highest amongst other polyolefins. Its high crystallinity results in better mechanical strength and it also provides a barrier to absorption of humidity and oxygen, which are key factors in degradation. Research is in progress for improving the UV stability of PE and extending its outdoor uses. This also includes the incorporation of various nanofillers in the polymer matrix.

In this work we have used graphene nanofiller to study the effect on properties of HDPE as well as UV stability. To the best of our knowledge, it is the pioneer effort in which graphene has been to enhance the weathering resistance of HDPE. *In-situ* polymerization technique was used, which helps in better dispersion of the filler and evaluation of the influence of nanofiller on the catalytic activity. The objective can be subdivided into the following tasks.

1.2 Obectives

1. Synthesize High Density Polyethylene (HDPE) and HDPE/graphene nano-composite using metallocene catalyst with MAO as co-catalyst.

2. Evaluate the effect of graphene on the activity of the catalyst.

3. Evaluate the effect of graphene on the melt crystallization of the synthesized nanocomposites.

4. Assess the influence of graphene on the thermal, mechanical and morphological characteristics of the synthesized nanocomposites.

5. Evaluate the inlfuence of graphene on flame retardency of the synthesized nanocomposites.

6. Investigate the influence of graphene on the molecular weight and MWD of the synthesized nanocomposites.

7. Study the effect of graphene on the natural weathering resistance of HDPE.

CHAPTER 2

LITERATURE REVIEW AND BACKGROUND

2.1 Polymer and graphene nanocomposites

Polymer nanocomposites derived from crabon based nano-fillers such as carbon black, carbon nanotubes (CNTs) and graphene have earned huge scientific and engineering interest. These nanocomposites posses improved mechanical, electrical and thermal properties [1,2]. Among these, Graphene based polymer nanocomposites has its own identity and importance because of its tremendous properties, low cost (compared to CNT's) and compatibility of uniform dispersion in variety of polymer matrices [3].

The structure of graphene is hexagonal honey comb like and is one atom thick comprising of sp^2 hybrdized carbon atoms. The recent successful isolation of graphene attracts the attention of the researchers, as it possesses some extra ordinary physical qualities including high surface area and high aspect ratio [4,5]. Beside this, the charge carrying capabilitiy and ballistic transport properties at ambient conditions make graphene as potential material in applications of electronic sensors, memory devices, solar cells and conductive polymer composites [6,7].

Graphite is naturally occurring material,from which bucky balls were derived in 1985 and the single-walled CNT were synthesized in 1991. In 2004, stable single layer graphene sheet was first prepared from graphite by using micromechanical cleavage [8].

The properties of single layer graphene are very high. It has young's modulus and ultimate strength of 1 Tpa and 130 GPa respectively, strongest material ever measured. The thermal and electrical conductivities are 5000 W/m.K and 6000 S/cm respectively. The available surface area in case of single walled graphene is 2630 m^2/g, calculated theoretically. All these properties along with gas impermeability make graphene as one of the potential material for ehnacing the properties of polymers like mechanical, thermal, electrical and gas barrier poperties [3].

S. Stankovich et al. first synthesized grapehen/polystyrene nanocomposites. A remarkable increase was found in the electrical conductivity [9]. Similary it has been observed that the T_g of polyacrylonitrile can be increased up to 40 °C by 1 wt.% of functionalized graphene, similarly the T_g of polymethyl methacrylate (PMMA) can be increased up to 300°C, just by addition of 0.05 wt. % [10].

2.1.1 Graphene dispersion in polymers

Apart from the inherent properties of the nanofillers, the properties of the nanocomposites are greatly affected by the dispersion of the nano-filler in the polymer. The dispersion of CNTs in polymers matix has been studied in a number of research studies [1]. Different techniques that includes, surface functionalization through fluorination [11], acid modification [12] and radical addition [13] improves solubility of CNTs in a particular solvent and polymer. However, uniform distribution and disentangling is not an easy task. But in case of graphene, its unique structure prevents the entangling the bundles. Futhermore, as a results of preparation of graphene from graphene oxide (G-O), some functional groups such as epoxide and hydroxide are left

behind. These functional groups facilitates functionalization of graphene [3]. However, restacking of flat graphene sheets is an issue and restacking reduces the effectiveness of graphene. One way to prevent the restacking is to add the surfactants, which can stabilize the reduced suspended particles [14] or blending of graphene with polymer before the chemical reduction [9]. The interfacial bonding between polymer matrix and the nano-filler is also essential. Several routes have been suggested to develop a covalent bonding between the polymer and graphene sheet. The functional groups on the graphene surface can facilitate this bonding [15].

Generally, the following methods are used for preparing graphene based polymer nanocomposites.

2.1.1.1 Melt blending and solution mixing procedure

One of the economical routes for prepration of polymer nanocomposites is melt blending. The melt blending is somewhat limited to the thermally reduced graphene oxide (TRG) because the chemicaly reduced graphene is thermally unstable. So, melt bleding can be used to prepare nanocomposites of stable elastomers and glassy polymers with TRG [16–19].

As the name indicates, in melt blending the polymer blend under high shear conditions are mixed with the nano filler (in dried powder form). Since there is no solvent used and directly mixing of polymer and filler is carried out, so this method is relatively cheap and is in practice generally. The challenging part is the difficulty in feeding graphene to the mixers due to low bulk density [20].

In solution blending procedure the mixing is carried out with the help of a solvent. A colloidal suspension of graphene and polymer is prepared by stirring or shear mixing followed by precipitation. The precipitation helps to encapsulate the nano-filler within the polymer chains. The resulting precipitate is then processed further for applications [20].

For water soluble polymers sonication is an effective technique for example polyvinyl alcohol and polyallylamine nanocomposites have been prepared by simple filtration [21,22]. Similarly vacuum filtration has been used for producing polyvinyl alcohol/G-O and polymethyl methacrylate/G-O nanocomposites [23]. Different techniques that include, Lyophilization methods [24], phase transfer techniques [25] and the use of surfactants [26], are implemented to speed up the solution mixing of graphene based composites. However, it has been reported that use of surfactants can reduce thermal conductivity of CNTs based nanocomposites [27].

2.1.1.2 *In-situ* polymerization

This method involved the mixing of the nano-filler with a monomer or a solution of monomer prior to the reaction. *In-situ* polymerization can be both covalent and non-covalent. Non-covalent *in-situ* polymerization has been used to produce nanocomposites that include PE/graphene nanocomposites [28], polymethyl methacrylate (PMMA)/graphene nanocomposites [29] and polypyrrole/graphene nanocomposites[30]. This methos provides good dispersion of the filler. Beside this, the steric and electronic effect of graphene can be used to tune the final product. For example it has been reported that graphene can be used to produce ultra-high molecular weight PE [31].

2.2 Crystallization kinetics of polymers

2.2.1 Theoretical background

M. Avrami first derived the general melt crystallization model [32]. This model is based on isothermal process and is given by relationship below

$$X_t = 1 - e^{-kt^n} \qquad (1)$$

n represents the Avrami exponent and it depends on the nucleation process. *k* corresponds to growth function that depends on crystal growth and nucleation. Avrami equation depends on time and the volume fraction of transformed material (X_t), by taking into account the nucleation rate. The increase in volume of lamellar crystals is considered as the main processes of the crystallization. Since Avrami equation deals with isothermal process, it is inadequate to be applied to practical processes which are mostly non-isothermal.

Owing to the inadequacy of Avrami equation, modifications have been made to compensate for the non-isothermal conditions. Ozawa method is one of them as shown in Equation 2,

$$X(T) = 1 - \frac{exp\big(-K(T)\big)}{\beta^m} \qquad (2)$$

in which the crystallization is described in terms of cooling function (K (T)), cooling rate (β), and the Ozawa exponent *m*, which is a temperature independent parameter [33]. However, Ozawa method is not good enough for polymers which exhibit secondary crystallization such as PE. Similarly other models based on modification of Avrami method can be found in literature like methods introduced by Mo et al. [34] and J. Kim

et al. [35]. Both of these models are based on combination of Avrami model and Ozawa model.

2.2.2 Activation energy and frequency factor

The general solid state reaction law is given as[36]

$$\frac{d\alpha}{dt} = kf(\alpha) \quad (3)$$

where α is the extent of conversion, k is the rate constant per unit time and $f(\alpha)$ is the reaction model in differential form. Equation 3 in integral form can be written as

$$g(\alpha) = k\,t \quad (4)$$

where, $g(\alpha)$ is the integral of $(d\alpha)/(f(\alpha))$.

For the non-isothermal case,Equation 3 can be written in terms of cooling rate $\beta = \frac{dT}{dt}$ as follows

$$\frac{d\alpha}{dT} = \frac{k}{\beta} f(\alpha) \quad (5)$$

The rate constant k can be written in the form of Arrhenius equation

$$k = k_o\, exp\left(\frac{-E_A}{R\,T}\right) \quad (6)$$

Whereas,

k_o is a frequency factor, s^{-1};

E_A is the activation energy, $J \cdot mol^{-1}$;

T is the absolute temperature, K;

R is the universal gas constant, $J \cdot mol^{-1} \cdot K^{-1}$.

There are two class of methods used in the analysis of kinetic data. These methods are discussed below:

2.2.3 Model Fitting Methods

In these methods the obtained data is fitted to various known models using best fit, which gives the activation energy and the frequency factor. The most common models are presented in Table 1. However, such methods have been criticized for their application in solid state kinetics by S. Vyazovkin [37,38].

2.2.4 Model Free Methods (Iso-conversional methods)

In model free methods, the activation energy is calculated independently from the reaction model, hence no assumptions are made. Iso-conversional methods require more than one heating or cooling rate to obtain E_A at progressive conversion. The iso-conversional methods are also called multicurves methods [39]. The most commonly used iso-conversional methods are differential Friedman method [40], integral Ozawa–Flynn–Wall method [41], Kissinger–Akahira–Sunose method [42,43] and advanced iso-conversional method by S. Vyazovkin [37,38].

Table 1-1 Some of the commonly used models for f(α) and g(α) [36].

Model	Differential format f(α)	Integral format g(α)
Power Law	$n\,\alpha^{\frac{1}{n}}$	$\alpha^{\frac{1}{n}}$
Avrami-Erofeev	$n(1-n)[-ln(1-\alpha)]^{\frac{1}{n}}$	$[-ln(1-\alpha)]^{\frac{1}{n}}$
Prout Tompkins	$\alpha(1-\alpha)$	$ln\left(\frac{\alpha}{1-\alpha}\right)+c$

2.3 Degradation of polyolefins

Like other polymers, polyolefins are also degraded by environmental factors through their service life.The process of degradation is complex and follows various complex mechanisms depending upon the chemical structure, composition and environment.

The degradation can be initiated by several processes which start by formation of a free radical. The radical then reacts in different ways to deteriorate the polymer and degrade its properties, so any process forming an active radical can initiate the degradation of polymer for example thermal factors, photo-oxidation and several other factors [44].

The alkyl radical so formed can further react with O_2 or it can take part in reaction of disproportionation resulting in formation of cross links or branches.Chemical reaction in polyolefins can also be initiated by exposure to shear stress, heat water and irradiation, hence starting the deterioration of polymer [45].

The mechanism of degradation in polyolefins can be classified in the following main categories.

- Thermal Degradation
- Oxidative degradation
- Photo Oxidative degradation
- Mechanical Degradation.

When polyolefins reacts with O_2, Oxygen containing functionalities are formed and this process is sequential also known as autoxidation. Similarly during outdoor exposure light or UV initiated deterioration starts which is followed by thermal break down [46].

Irradiation can initiate degradation resulting in cross linking or scission of PE chains.

2.3.1 Degradation of polypropylene (PP)

2.3.1.1 Thermal and oxidative degradation of PP

Thermal degradation of PP follows the phenomena of random scission. Along with random scission large radical fragments are also formed during the initial stages. Since there are no volatile compounds formed during the initial stages so the weight loss in negligible. After this intramolecular chain transfer starts, which produces lower molecular weight hydrocarbons and weight loss is evident [47].

Initiation step in which formation of secondary or tertiary radicals take place under the influence of shear, heat or photo initiation.

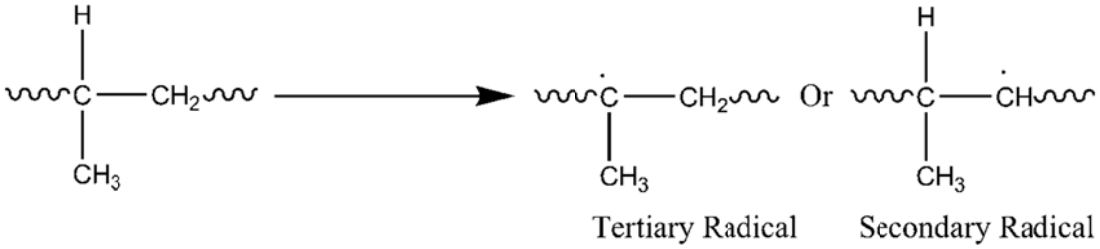

Scheme 1-1 Initiation step of degradation under influence of shear, heat or photo initiation

Chain Transfer is the second step in which tertiary peroxide is formed by reaction of oxygen with tertiary alkyl. A secondary hydroperoxide may also form by reaction of oxygen with secondary alkyl, but this reaction seldom occurs. The peroxide will be converted into hydroperoxide and then may decompose either by reacting with hydrogen atom to form alcohol or it can undergo β-Scission to form ketone. The end products will be aldehyde or alcohol and water [48].

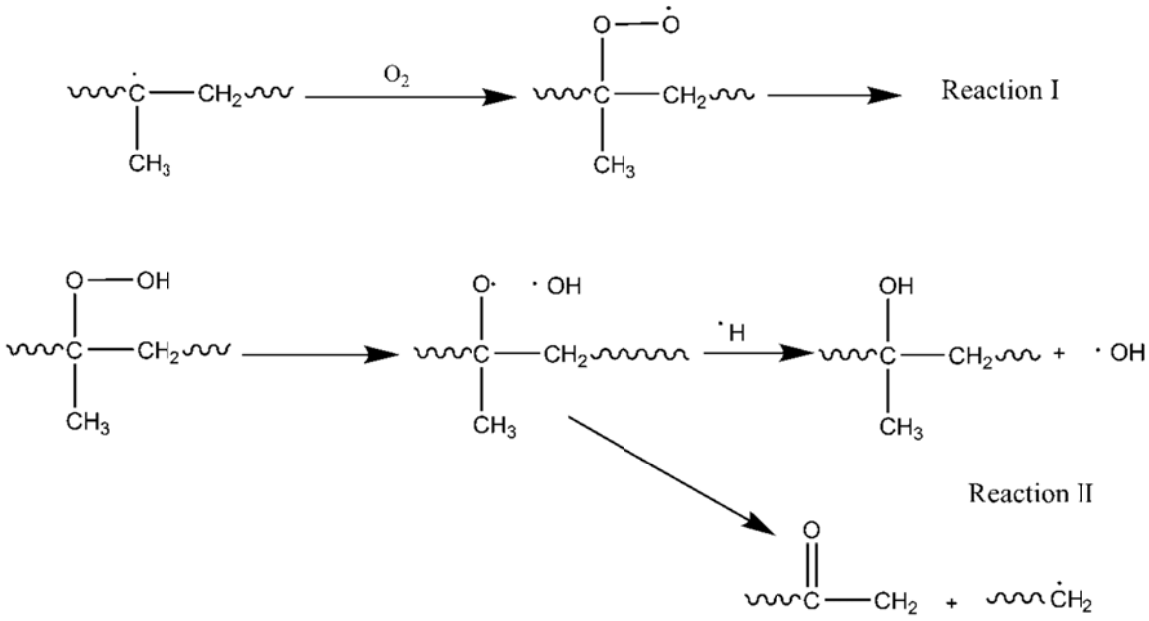

Scheme 1-2 Reaction 1 shows the reaction of tertiary alkyl with oxygen and Reaction 2 shows the decomposition of tertiary hydroperoxide

Termination step is the last step in which several disproportionation reactions may take place. Termination of PP is different from the termination of PE, in which mainly combination of cross linking and disproportionation reactions occur. Terminal Vinylidene groups form during decomposition reactions in PP.

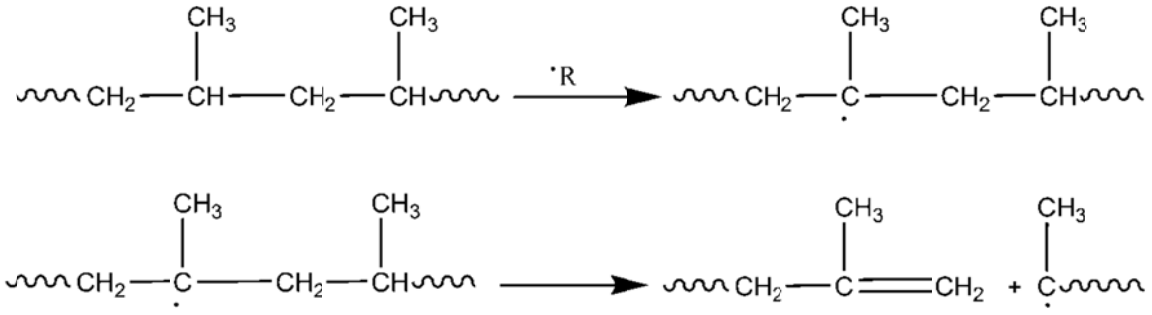

Scheme 1-3 Formation of Terminal Vinylidene groups in radical decomposition of PP

2.3.1.2 Photo-oxidative degradation of PP

The hydroperoxide and carbonyl groups formed due to thermal oxidation at the initial stages of the processing of polymer plays a significant role in initiation step of photooxidation. Both these groups act as absorption sites for UV radiation [47]. Similarly studies by N.S Allen [48] reveal that carbonyl and hydroperoxy groups strongly influence the photo-oxidation rate. However, removing these groups does not have a significant effect on stability, because the role of both these groups is only as initiator. Once the photooxidation is initiated then hydroperoxy group account for most of the degradation process, at the early stages. At higher stages the carbonyl group is predominant specie for absorbing UV radiation [47].

The degradation of PP is shown to be promoted by metal contamination and catalyst residues. Similarly the presence of pigments and stabilizers was found to change the

degradation to a significant extent. Pigments for example titanium oxide were found to limit the depth of degradation. Pigments may reflect or scatter UV light and this may limit the exposure of deeper layers to the UV light. Carbon black also effectively decreases photooxidation [49].

2.3.2 Degradation of polyethylene

Degradation of PE has been studied extensively. Different mechanisms of degradation of PE are explained below.

2.3.2.1 Thermal degradation of PE

Thermal degradation of PE is initiated by random scission or by initiation at weak links. Chain depolymerization is negligible at the start of the process because inter and intra-molecular free radical transfer produces other lower molecular weight products. L.A. Wall and S. Straus [50] reviewed the effect of chemical structure on the mechanism of the degradation. Different structured hydrocarbon polymers have been studied and compared according to the rates of volatilization. According to this review, the linear PE followed the theory of random scission while the branched chain did not follow the theory of random scission. The rate of depolymerization increases with branching. The product formation can be explained by free radical mechanisms as followed.

1) **Initiation**

Initiation is the formation of polymer radicals, resulting from any of the process like thermal process, chemical attack or mechanical process. The most common pathway of radical formation can be abstraction of hydrogen from main chain or the breaking of polymer chain by absorbing some energy or due to chemical attack. The radical once

formed then starts reacting with different species like reacting with one another, reacting with molecular oxygen. The general initiation reactions are as follows [51].

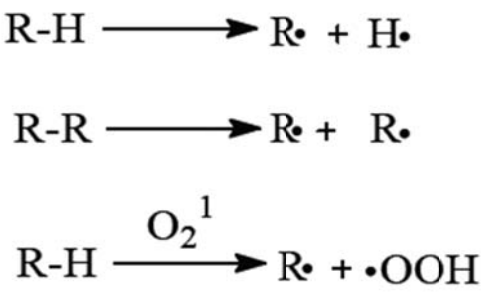

Scheme 1-4 General Initation reaction in Polymers

Scission of polymer chains, i.e. cleavage of R-R or R-H bond is the result of severe deformation or elevated temperature. It requires energy that is provided by a high temperature like in molten state or by another source such as UV. This step is rare as compared to a scission of bonds that occur by chemical attack or irradiation e.g. reaction of oxy radical with polyethylene chain may result in the removal of a hydrogen atom from C-H bond and result in the formation of products like alcohol and other alkyl radical.

Scission by high energy radiation results in removal of hydrogen from C-H bonds and this produces an alkyl radical. The hydrogen atom so formed can recombine with the alkyl radical or it can react with another radical and the process continues which is termed as degradation. In crystalline structured polymers, the probability of recombination of hydrogen atom with the radical is high because the crystalline structure restricts the mobility and the atom is trapped at its own position. Hydrogen atom may

also move inter or intramolecular known as hydrogen transfer and hence can take part in reactions [52].

Initiation or radical formation due to UV or irradiation needs some impurities to be present in the polymer because pure polymer does not absorb light. The presence of molecules that have UV absorber or UV absorbed group cause unsaturation which then leads to degradation. The impurities can be catalyst residues, dyes and stabilizers etc. [52].

2) Propagation

In Propagation alkyl radicals reacts with oxygen to produce hydroperoxides. One possible mechanism for this reaction is that the alkyl radical reacts with oxygen molecule to form peroxy as shown by the first reaction and it is followed by removal of hydrogen atom from polymer by this peroxy radical. This step results in formation of hydroperoxide and new alkyl radical, and the sequence goes on [53,54].

A decrease in molecular weight will occur when β scission occurs and this effects the crystallinity of the polymer resulting a degradation of the mechanical properties. In crystalline structure the oxygen solubility is low and hence the degradation in crystalline phase is low [55].

The general reactions of propagation mechanism are as follows

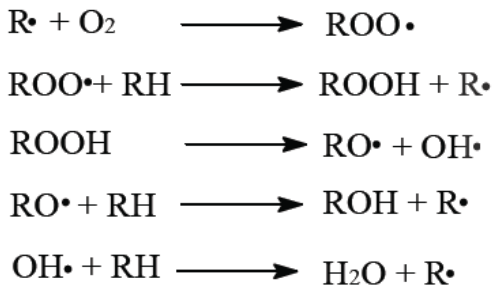

Scheme 1-5 General mechanism of propagation reactions

3) Termination

Termination is characterized by various reaction such as the reaction of alkyl radicals with atomic hydrogen quenching the reaction or reaction of the alkyl radicals with one another resulting in a cross linked material like formation of gels which is highly cross linked material. The possibility of cross linking is high when oxygen concentration is very low [53,55].

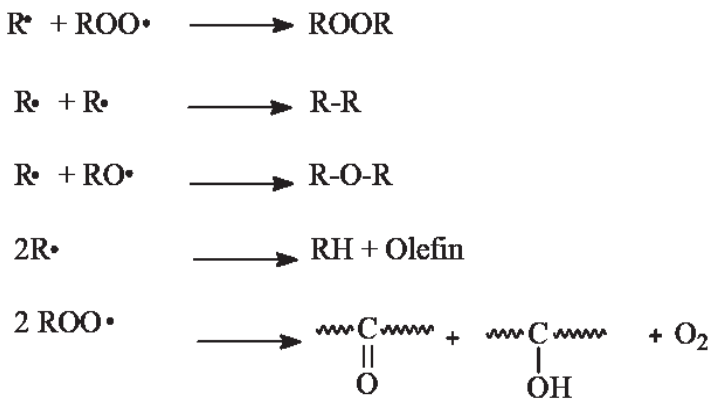

Scheme 1-6 General mechanism of termination step

Intramolecular transfer is the predominant process for the formation of volatile products. W.G. Oakes and R.B. Richard studied the changes in molecular weight during pyrolysis; they observed a decrease in molar mass of branched PE above a temperature of 290 °C and a negligible loss in weight up to 370 °C. These observations conforms the phenomenon of rupture at weak links.Furthermore the authors showed three routes for hydrogen transfer during pyrolysis, which leads to three types of unsaturation [56].

L.W. Jelinski et al. [57] studied the thermal degradation of PE and carried out its analysis in PE. The authors observed that O_2 containing groups in PE act as traps and hinders the mobility of H_2O molecules. Water molecules move easily by pore diffusion through the hydrocarbon matrix, but hindrance occurs in these traps. Through different techniques, the authors found that primary oxidized species include ketones, secondary alcohol, secondary hydroperoxides and carboxylic acids.

Furthermore, the authors observed a large variation in the oxidation species of LLDPE and LDPE. The differences in patterns were due to variations in branched content as well as difference in thermal treatment of materials.

From macroscopic point of view the scission in PE can be random or chain end scission [58]. Through the quantitative analysis of PE degradation products by T. Ueno et al. It was observed that the scission products obtained had a broad range of carbon molecules, includingparaffin, olefins and diolefins. These paraffin, olefins and diolefins were independent of carbon number of the scission product. However, the distribution of degradation products was temperature depenedent. Increasing temperature increases the ratio of diolefins and decreases ratio of paraffin [59].

Chain scission follow two path ways. One is C-C bond scission which produces radicals at the ends of the chain. The other pathways is C-H scission, which promotes the C-C scission by formig a free radical on C-C bond at β position. When the bond energy of β position chain is leass then bond energy of C-C bonds. Direct scission then occurs which is known as depolymerization [60].

2.3.2.2 Photo degradation of PE

Studies on photo degradation of PE has revealed that the later stages of degradation are similar to the thermal oxidation i.e. it involves radical chains; however there are still discrepancies about the primary stages [61].

According to W.L. Hawkins [47] the degradation effect in LDPE is high at the exposed surface and this effect decreases sharply towards the bulk of the polymer. Scientific studies of photo-degradation, under natural or artificial weathering reveals that carbonyl content of LDPE decreases rapidly below the surface and is finally negligible at the center of the polymer. This decrease in degradation is attributed by low permeation of oxygen into the polymer and this conclusion was confirmed by an experiment in which one surface was laminated with metal films, that prevented oxygen permeation and the results showed no degradation on the laminated surface, because of no oxygen penetration, in spite of intense UV radiation.

A.M. Trozzolo et al [61] proposed a mechanism for the photo degradation of PE with experimental evidence supporting it. The proposed mechanism has the four main steps which are described below.

1) Absorption of light by carbonyl group

Due to paraffinic structure PE cannot absorb light with wavelength higher than 300 mμ. It has been shown that during polymerization process several carbonyl functionals groups are prodouced which are responsible for absorption of light. The absorption of light in the range of 270-290 mμ by a ketone group excites the electron in a non-bonding *n*-orbital. This electron is promoted towards a more delocalized anti bonding orbital [62].

2) Norrish type cleavage

Polymers which have ketone group exhibit two types of photochemical reaction. Norrish Type I reaction which yields two end polymeric radicals and carbon monoxide, also called as alpha cleavage. The other reaction is Norrish Type II reaction, in which there is an intermolecular abstraction of hydrogen through a cyclic six membered intermediates, which are directly rearranged to form a ketone and olefin [47]. The Norrish Type I and Type II reactions depend on polymer structure. These reactions are much limited below T_g [62].

3) Formation of singlet O_2 molecule

The role of O_2 is important in the degradation process. The diffusion of exited O_2 results in the long range oxidation. Beside this, during the early stages of the photo-oxidation process, the oxygen molecules quench the n-π triplet states of ketone groups. This results in an electronically active oxygen molecule. This oxygen molecule then initiates the further degradation process.

4) Reaction of singlet O_2 with vinyl groups

As a results of Norrish Type II reactions the vinyl groups are formed. These vinyls groups react with singles O_2 resulting formed during the quenching process to produce hydroperoxides.

2.3.2.3 Weathering studies of PE

The effect of natural weathering on the chemical structure of LDPE was studied by G. Akay et al.[63]. This study showed the formation of carbonyl and vinyl groups. IR spectroscopy revealed that most evident changes occurred in carbonyl region, while the changes in vinyl groups were of secondary importance.

Rasoul and Hameed [64] studied degradation of PE by exposure to natural environment. It was observed that IR spectra of PE changes very much during summer exposure. The observed peaks grew higher with exposure time. Moreover, the outdoor weathering of coloured films of PE was studied. The results showed that PE films having yellow and pink pigments degraded quickly as compared to films having blue, green and black pigment. The formation of hydroperoxides groups was also confirmed.

M. Mlinac et al. [65] studied the weathering of coloured PE under natural and artificial conditions and concluded that deterioration of coloured PE depends upon the nature of pigments used. Environmental degradation study of PE revealed that optical density of vinyl and carbonyl groups rise at the early stages and a minor change in optical density of vinylidene groups was observed [66,67].

The degrees of unsaturation also affect the thermal and photo-chemical oxidation. In case of HDPE the degree of unsaturation is more important then metal impurities. It has been reported that PE with low unsaturation content is less susceptible to degradation due to high crystallinity [68].

The crystallinity of PE has been found to increase due to degradation. The increases in crystallinity also depends on the exposure duration. Similarly, the gas permeation decreases with the exposure time. The increase in crystallinity is due to formation of short chains molecules which are more mobile [66,67,69].

During the degradation process several functional groups are formed in the amorphous region such as of –CO, -OH, -OOH. These functional groups replace the $–CH_2$ group. This phenomenon is referred as chemicrystallization. In chemicrystallization, the crystallinity is increased because the chain mobility is increased after degradation [70].

A.B. Mathur et al. [71] found that although the crystallinity of exposed PE samples increases however, the crystalline melting temperature remains the same and hence the authors concluded that the weathering promotes secondary crystallization and this may be due to the formation of new intermolecular polar bonds of carbonyl groups.

2.3.2.4 Effect of degradation on mechanical properties of PE

Mechanical properties of polymers are of prime consideration in the determination of its utility. Polymers are differentiated from lower molecular weight compounds by nature of physical state or morphology. Generally polymers possess the characteristics of crystalline solids as well as viscous liquids at the same time [72].

The effect of weathering on mechanical behavior of polymers is of keen interest. Tensile properties are being in use for quality control purpose and in specification of plastic materials. Transition from ductile to brittle can be indicated by elongation at break [73]. Flexibility of polymer chains and structure arrangements affect the properties of polymer. The semi crystalline structure of polyolefins provides a high strength and toughness. The distinctive mechanical behavior of polymers is due to high molecular weights. The decrease in molecular weight by chain breaking degrades the mechanical strength of polymer.

Polymer chains are broken directly when certain groups absorb UV radiations. Usually the ultimate tensile strength, brittle temperature and softening point are most adversely affected by chain breaking. Cross linking behavior will cause an initial hardening and increase in tensile strength [74,75].

E.G. Bobalek et al. [76] studied the oxidative degradation of PE and observed a drastic drop in elongation of Alathon 34 PE and branched PE DYNH-3, due to oxidation in air at 100 °C. In about 3 days , the percent elongation of Alathon PE decreased from 500% to 100% and further decreased linearly to 0%. In case of branched PE, elongation first increased a little during the initial stages and then decreased sharply from 650% to 150% in 6 days.

G. Akay et al. [63] in his study of wreathing of PE observed an increase in strain at break during the initial stages, due to cross linking and then later on a steady decrease was observed until the sample was completely brittle.

Since, the photo-chemical degradation of PE is not uniform and this damage is decreased with the depth of material, internal stresses arise due to this localized gradient and weak centres are formed due high amount of surface irregularities which causes micro cracks [77,78].

In a study on oxidative stability of LDPE under static and dynamic condition, it was observed that induction period is inversely proportional to vinyl content of polymer, and oxygen uptake is related to chain branching. It was also concluded that life time of polymers can be increased up to 33 months in comparison with 4 or 5 months by using selective stabilisers [77,79].

2.3.2.5 Effect of different nano fillers on degradation of PE

Research has been done on the effect various fillers on degradation of PE, however, this research is somehow limited to commonly used fillers such as Titanium oxide and Zinc oxide. Recently some studies have also been conducted on the effect of CNTs which showed fruitful results. However there is still a lot to be explored in this area.

A. Holmström et al. [80] studied the thermo oxidative degradation of LDPE and the effect of TiO_2 on this degradation. The authors observed that different samples of TiO_2 effect degradation in various ways like uncoated rutile accelerates the degradation and coated rutile have a stabilization effect. However the stabilization is more pronounced for a shorter time about 5 hrs. According to the authors, the coating inactivates the surface and also acts as a trap for radicals and oxidized products resulting from degradation, and later on due to saturation of the coated surface, the stabilization ability is lost.

R. Davidson [81] studied photooxidation of PE/TiO_2 nanocomposites. The results indicated that PE containing TiO_2 had small photo induced oxygen absorption. Since the photo induced absorption of O_2 results in formations of carbonyl compounds and hydroperoxides, so the addition of TiO_2 had a retarding effect on production of carbonyls and hydroperoxides. This stabilization effect of TiO_2 increased with increased loadings. The authors stated that the effect of TiO_2 upon the durability of polymer is affected by the photo reactivity of pigment as the results showed that the least photo reactive pigment lead to a high degree of stabilization.

S.K. Esthappan et al. [82] also studied the effect of TiO_2 nano composites on thermal and mechanical stability of PE, although the authors studied the effect on PE fibers. The results revealed a very good enhancement on thermal stability of PE fibers, at 0.5% loading the starting temperature of degradation of PE shifted from 324 °C (Pure PE) to 377.8 °C, similarly the maximum degradation temperature increased by 37 °C. By DSC analysis it was observed that TiO_2 acts a nucleating agent for crystallization [82].

R. Yang et al. [83] studied the effect of ZnO nano particles on UV degradation of LDPE. The extent of degradation was measure by the amount of CO_2 evolved. It was observed that carbonyl index of ZnO composites was less then that of TiO_2 nanocomposites. However, the amount of CO_2 evolved in ZnO nanocomposites was higher. This lead to the conclusion that the presence of semiconductor nano-particles the degradation mechanism is altered. The carbonyl formed readily reacts to form CO_2, which lead to a less carbonyl content of ZnO nanocomposites.

The influence of multiwall CNTs on the dispersion and thermal properties of PE was investigated recently by S. Barus et al. [84]. The addition of CNTs to the polymers greatly enhances its mechanical durability, but this enhancement is effected significantly by dispersion of CNTs, similarly the dispersion of CNTs has also an impact on thermal stability and morphology of PE composites. The results of this study indicated the thermal stability of MWCNT/PE composites is not significantly improved against nitrogen environment, however the stability against thermal degradation was improved significantly. Results indicated stability of about 50 °C with 0.5 wt.% and 100 °C with 2 wt.% loading [84]. The authors also concluded that thermal properties were severely affected by dispersion efficiency. The CNTs form a protective shield on the surface and acts an oxygen filtering or reduces the formation of oxidized compounds.

I. Grigoriadou et al. [85] in his research studied the influence of various nano-particles on UV stability of HDPE concluded, that SiO_2 and modified monmorillonite have an accelerating effect on photo-oxidation of HDPE while MWCNTs give the highest stability. Mechanical tests also showed that HDPE/MWCNTs have the highest UV stability. The FTIR observation of the samples also indicated that SiO_2 has the highest accelerating effect on UV degradation as it promotes the propagation step of photo-oxidation.

CHAPTER 3

RESEARCH METHODOLOGY

3.1 Synthesis of nanocomposites

3.1.1 Materials

Zirconocene (catalyst), Toluene (solvent) and methylaluminoxane (MAO) (co-catalyst), were obtained from Aldrich Chemicals and kept in glove box (nitrogen environment) to prevent any contamination.Graphene (96-99%, 50-100nm) was purchased from Grafen Chemical Industries Co (Turkey).

3.1.2 Ethylene polymerization

The polymerization of ethylene was performed in a Schlenk flask. Prior to reaction the required amount of catalyst (6 mg), solvent (80 mL) and graphene (5, 10, 15 and 30) mg were added to the flask inside the glove box. Afterwards the reactor was immersed in a constant temperature bath at 40 °C. Once the reactor and bath temperature had been equilibrated, nitrogen from the reactor was removed by a vacuum pump and ethylene was introduced. The co-catalyst was added after absorption of ethylene into toluene reached the saturation point. The reaction time was kept at 30 minutes and stirring speed was 1000 RPM, after which the polymerization was quenched by adding acidified methanol (5 vol. % HCl). The product was filtered and washed with excess amount of methanol and then kept in an oven at 50 °C. All the samples were prepared inthe same conditions. The weight fraction of graphene in the nanocomposites was calculated on the basis of

weight of graphene added during the polymerization process. 5, 10 and 15 mg were 0.14, 0.25 and 0.41 wt. %, respectively. The corresponding abbreviations used here are G1/HDPE, G2/HDPE, and G3/HDPE for 0.14, 0.25, and 0.41 wt. %, respectively.

3.1.3 Preparation and exposure of samples to natural environment

Thin sheets of the nano-composites were prepared by using the carver hydraulic pressat a temperature of 160 ℃. The sample dimensions were 4 mm wide, 10 mm long and 1 mm thick. The samples were exposed outdoors at the exposure site located at King Fahd University of Petroleum and Minerals, Dhahran, Saudi Arabia. The samples were placed on racks placed at 45 ˚ angle in the basement and facing to the east. Samples were collected and tested for degradation after different spans of time.

3.2 Characterization Techniques

The samples were characterized before and after exposure by the following techniques

3.2.1 Differential scanning calorimetry (DSC)

DSC tests were performed using DSC-Q1000, TA instrument. The equipment was calibrated by melting characteristics of Indium. Nearly 5 mg of each sample was taken. The samples are first heated to 160°C at a rate of 10 °C/min, then cooled at 10 °C/min to 30 °C under nitrogen flow of 50 ml/min. 2 heating cycles of were carried out for each sample and data of the second heating cycle was used for calculating T_m and percent crystallinity.

Percent crystallinity was calculated by the following relationship.

$$x = \frac{\int_{T}^{T_\infty} \left(\frac{dH}{dT}\right) dT}{293.6} * 100$$

Where as, 293.6 J/g is the melting enthalpy of 100 % crystalline PE [86].

DSC was also used in the study of the non-isothermal melt crystallization kinetics. Nearly 5 mg of each sample was first heated to 160°C and then cooled down at rates of 5, 10, 15 and 20 °C/min.

DSC study was also carried out for the exposed samples, in order to observe the changes in T_m and crystallinity of the nanocomposites with the extent of degradation.

3.2.2 Dynamic mechanical analysis (DMA)

DMA can measure properties such as storage modulus, loss modulus and mechanical friction or damping factor (Tan δ). When sinusoidal stress is applied to a viscous material. The material will also respond with a sinusoidal strain. However, this strain lags by a phase angle δ. This is the result of slow chain movement as relaxation of viscoelastic materials need excess time. The storage modulus refers to the energy stored in the material (elastic portion) while the loss modulus refers to the dissipated energy inside the material (viscous portion). Since polymeric materials are viscoelastic in nature. DMA analysis provides a better insight of their mechanical strength with varying temperature or frequency.

Rectangular films of HDPE and HDPE/graphene nanocomposites were analyzed by the temperature ramp test using DMA Q800, TA instruments. The samples were heated from

30 ℃ to 90 ℃ at a heating rate of 5 ℃ /min . Stimulus was applied at frequency of 1 Hz. Storage modulus, loss modulus and Tan δ were compared for HDPE and HDPE/graphene nanocomposites.

The extent of degradation in terms of loss in mechanical properties was assessed through DMA testing. The results were compared for the exposed and the unexposed samples in order to see the effect of degradation.

3.2.3 Crystallization analysis fractionation (CRYSTAF)

CRYSTAF was used to study the chain microstructure of the synthesized nanocomposites. This study was used as supporting evidence for the DSC results as it also helps in studying the crystallinity of polymers. Nearly 5 mg of each sample was dissolved in 1,2,4-trichlorobenzene solvent at 160 °C. The solution was then cooled down at 0.1 °C/min to nearly 30 °C. The equipment (Polymer ChAR CRYSTAF 200) was calibrated by using polystyrene standards.

For the exposed samples CRYSTAF study was used in the investigation of the soluble fraction and shift in crystallization temperature for the samples.

3.2.4 Pyrolysis combustion flow calorimetry (PCFC)

PCFC tests were conducted for HDPE and HDPE/graphene nanocomposites by using an FAA micro calorimeter. This helped in the analysis of the flame retarding capabilities of the nanocomposites. Nearly 3 to 5 mg of each sample was heated to 900 ℃ at 1 ℃ per minute. The heat release rate and total heat released were recorded as a function of time and temperature.

3.2.5 Gel permeation chromatography (GPC)

The molecular weight of the nanocomposites was determined by Triple Detection High Temperature Gel Permeation Chromatography (HT GPC). The equipment was calibrated using Polystyrene standards. About 25 mg of each sample was dissolved in an accurately measured 10 mL 1, 2, 4-trichlorobenzene, in a 40 mL glass vial. The vial was sealed with a teflon coated cap and placed for 3 hours in auto sampler vortex to dissolve. The temperature was maintained at 160 °C while stirring gently. M_n and M_w were calculated using calibration standards of polystyrene.

This technique was also used to study the extent of degradation in samples by measuring the molecular weight of the exposed and unexposed samples.

3.2.6 Fourier transformed infrared spectroscopy (FTIR)

FTIR scans of the samples was recorded by using Nicolet 6700 spectrometer with a resolution of 4 cm^{-1} and 32 scans. 4 spectral readings were taken for each sample at different positions and then an averaged spectrum was obtained using the OMNIC software, available with the equipment.

With the help of FTIR the functional groups formed during the degradation process were analyzed. The extent of degradation was measured by looking at the carbonyl, hydroxyl and vinyl index of the exposed and the unexposed samples.

CHAPTER 4

RESULTS AND DISCUSSION

4.1 Activity of the catalyst

The effect of graphene on the activity of the catalyst is shown in Figure 4-1. It shows that the activity of the catalyst has been decreased with the addition of the filler. This decrease can be attributed to the steric hindrance of graphene. The heterogeneous nature of the process also favors the decrease of catalyst activity due to the reduced inductive effect of the alkyl group [87].

The effect of graphene on the activity of the catalyst is summarized in Table 4-1

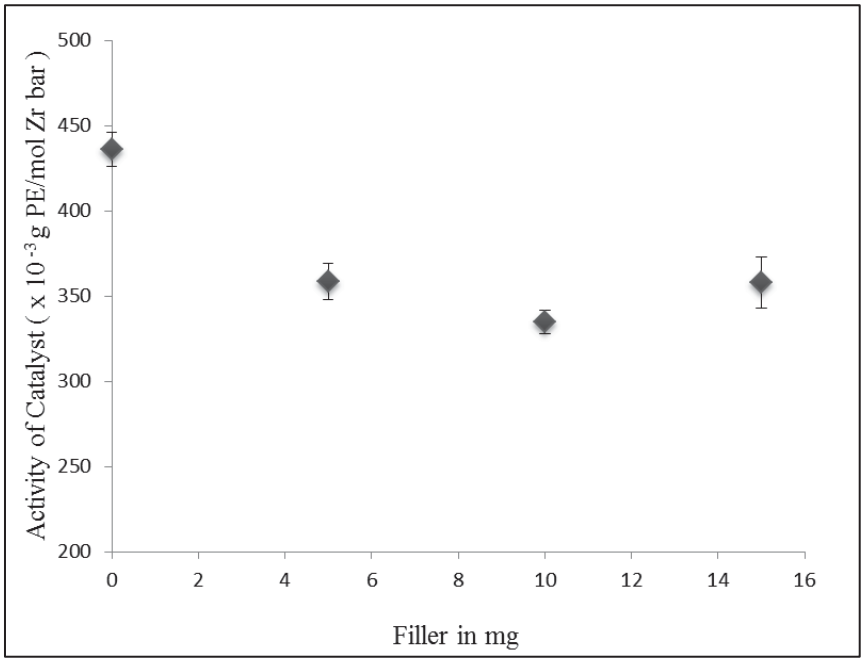

Figure 4-1 Effect of graphene on the activity of catalyst

Table 4-1 Activity of the catalyst at various loadings of filler

No.	Catalyst / Filler in mg[a]	Temp (°C)	Time (mins)	Activity [b]
1	6/ 0	30	30	435.81 ± 10.04
2	6 / 5	30	30	358.45 ± 10.60
3	6 / 10	30	30	334.75 ± 6.98
4	6/ 15	30	30	357.93 ± 15.25

[a]Graphene, zirconocene is catalyst and MAO (5 ml) is co-catalyst

[b] x 10^{-3}gPE/mol h bar

4.2 Melting temperature and degree of crystallinity

The effect of graphene on the crystallinity of HDPE is studied by using DSC. It has been found that the degree of crystallinity is reduced due to addition of graphene. The decrease in the crystallinity may be due to the restriction of chain movement caused by graphene nano-particles. The chain in the crystalline melting temperature is not significant and it again reinforces the hypothesis that graphene is not altering the branching of HDPE chains except restricting the chain movements.. The DSC data are summarized in Table 4-2. The DSC melting thermograms of HDPE and HDPE/graphene nanocomposites can be seen in Figure 4-2, it is clear that there is a slight shift in the T_m. Since, the changes in T_m are less pronounced this suggests that reduction of crystallinity can be only by restriction of chain mobility. If there would have been any effect on the branching of monomers, then it would have been reflected *via* a change in the T_m. Further insights of the chain microstructure can be assessed through CRYSTAF analysis.

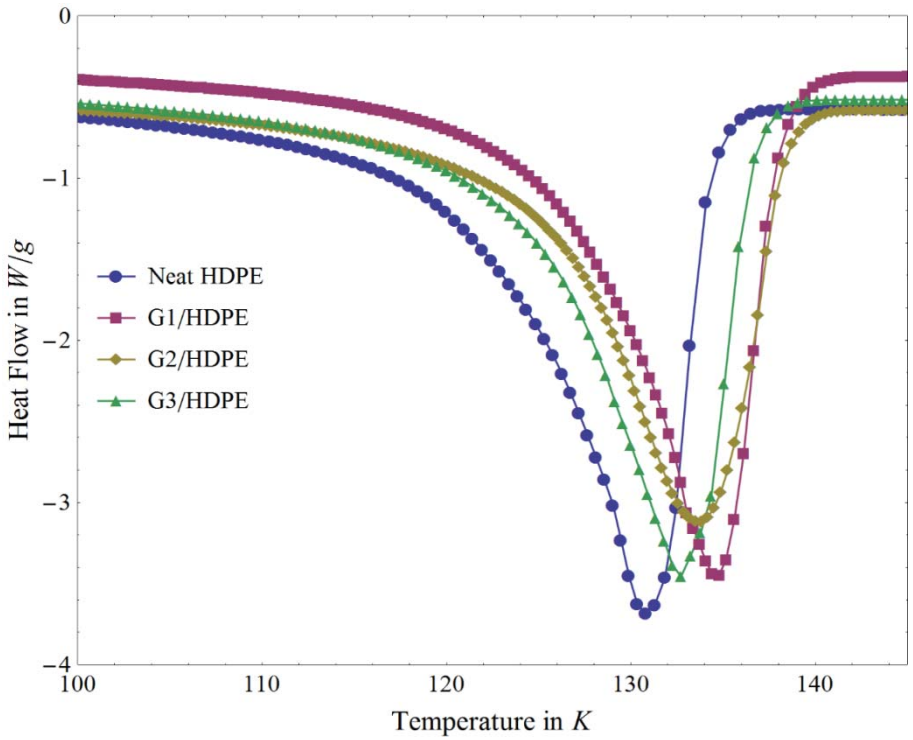

Figure 4-2 DSC heating thermogram for HDPE and HDPE/graphene nanocomposites

Table 4-2 DSC data for HDPE and HDPE/graphene nanocomposites

No.	Sample	T_m °C	% Crystallinity (DSC)[a]
1	HDPE	131.28 ± 0.59	62.04 ± 4.19
2	G1 / HDPE	132.08 ± 0.58	57.592 ± 2.47
3	G2 / HDPE	132.14 ± 0.374	56.500 ± 2.32
4	G3 / HDPE	132.20 ± 0.42	60.770 ± 2.14

[a] Calculated based on Enthalpy of melting of 100 % crystalline PE, 293.6 J/g

4.3 CRYSTAF analysis of the nanocomposites

The chain hetrogenity and chain micro-strucutre can be analyzed by CRYSTAF. CRYSTAF profiles represent the distribution of thickness of crystals. The precipitation of polymer chains from a solution depend upon the longest methylene sequence at a specific temperature [88]. The CRYSTAF results obtained for HDPE and HDPE/graphene nanocomposites are summarized in Table 4-3. The T_{peak} obtained for all samples is nearly the same and close to that of linear polyethylene i.e. 85 °C. This indicates that all the samples have nearly same and very less chain branching. However, it can be seen from Figure 4-3 that the CRYSTAF profile for all the HDPE/graphene nanocomposites are narrower. This narrow distribution can be assigned to change in molecular weight and MWD of the HDPE/graphene nanocomposites. Although, the changes in molecular weight effect the CRYSTAF profile to a vey less extent. However, the observation of T_m and T_c lead to the idea that this change can only be due to changes in M_w. This hypothesis was supported by GPC results which showed that M_w and M_n for all HDPE/graphene nanocomposites were higher as shown in Table 4-. The broad profile of the neat HDPE observed in Figure 4-3, indicates that it has less uniform inter chain branching distribution as compared to neat HDPE. Broader CRYSTAF profiles have been reported in literature for PE with low M_w [89]

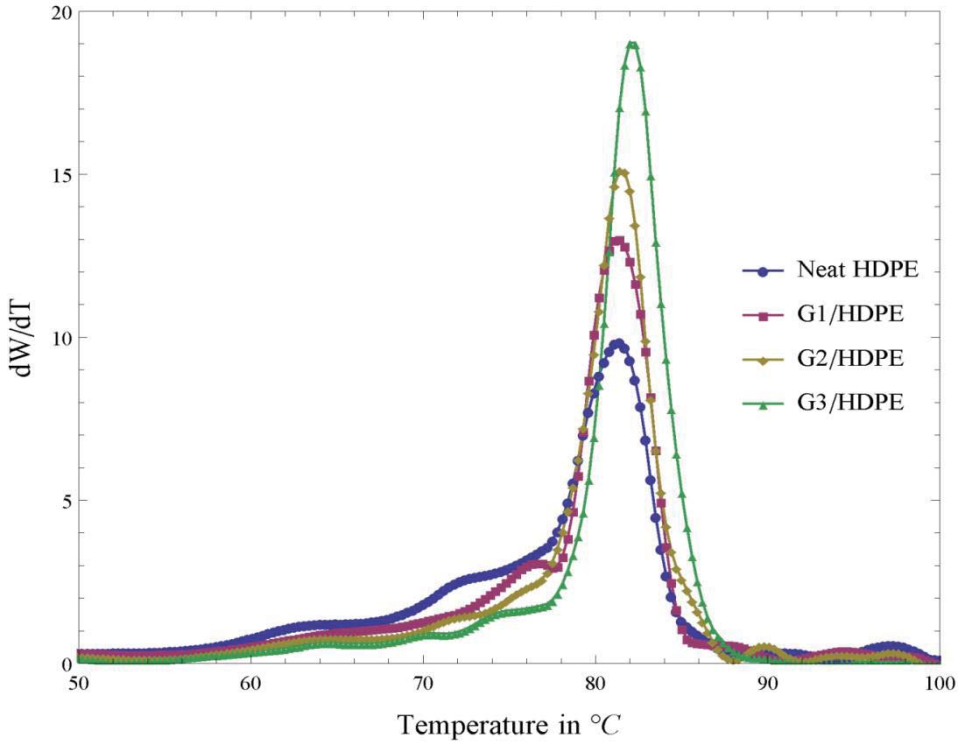

Figure 4-3 CRYSTAF comparison of HDPE and HDPE/graphene nanocomposites

Table 4-3 CRYSTAF data for HDPE and HDPE/graphene nanocomposites

No	Sample	T_{peak}	A_{peak}	T_w	T_n
1	HDPE	81.40	53.10	73.93	70.61
2	G1/HDPE	81.30	68.40	75.99	73.11
3	G2/HDPE	81.50	72.30	76.93	74.13
4	G3/HDPE	82.10	87.50	80.01	80.09

4.4 Dynamic mechanical properties of the nanocomposites

All semi crystalline polymeric materials show viscoelastic behavior. It means that they show characteristics of both elastic and plastic materials. Dynamic mechanical testing helps to measure the two different responses of materials, i.e. elastic response and viscous response. These responses are temperature dependent. The details of the dynamic mechanical properties of HDPE and HDPE/graphene nanocomposites are discussed below:

4.4.1 Storage modulus

Storage modulus refers to the stiffness of the material. It is the measure of the elastic response of a material. The storage moduli of HDPE and HDPE/graphene nanocomposites are shown in Figure 4-4. There is a continuous decreasing trend in the storage module with rise in temperature for all the samples. Similarly, there is no detectable transition as well. However, the storage moduli have an increasing trend with the filler concentration. For all the graphene filled HDPE nanocomposites the storage moduli is higher than pristine HDPE. Similar observations were made by other researchers like [90,91]. It has been reported that addition of the rigid filler in the polymer matrix enhances the dynamics storage modulus.

4.4.2 Loss modulus

Loss Modulus is the measure of the viscous response of a material. It reflects the measure of mechanical energy dissipation within a material. Figure 4-5 represents the storage moduli of HDPE and HDPE/graphene nanocomposites. It is evident that for

HDPE/graphene nanocomposites the loss moduli is higher than neat HDPE. This increase in the loss moduli indicates the restriction in chain mobility of the nanocomposites. This restriction is caused by incorporation of graphene in the polymer matrix. These observations are in agreement with the results obtained by F.C.Fim et al. [92]. Such observations indicate that there is an interaction between the filler and the polymer matrix. However, this interaction is physical and is due to differential thermal shrinkage of HDPE and graphene [93].

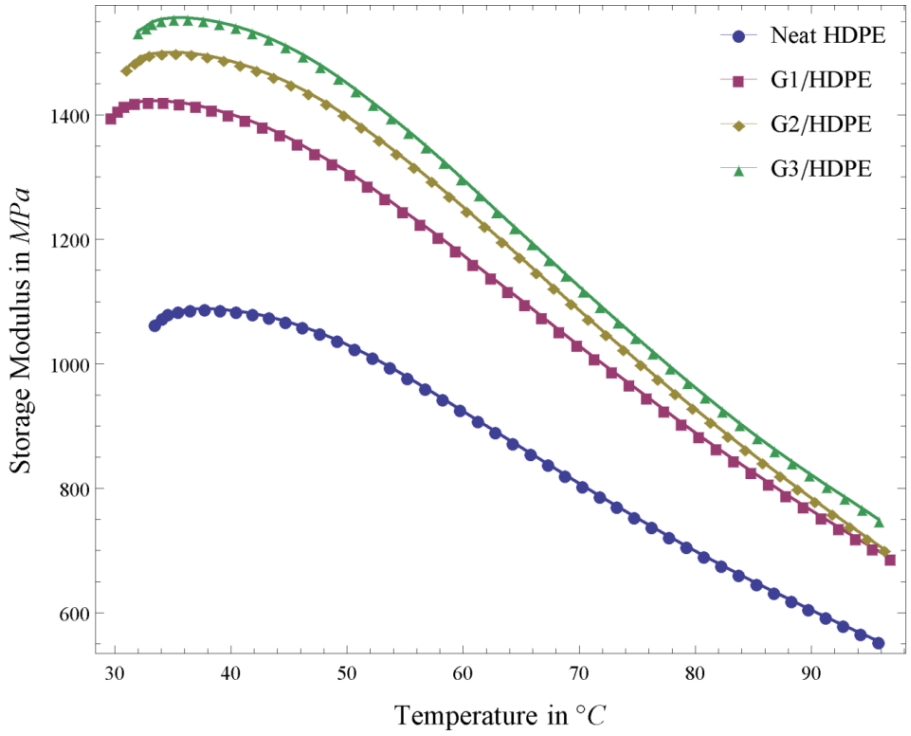

Figure 4-4 Storage Modulus of HDPE and HDPE/graphene nanocomposites

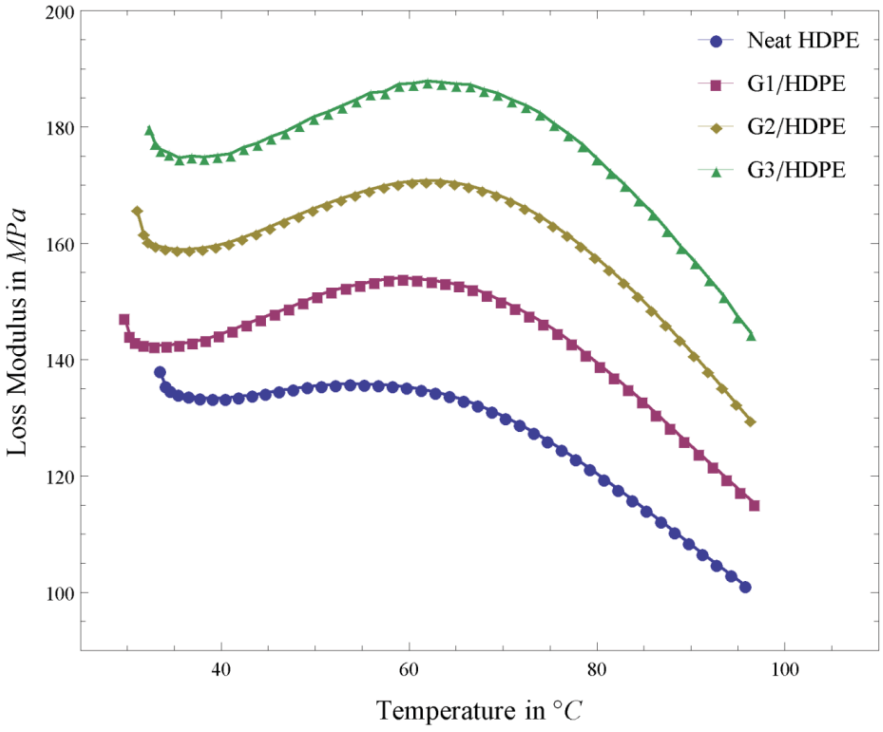

Figure 4-5 Loss Modulus of HDPE and HDPE/graphene nanocomposites

4.4.3 Damping ratio (Tan δ)

Damping factor or Tan δ is the measure of the ratio of viscous response to elastic contribution. Tan δ indicates how near or far a material is from elastic materials. For a pure elastic material, there is no Tan δ or the energy dissipation is zero. On the other hand, for a pure viscous material, all the energy applied is dissipated as heat and hence there is no elastic response, indicating a Tan δ of infinity. If a material has high Tan δ then another it means it dissipates higher energy. For HDPE and HDPE/graphene nanocomposites, the Tan δ curves are shown in Figure 4-6. From this figure, it can be observed that all HDPE/graphene nanocomposites have low Tan δ as compared to neat HDPE. This shows that the material has moved towards elastic material. This anomalous behavior of G2/HDPE and G3/HDPE can be attributed to high the PDI of these samples as it can be seen in Table 4-, G3/HDPE is highly polydisperse as compared to the G1/HDPE and G3/HDPE. Therefore, it has relatively large number of low molecular weight chains present, which increases the free volume of material. This effect becomes more pronounced at high temperature, thereby increasing the chain mobility. Therefore, the loss factor or heat dissipation is increased. Further more, at low temperature the presence of graphene restricts the chain movements, but at a high temperature this effect is compromised very low flow activation energy and the material behave like lower M_w neat HDPE [94–96].

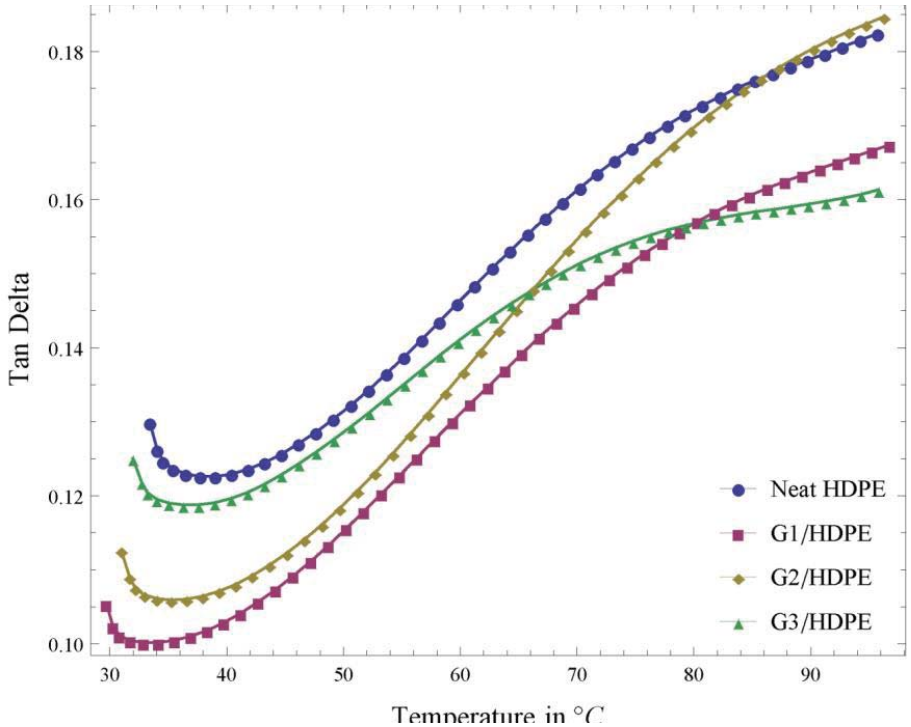

Figure 4-6 Mechanical damping factor for HDPE and HDPE/graphene nanocomposites

4.5 Non-isothermal crystallization of the nanocomposites

Multiple cooling DSC scans were used to study the non-isothermal melt crystallization of the nanocomposites. Figure 4-7 shows the endotherms for HDPE at four distinct cooling rates. It is evident from the figure that by increasing cooling rate the peak becomes broader and peak temperature (T_p) is decreased or shifted to the lower region. This indicates that at lower cooling rate there is enough time for the polymer chains to transform from melt to crystalline phase, therefore the transformation occurs at hight temperature [97]. When the cooling rate is high, motion of polymer chains cannot follow the cooling rate, so more super cooling is needed for the crystalliztion which is indicated by the broadness of the curve at higher cooling rates. Similar results were observed by J.Kim et al. [35] in crystallization of HDPE/MWCNTs nanocomposites.

The data for thermal analysis has been summarized in Table 4-4, which shows that for a given cooling rate such as 10 °C/min, the T_p of HDPE/graphene nanocomposites is higher than the pristine HDPE. This change in T_p is due to the nucleation caused by graphene and therefore the crystallization occurs at higher temperatures. This phenomena can also be observed from Figure 4-8, which compares the endotherms of HDPE and HDPE/graphene nanocomposites at 10 °C/min cooling. It is evident that for HDPE/graphene nanocomposites, T_o has shifted to a higher temperature indicating that unlike pristine HDPE the crystallization process starts at a high temperature in HDPE/graphene nanocomposites.

Table 4-4 DSC data at different cooling rate for all samples

Sample	β (°C/min)	T_{on} °C	T_p °C	$t_{(1/2)}$ min
	5	119.47	116.53	0.92
	10	118.51	113.98	0.56
	15	117.82	111.87	0.19
HDPE	20	117.35	110.87	0.12
	5	121.81	118.75	0.81
	10	120.77	116.72	0.52
	15	120.51	115.77	0.17
G1/HDPE	20	119.42	113.59	0.11
	5	121.16	116.79	1.31
	10	120.51	113.81	0.74
	15	119.29	112.21	0.52
G2/HDPE	20	118.65	110.83	0.16
	5	121.53	117.52	0.94
	10	120.56	114.96	0.58
	15	120.14	113.06	0.23
G3/HDPE	20	119.28	111.96	0.12

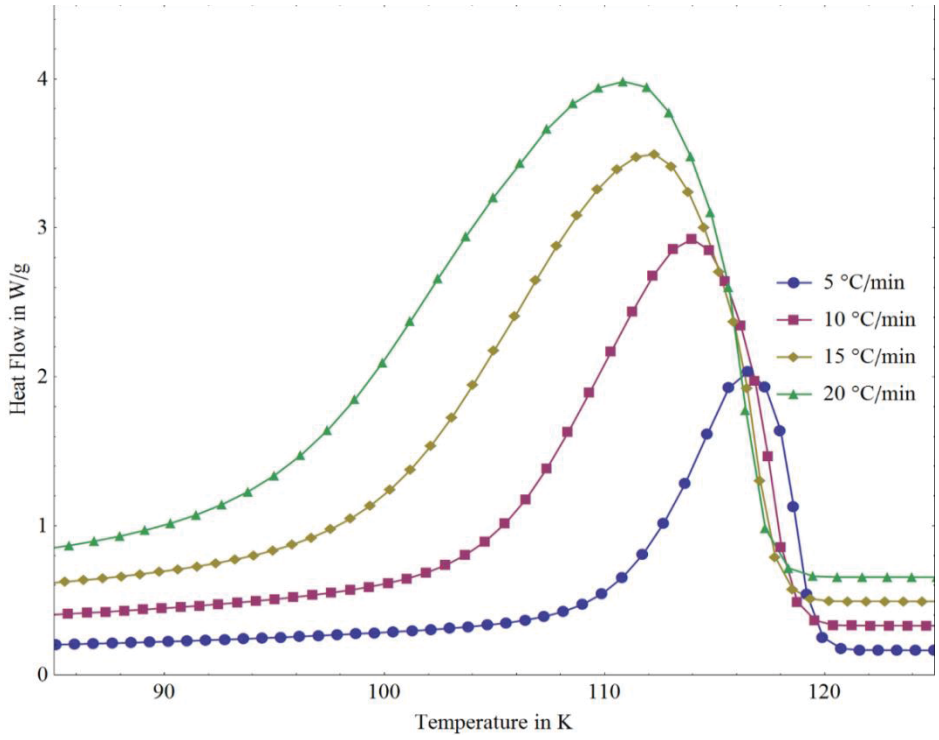

Figure 4-7 DSC cooling scans for HDPE at different cooling rates

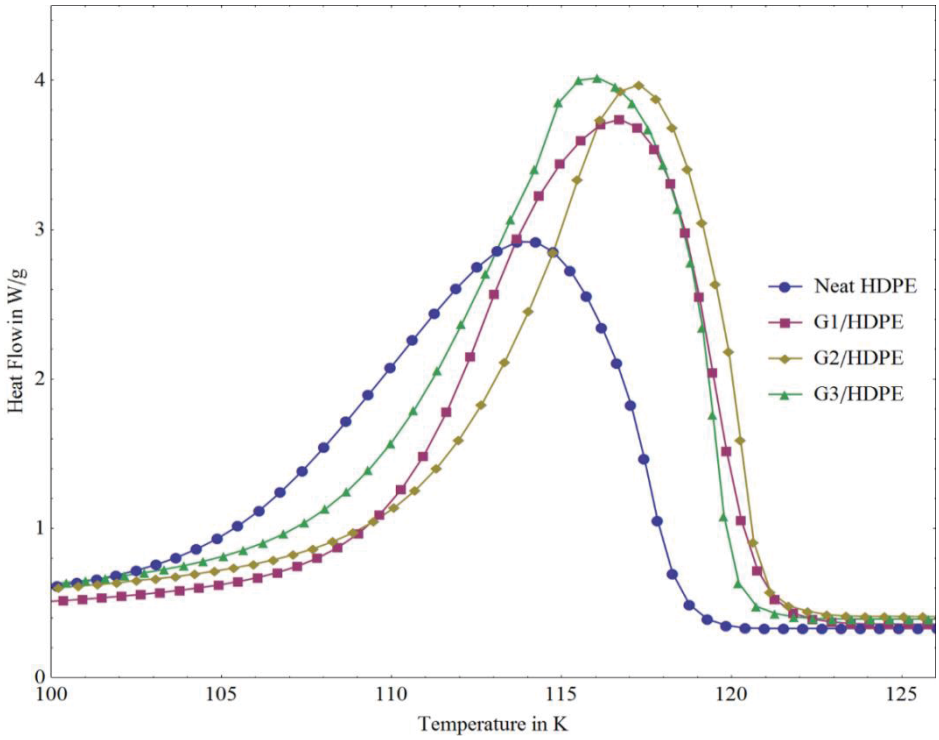

Figure 4-8 DSC cooling scans at 10 °C/min for HDPE and HDPE/graphene nanocomposites

The heat released in the non-isothermal crystallization of polymers is a function of temperature instead of time. $X(T)$ can be calculated from the weight fraction $\alpha_w(T)$, given by the following relationship [86].

$$\alpha_w(T) = \frac{\Delta H(T)}{\Delta H_{total}} = \frac{\int_{T_o}^{T} \left(\frac{dH}{dT}\right) dT}{\int_{T}^{T_\infty} \left(\frac{dH}{dT}\right) dT} \quad (7)$$

whereT_o, T and T_∞, are the onset, arbitrary and end crystallization temperatures respectively. *dH* is the heat released in an very small temperature interval *dT*. The weight fraction can be converted to volume fraction by the formula given below:

$$X(T) = \frac{\alpha_w}{a_w + \frac{\rho_c}{\rho_a[1-a_w]}} \quad (8)$$

where, $\rho_c$and ρ_a are the densities of crystalline and amorphous phases respectively. The values of $\rho_c$and ρ_a are 1.004 and 0.853 for PE [86]. Figure 4-9 (a, b,c and d) shows temperature dependence of X_T for HDPE as well as HDPE/graphene nanocomposites.

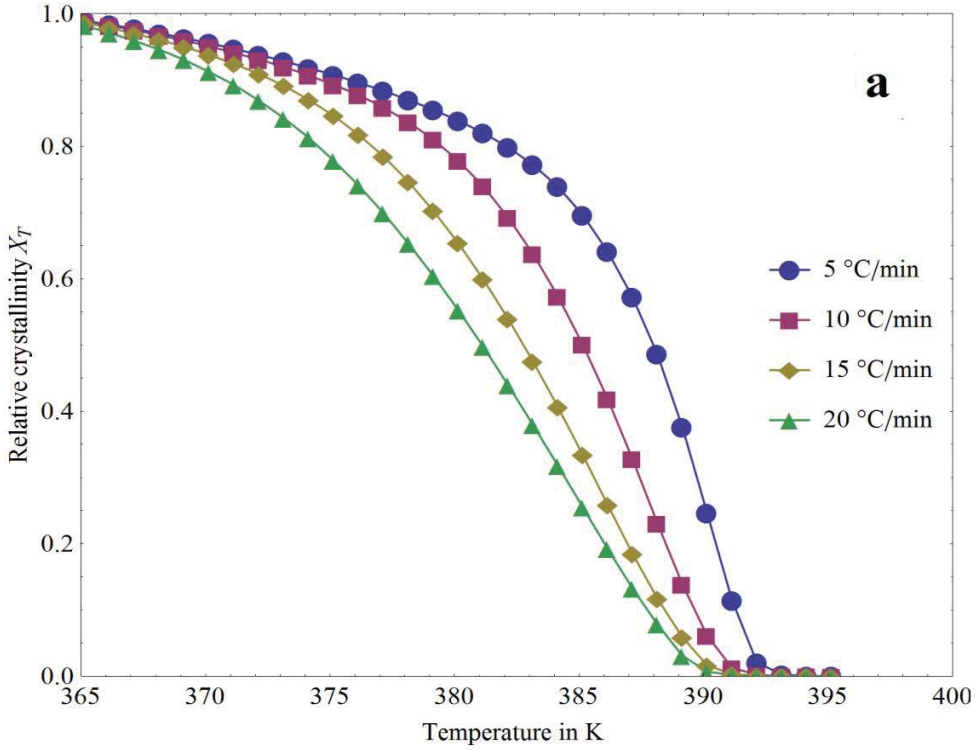
a
Relative crystallinity X_T
Temperature in K
5 °C/min
10 °C/min
15 °C/min
20 °C/min
1.0
0.8
0.6
0.4
0.2
0.0
365
370
375
380
385
390
395
400

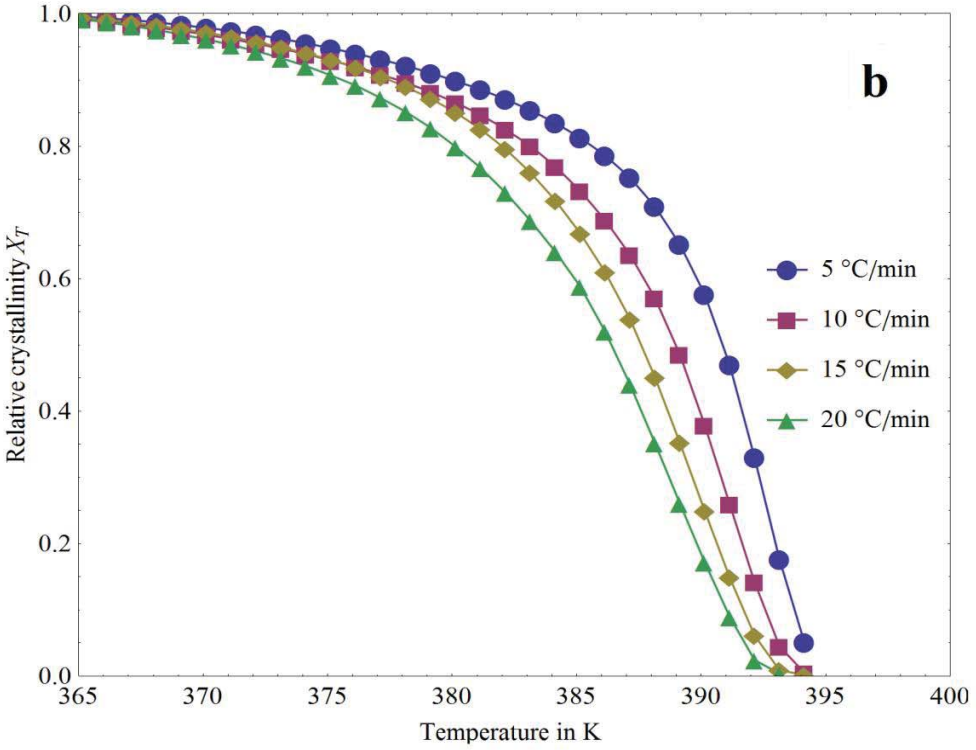
b
Relative crystallinity X_T
Temperature in K
5 °C/min
10 °C/min
15 °C/min
20 °C/min
1.0
0.8
0.6
0.4
0.2
0.0
365
370
375
380
385
390
395
400

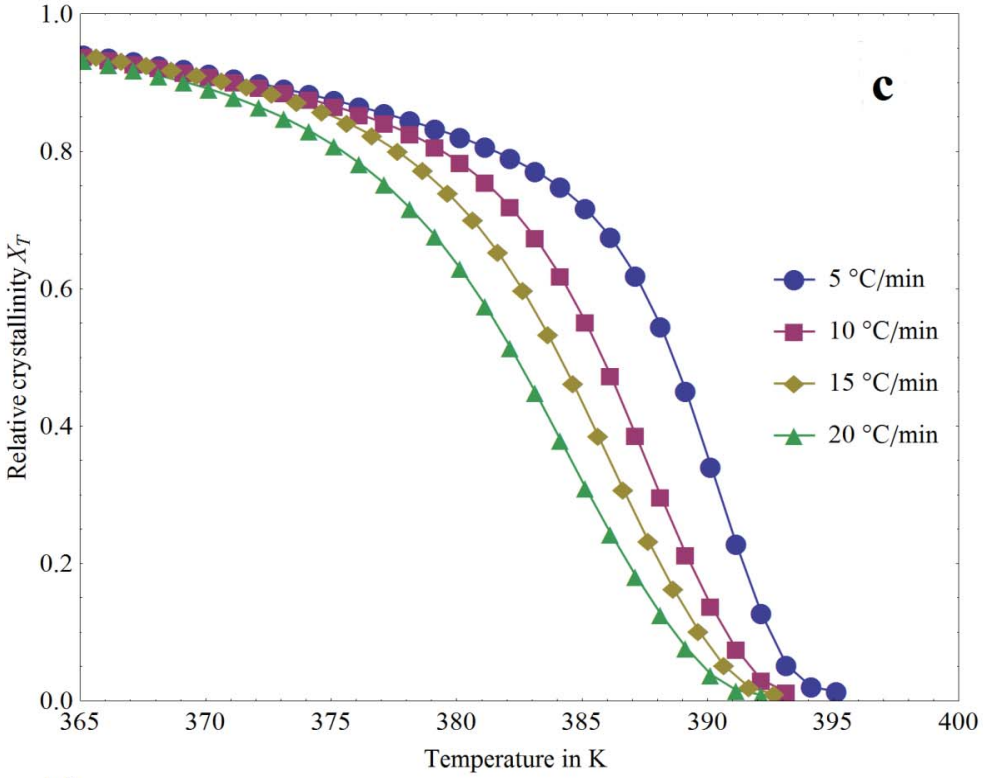

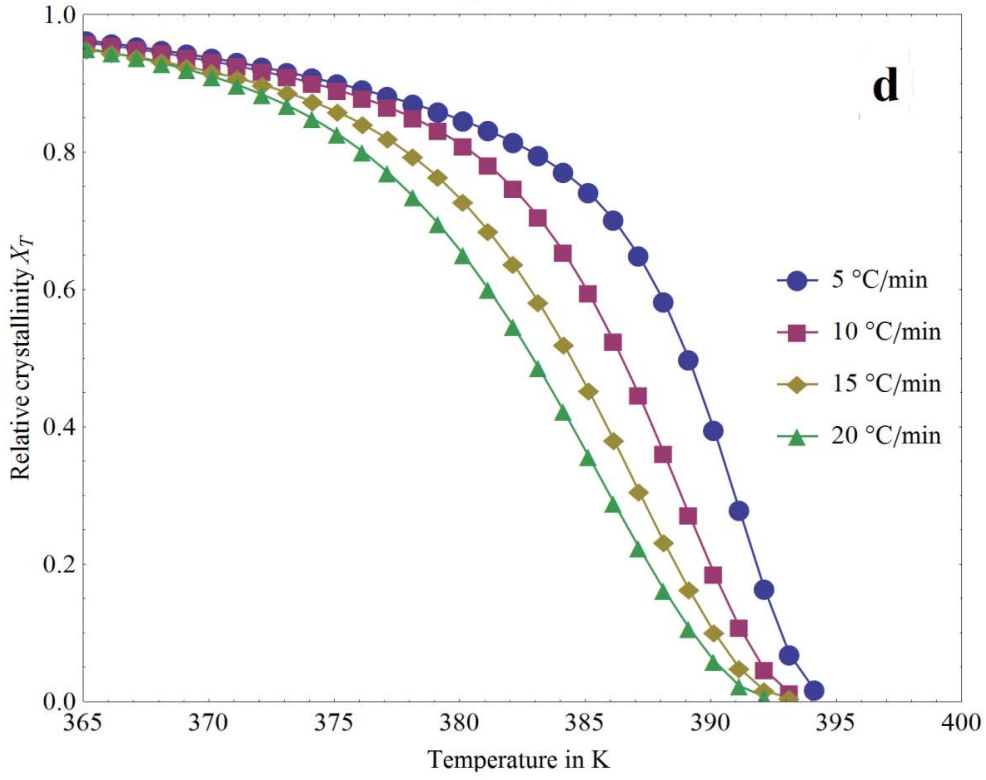

Figure 4-9 Relative crystallinity vs. temperature plots for a) HDPE, b) G1/HDPE, c) G2/HDPE and d) G3/HDPE

The instantaneous crystallization temperature *T* is changed to time by the given relationship, $t=(T_o-T)/\beta$

From the analysis of Figure 4-8, it is clear that the curvesshifted to the left hand side by an increase in the cooling rate. $t_{1/2}$ the time required to attain 50 % *X(T)*. $t_{1/2}$ can be obtained from the curves in Figure 4-9 and the respective values are given in Table 4-4.

The $t_{1/2}$ values show a slow rate of crystallization in G2/HDPE and G3/HDPE as compared to G1/HDPE and pristine HDPE. The reason for this may be the continuously changing temperature. Non-isothermal crystallization occurs at lower temperatures (from 122 °C to nearly room temperature) and the growth of crystals depend on the cooling rate and filler amount. The presence of graphene obstructs the crystal growth process; hence $t_{1/2}$ is increased. However, this effect is not observed in case of G1/HDPE nanocomposites probably due to very less amount of nano-filler. Same retarding effect was also observed by X. shi et al. [98] for non-isothermal crystallization of HDPE/graphite sheets nanocomposites as well as by C.I Ferreira et al. [99] in the study of polypropylene and exfoliated graphite nanocomposites. In the case G1/HDPE, the amount of nano-filler is very less compared to the other two and the possibility of random distribution of the filler in the matrix can be thought of. For the quantitative description of crystallization process, we will use various models that have been proposed so far.

4.5.1 Jeizorny method

Jeizorny [100] proposed a compensation for the non-isothermal condition in the isothermal Avrami equation. The correction was made in the rate parameter k_c given by the following equation

$$Log(k_c) = \frac{Logk_t}{\beta} \quad (9)$$

$$X(T) = 1 - e^{-k_t t^n} \quad (10)$$

By linearization of equation 10, we get

$$Ln\big(-Ln(1 - X_t)\big) = nLn(t) + Ln(k_t) \quad (11)$$

From Equation 11, if the system follows the Avrami equation then the plot of $Ln\big(-Ln(1 - X_t)\big)$ should be a straight line with the slope of *n* and intercept of *L*n(k_t). It is worth noting that unlike in isothermal condition the Avrami exponent *n* and k_t have no physical interpretation in this case of non-isothermal crystallization. This is because the temperature is changing in this case. Here *n* and k_t can be thought of as two parameters for data fitting [101,102]. Selected results of the Avrami method modified by Jeizorny are shown in Figure 4-10. The poor linearity of plots shows the insufficiency of modified Avrami method for HDPE and HDPE/graphene nanocomposites. Therefore, due to unsatisfactory results of this model further discussion is not made here.

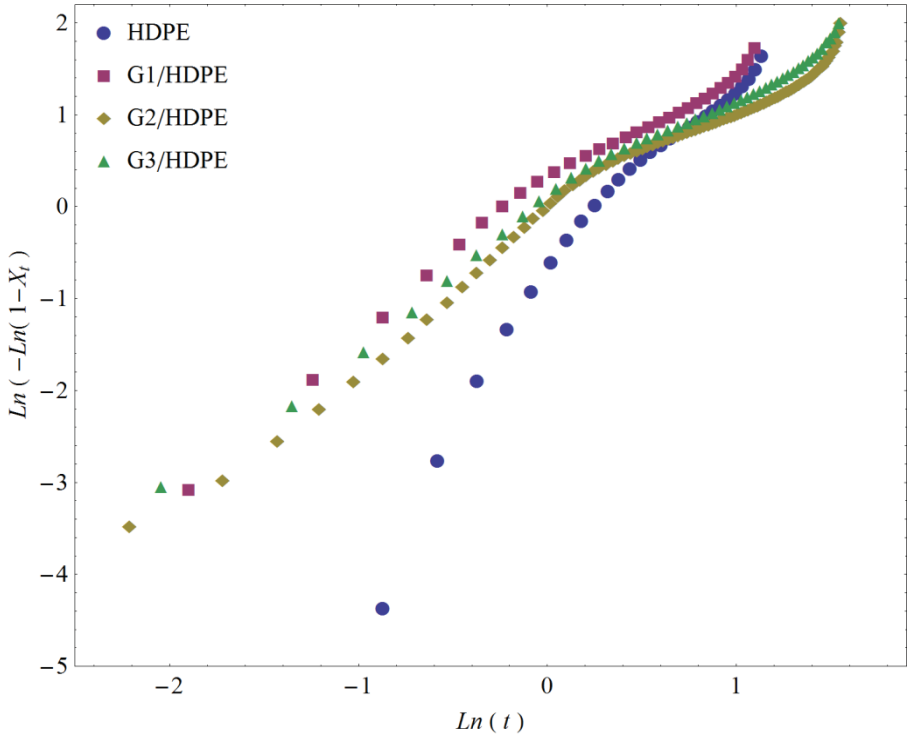

Figure 4-10 Avrami plots for a) HDPE, b) G1/HDPE, c) G2/HDPE and d) G3/HDPE

4.5.2 Ozawa method

Ozawa [33] proposed a model for non-isothermal crystallization of polymers. Unlike Avrami model, in Ozawa model *X(T)* is temperature dependent. Ozawa model is given as follows:

$$X(T) = 1 - \frac{e^{-K(T)}}{\beta^m} \qquad (12)$$

whereas, β is cooling rate. *K(T)* is cooling function representing the overall rate of crystallization. *m* is Ozawa exponent.

Equation 12 is linearized by taking double logarithm and is given by:

$$Ln\left(-Ln(1-X_t)\right) = Ln(K(T)) - mLn(\beta) \qquad (13)$$

According to Equation 13, if Ozawa model correctly describes the crystallization behavior then plot$Ln\left(-Ln(1-X_t)\right)$vs. $Ln(\beta)$ should be a straight line, with the slope and the intercept equal to *n* and *Ln*(*K*(*T*)) respectively. Such plots can be generated by taking a temperature *Ta*, and plotting the crystallinity at that temperature, against the corresponding cooling rate.

The plots show a good linear behavior at early stages of crystallization,however, at later stages the plots are no more linear, Figure 4-11,indicating the insufficiency of Ozawa method to predict secondary crystallization. It shows that *m* is changing with temperature. In Ozawa theory the secondary cystallization is not taken into consideration. Similarly the dependence of chain folding and *m* on temperature is not considered. It has been reported that that Ozawa method cannot not describe the crystallization process of those polymers, whose crystallization process involves a major portion of secondary crystallization for instance PE, PEEK and Nylon11 [33,103]. The results of Ozawa model are summarized in Table 4-5. Figure 4-11 shows the Ozawa plots for all the samples.

Table 4-5 Results of Ozawa analysis for HDPE and HDPE/graphene nanocomposites

Sample	T °C	*m*	*Ln* [*K* (*T*)]
Neat HDPE	118	0.09	0.25
	115	0.42	1.33
	110	0.77	2.73
	100	0.80	4.04
G1/HDPE	118	0.47	1.39
	115	0.90	2.9
	110	0.95	3.86
	100	0.74	4.95
G2/HDPE	118	0.18	0.53
	115	0.47	1.52
	110	0.62	2.51
	100	0.20	2.59
G3/HDPE	118	0.22	0.67
	115	0.51	1.67
	110	0.69	2.69
	100	0.33	3.06

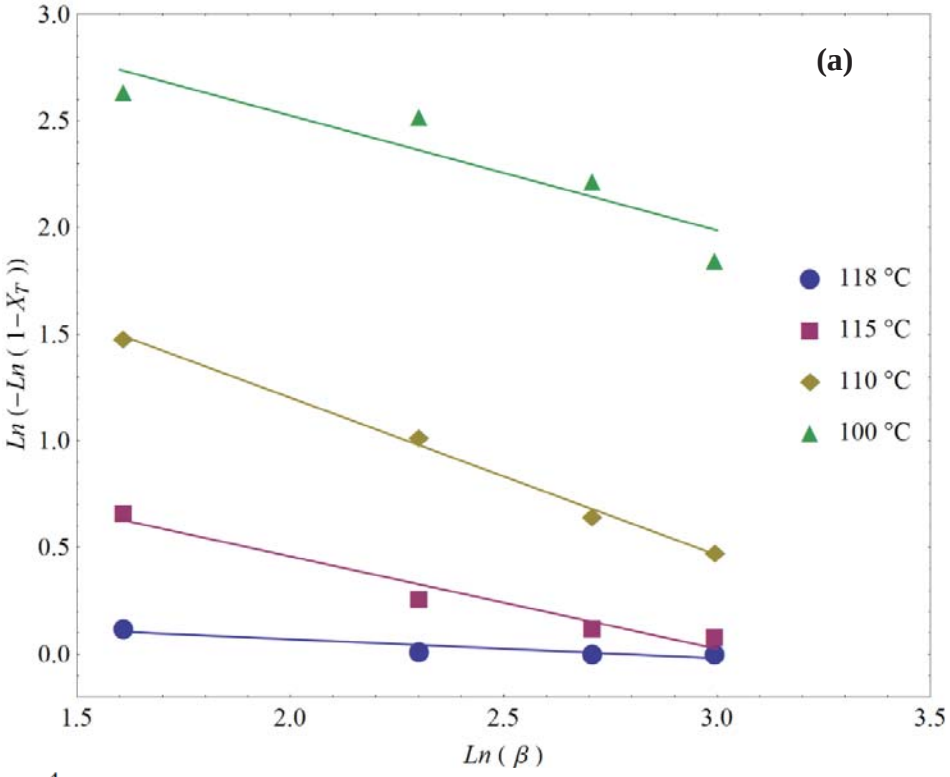
(a)
3.0
2.5
2.0
1.5
1.0
0.5
0.0
Ln (−Ln (1−X_T))
1.5
2.0
2.5
3.0
3.5
Ln (β)
118 °C
115 °C
110 °C
100 °C

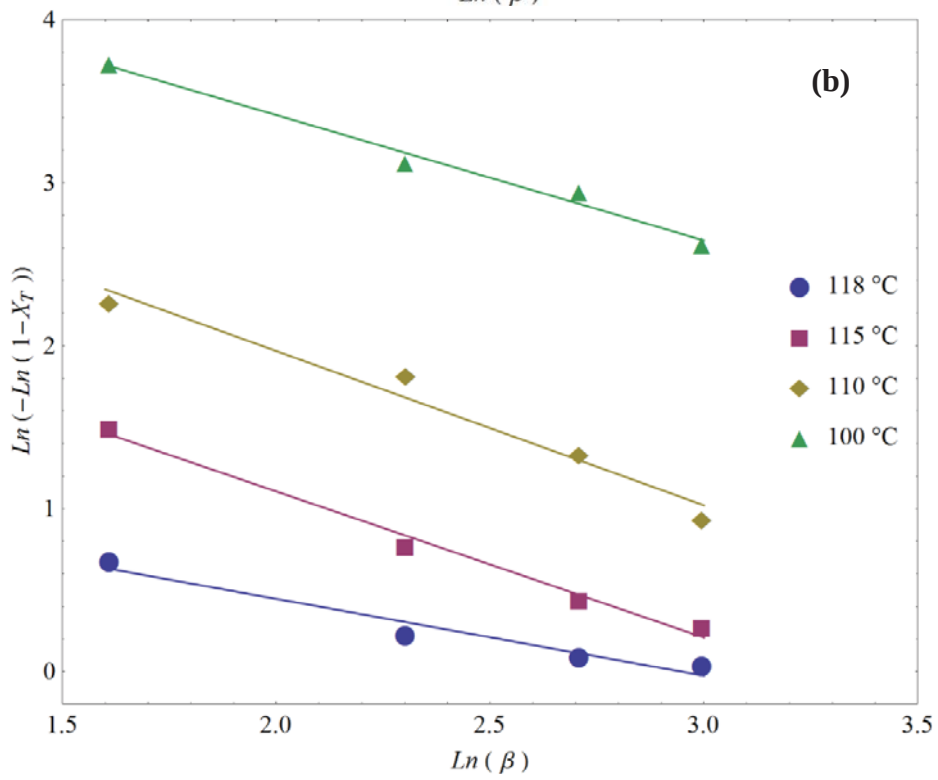
(b)
4
3
2
1
0
Ln (−Ln (1−X_T))
1.5
2.0
2.5
3.0
3.5
Ln (β)
118 °C
115 °C
110 °C
100 °C

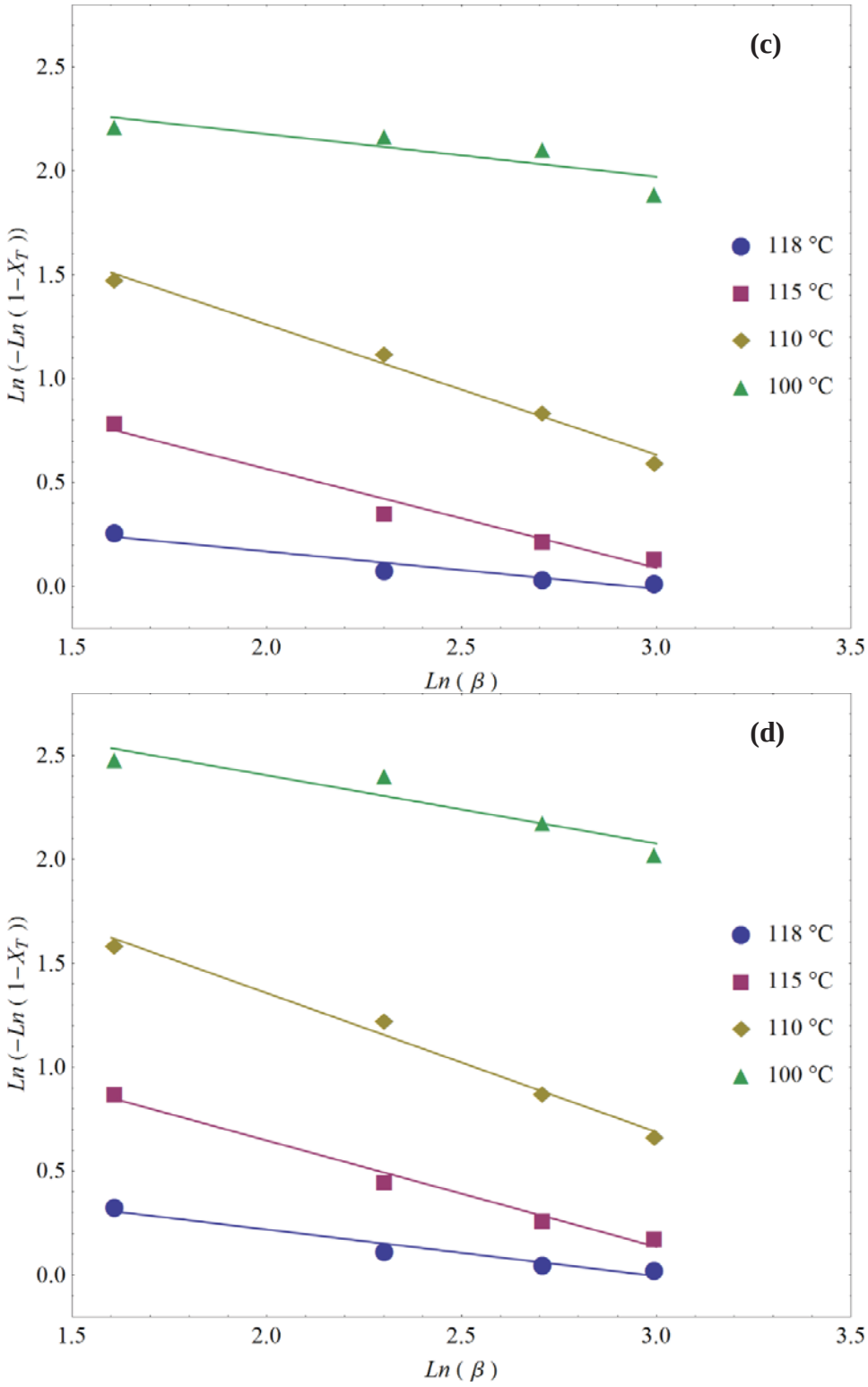

Figure 4-11 Ozawa plots for a) HDPE, b) G1/HDPE, c) G2/HDPE and d) G3/HDPE

4.5.3 Mo-method

Mo et al. [34] derived a new method for the analysis of non-isothermal melt crystallization of polymers. It takes into account both the Avrami and Ozawa models.. The combination of Equation 11 and 13 gives the following equation

$$nLn(t) + Ln(k_t) = Ln\big(K(T)\big) - mLn(\beta) \quad (14)$$

Upon simplification, the above equation is reduced to:

$$Ln[\beta] = Ln[F(T)] - \aleph Ln[t] \quad (15)$$

whereas, $F(T) = \left[\frac{K(T)}{k_t}\right]^{1/m}$ is the cooling function and $\aleph = n/m$. Although the exact physical significance of *F* (*T*) is still not clear. Theoretically, it can be related to the amount of cooling required to attain a specific degree of crystallinity in unit time [34]. Smaller value of *F* (*T*) indicates an easier crystallization process. Hence, by comparing the required degree of cooling at certain degree of relative crystallinity one can compare the rates of crystallization.

According to equation 15 for Mo-method to be valid, the plot of $Ln[\beta]$ against $Ln[t]$ for a specific value of crystallinity should be a straight line. The intercept and slope of that straight line can be used to get *F* (*T*) and $\aleph$ respectively. The Mo plots for all the samples are shown in Figure 4-12 and the results are presented in Table 4-6. From Figure 4-12 it is evident that Mo-method can be used to analyse the non-isothermal crystallization of HDPE as well as HDPE/graphene nanocomposites. Similar results were obtained with different nanocomposites of HDPE [101–104].

Form the analysis of the results in Table 4-6, it can be seen that $F(T)$ value increases with increase in $X(T)$ for all the samples. This means that in a unit time, higher degree of crystallinity can be achieved by higher cooling rate [102,104]. For a given value of $X(T)$, $F(T)$ for HDPE/graphene nanocomposites is high as compared to neat HDPE, indicating a slower rate of crystallization in HDPE/graphene nanocomposites. This is due to the fact that graphene at later stages of crystallization is acting as physical hindrance in the motion of polymer chains. This retarding effect may be due to the arrangement of polymer chains in 2D structure instead of 3D heterogeneous structure of neat HDPE, as observed in case of HDPE/MWCNTs nanocomposites by H. Kim et al. [35]. However, a clear indication about nucleation of graphene, is shown by the increase in T_{on} of HDPE/graphene nanocomposites. The nucleation hypothesis can be corroborated by E_A. It is also evident that the changes in value of α are very less, indicating that Mo-method can suitably used to analyse the crystallization process.

Table 4-6 Results of Mo analysis for HDPE and HDPE/graphene nanocomposites

Sample	X(T)	20%	40%	60%	80%
Neat HDPE	F(T)	0.85	2.51	6.10	13.86
	α	1.80	1.81	1.64	1.29
G1/HDPE	F(T)	1.17	2.42	4.81	10.48
	α	1.61	1.65	1.68	1.46
G2/HDPE	F(T)	2.11	4.55	8.10	15.10
	α	1.61	1.59	1.51	1.20
G3/HDPE	F(T)	1.62	3.26	6.78	15.20
	α	1.50	1.58	1.53	1.35

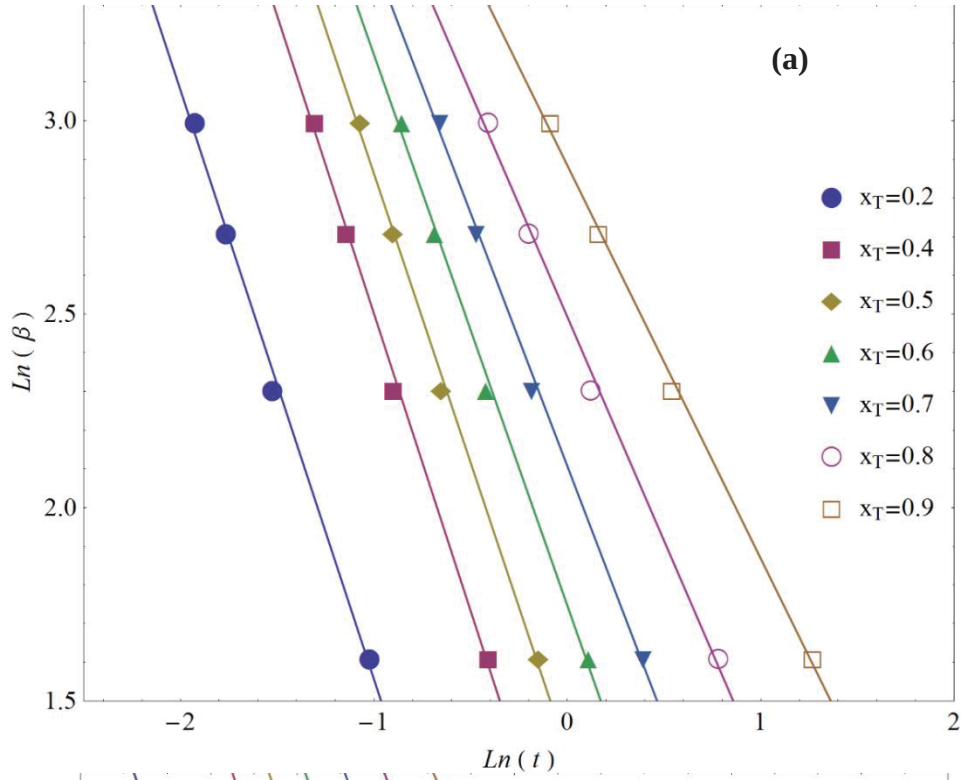
(a)
3.0
2.5
2.0
1.5
Ln (β)
−2
−1
0
1
2
Ln (t)
x_T=0.2
x_T=0.4
x_T=0.5
x_T=0.6
x_T=0.7
x_T=0.8
x_T=0.9

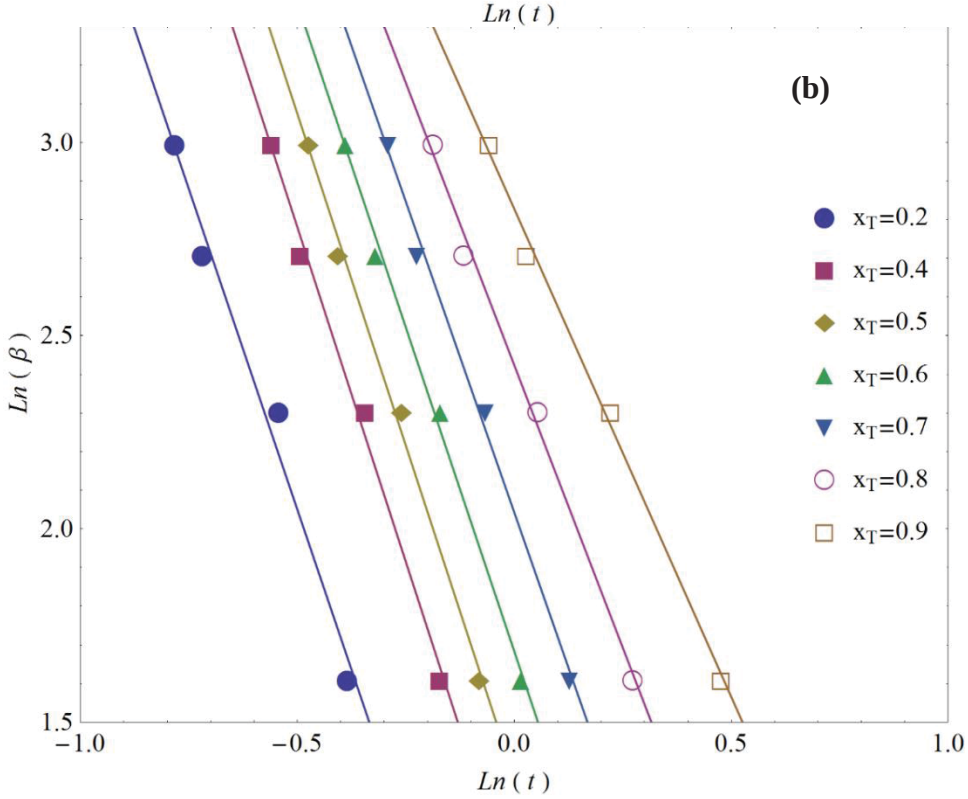
(b)
3.0
2.5
2.0
1.5
Ln (β)
−1.0
−0.5
0.0
0.5
1.0
Ln (t)
x_T=0.2
x_T=0.4
x_T=0.5
x_T=0.6
x_T=0.7
x_T=0.8
x_T=0.9

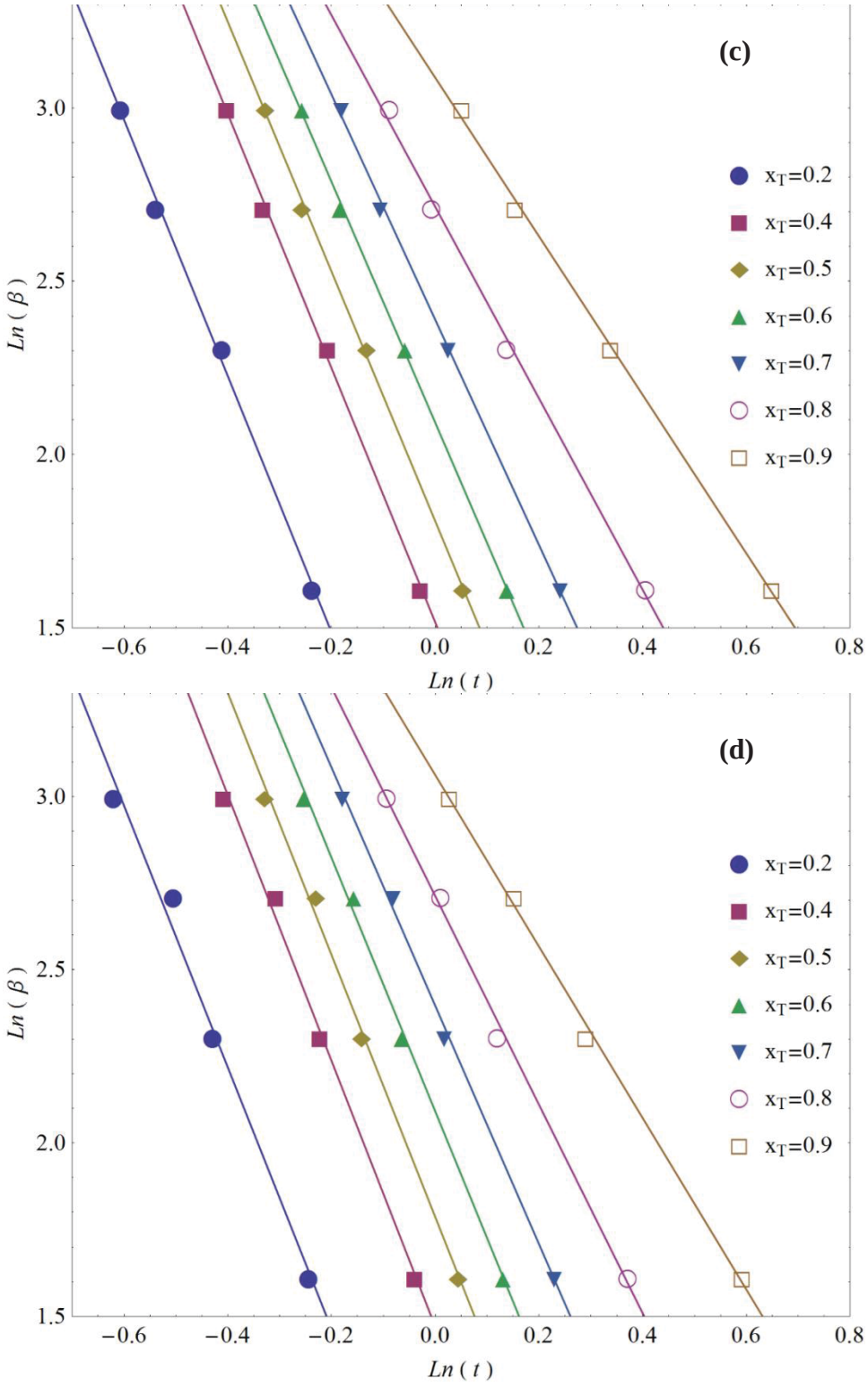

Figure 4-12 Mo- Plots for a) HDPE, b) G1/HDPE, c) G2/HDPE and d) G3/HDPE

4.5.4 Activation energy (E_A)

One of the two factors of crstallization process is activation energy. E_A is the dynamic factor controlling the crystallization of polymers. It is related to the energy required for the transport of crystalline chains across the phase. The second factor, which is the static factor, accounts for the free energy barrier of nucleation [104,105].

Vyazovkin [37] has criticized the term activation energy in for the process of melt crystallization. It has been stressed that it is the effective activation energy which accounts for all the multiple steps involved in the crystallization process. As discussed previously, generally E_A can be calculated by two class of methods. One class includes the fitting methods and second includes the iso-conversional methods. In the case of solid state kinetics, E_A changes with temperature and extent of conversion, probably due to change in the reaction medium or due to multiple steps involved in the process. Hence, a single value of E_A can be erroneous in case of solid state reactions. Keeping in mind this uncertinity, we have followed the iso-conversional method proposed by Vyazovkin [106] for the melt crystallization. This method relies on the fact that E_A is independent of heating or cooling rate and so for experiments carried out at *n* heating or cooling rates, the ratio of the temperature integral at each extent of conversion remains constant. Mathematically, we can write [38,107].

$$g(\alpha) = \frac{k_o}{\beta} \int_{o}^{T_\alpha} Exp\left[-\frac{E_{A\alpha}}{RT}\right] dT = \frac{I[E_{A\alpha}, T_\alpha]}{\beta} \qquad (16)$$

$$\frac{k_o}{\beta_1} I\left[E_{A\alpha_1}, T_{\alpha_1}\right] = \frac{k_o}{\beta_2} I\left[E_{A\alpha_2}, T_{\alpha_2}\right] = \cdots = \frac{k_o}{\beta_n} I\left[E_{A\alpha_n}, T_{\alpha_n}\right] \quad (17)$$

while α ranges from 0 to 1. According to nonlinear iso-conversional method Equation 17 follows the strict fulfillment of the following equality [107].

$$\sum_{i=1}^{n} \sum_{j \neq i}^{n} I\left[E_{A\alpha_i}, T_{\alpha_i}\right] \beta_j) / (I\left[E_{A\alpha_j}, T_{\alpha_j}\right] \beta_i) = n(n-1) \quad (18)$$

Keeping in mind the errors in the experimental data. The strict equality of the above equation can be relaxed to the absolute minimum of the function. i.e. the closest value to zero.

Mathematically,

$$\left| \sum_{i=1}^{n} \sum_{j \neq i}^{n} I\left[E_{A\alpha_i}, T_{\alpha_i}\right] \beta_j) / (I\left[E_{A\alpha_j}, T_{\alpha_j}\right] \beta_i) - n(n-1) \right| = minimum \quad (19)$$

Equation 19 was solved by using MATHEMATICA 9.0, and temperature integral was approximated using Senum and Yang approximation [108] in order to avoid excess computation time. The range of α was selected from 0.1 to 0.9 with a step size of 0.01. The results of the simulated data are shown in Figure 4-13. From this figure we can observe the variation of the E_A with the α and it is clear that E_A has decreased significantly in HDPE/graphene nanocomposites. This shows that graphene nucleates the the crystallization of HDPE/graphene nanocomposites. Similar observations were noticed in the study of virgin kevlar fiber/PE and grafted kevlar fiber/PE nanocomposites by R. Ou et al. [101]. The E_A data for selected data points are given in Table 4-7. Therefore, by

using the nonlinear iso-conversional method we have avoided the dropping of negative sign of cooling rate which is $-\beta$, confronted in the application of Kissinger method [37].

Table 4-7 Effective activation energy at progressive conversion

α / *X(T)*	-E_A (kJ/mol)			
	HDPE	G1/ HDPE	G2/ HDPE	G3/ HDPE
0.1	493.45	655.30	638.28	695.95
0.2	388.75	562.57	549.79	574.11
0.3	325.87	488.59	470.40	489.59
0.4	280.90	435.30	409.55	429.87
0.5	248.76	393.87	367.14	382.87
0.6	225.94	357.98	341.05	331.12
0.7	211.85	323.30	314.57	287.20
0.8	217.08	316.52	297.99	256.19
0.9	302.89	385.08	337.99	256.87

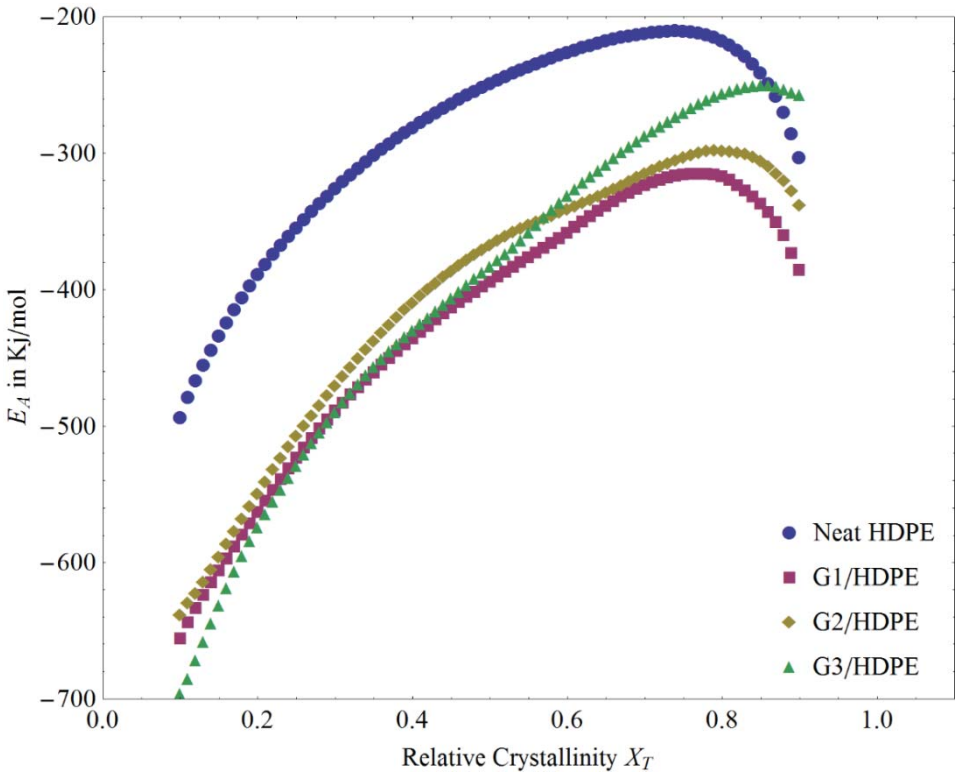

Figure 4-13 E_A at progressvie conversion for HDPE and HDPE/graphene nanocomposites

4.5.5 Nucleation activity

The nucleation activity for non-isothermal process can be calculated by Dobvera method [109]. According to this method, the following relation is valid for non-isothermal crystallization process.

$$\varphi = \frac{B_s^*}{B_s} \tag{20}$$

$$Ln[\beta] \approx const - \frac{B_s^*}{2.3\ \Delta T_P^2} \tag{21}$$

$$Ln[\beta] \approx const - \frac{B_s}{2.3\ \Delta T_P^2} \tag{22}$$

whereas, ΔT_P is the difference between T_{on} and T_p. The parameters $B_S^*$and B_S can be calculated from the plot of $Ln[\beta]$ against $1/(2.3\Delta T_p^2)$ for neat HDPE and the nanocomposites respectively.

For highly active nanofillers, φ approaches 0 and for inert ones it is one. Figure 4-14 shows the plots of $Ln[\beta]$ vs. $1/(2.3\Delta T_p^2)$ for HDPE and HDPE/graphene nanocomposites. The results are shown in Table 4-8. For all the nanocomposites φ is less than 1 and decreases with increasing wt.% of graphene. This indication also supports the postulate of nucleation of graphene.

Table 4-8 Nucleation activity data for HDPE and HDPE/graphene nanocomposites

Nanocomposite	G1/HDPE	G2/HDPE	G3/HDPE
Nucleation Activity ϕ	0.62	0.59	0.57

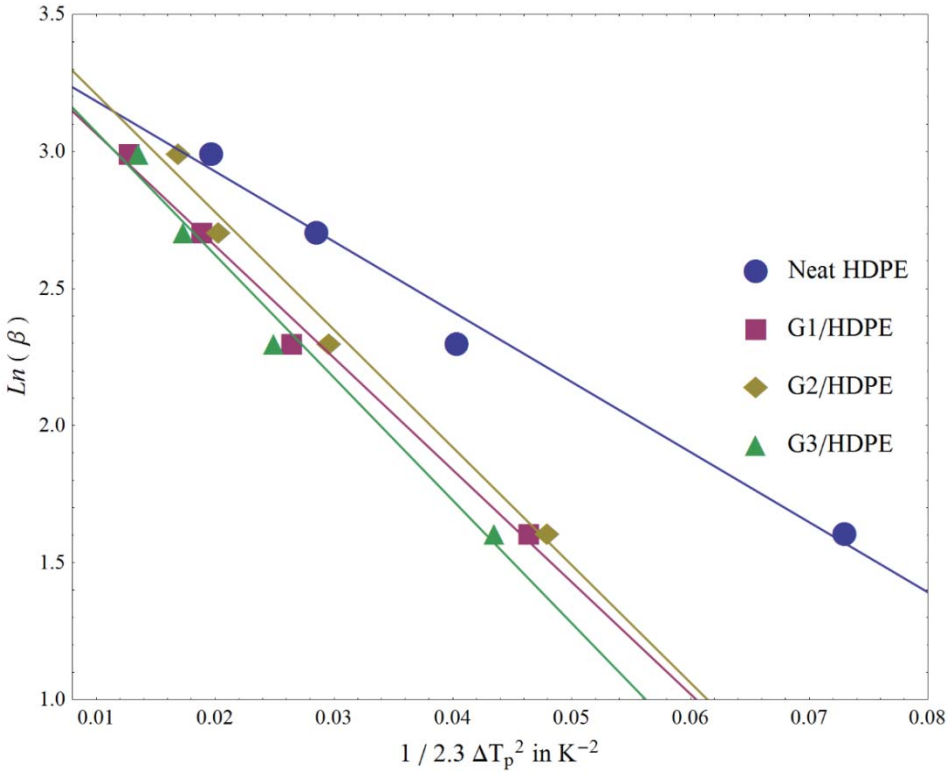

Figure 4-14 Nucleation activity plots for HDPE and HDPE/graphene nanocomposites

4.6 Flammability testsof the nanocomposites

The combustibility of the synthesized nanocomposites was assessed by measuring the peak heat release rate (Peak HRR), total heat released (Total HR) and peak decomposition temperature (T_p). The tests were carried out by using Pyrolysis Combustion Flow Calorimeter (PCFC) also known as Micro calorimeter (MC). The obtained results are presented in Table 4-9.

Table 4-9 Data for combustion analysis of HDPE and HDPE/graphene nanocomposites

No	Sample	Peak HRR (W/g)	Total HR (kJ/kg)	T_p (°C)
1	HDPE	1039.68± 32.21	39.25± 3.09	507.21± 1.53
2	G1/HDPE	665.28 ± 18.87	29.18 ± 2.27	496.02 ± 2.55
3	G2/HDPE	648.16 ± 19.46	28.73 ± 2.34	489.76 ± 1.81
4	G3/HDPE	788.90± 25.59	33.34± 0.89	499.61± 1.88

It was observed that both the Peak HRR and Peak decomposition temperatures are profoundly decreased in HDPE/grapehene nanocomposites. This decrease illustrates the improvement in flame retardant capability of the nanocomposites. This behavior is due to layered structure and gas barrier properties of graphene nano-particles, which prevents the evolution of combustion gases, thereby reducing the combustibility of material [110,111]. The results for PCFC test are also graphically presented in Figure 4-15 to Figure 4-17. It can be observed that the decreasing trend of the PHRR and T_p is vanishing at higher loadings of graphene. This effect could be the result of restacking of graphene due to strong Van der Waals forces between sheets of graphene. However, this issue can be addressed by using graphene hybrids such graphene cobalt oxide and graphene nickel oxide etc. to enhance the flame retarding efficiency of graphene [110–112].

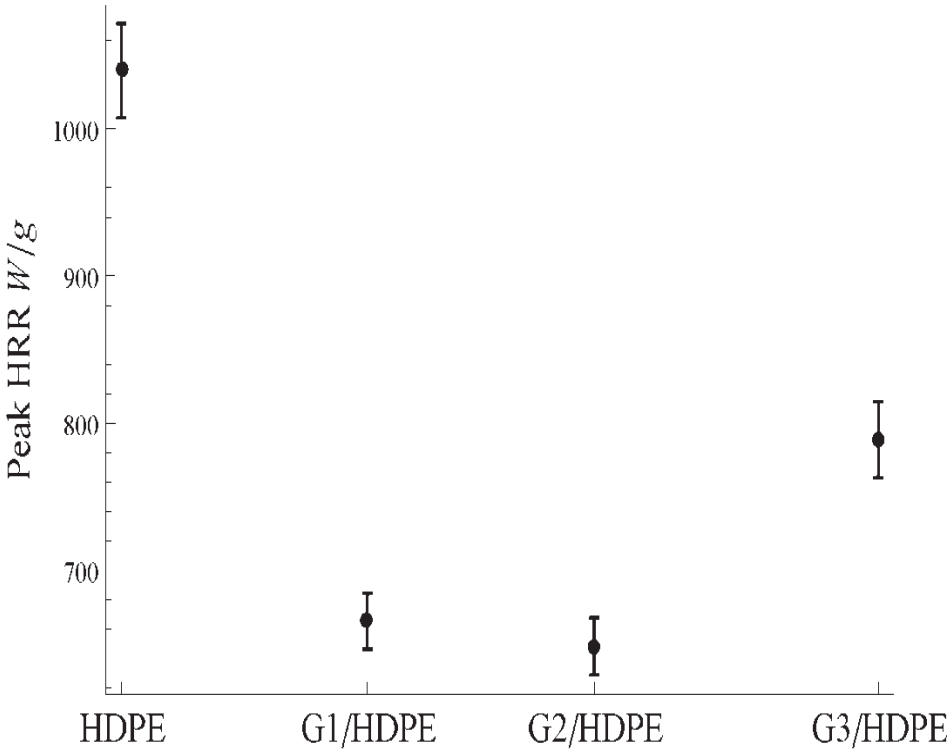

Figure 4-15 Peak heat released rate for HDPE and HDPE/graphene nanocomposites

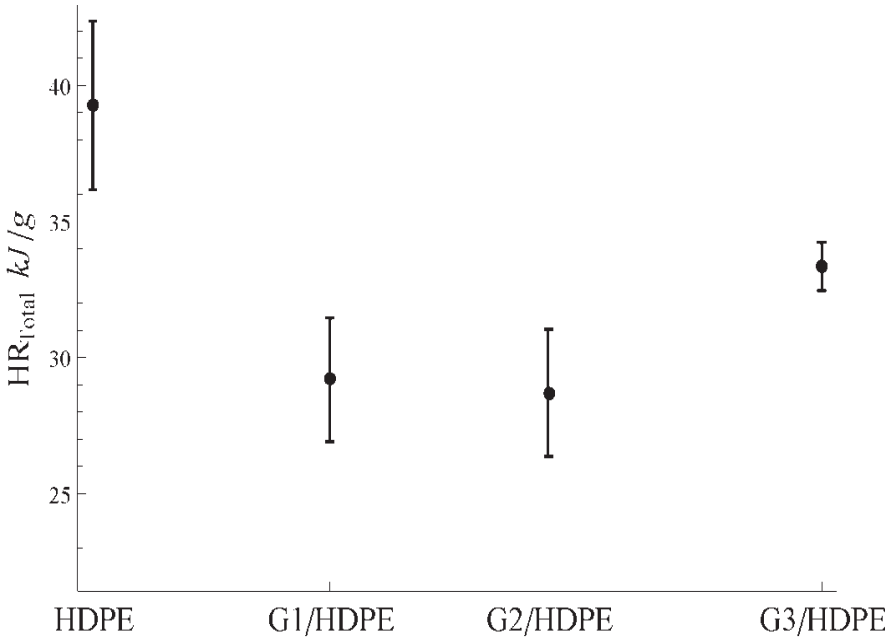

Figure 4-16 Total heat released per unit mass for HDPE and HDPE/graphene nanocomposites

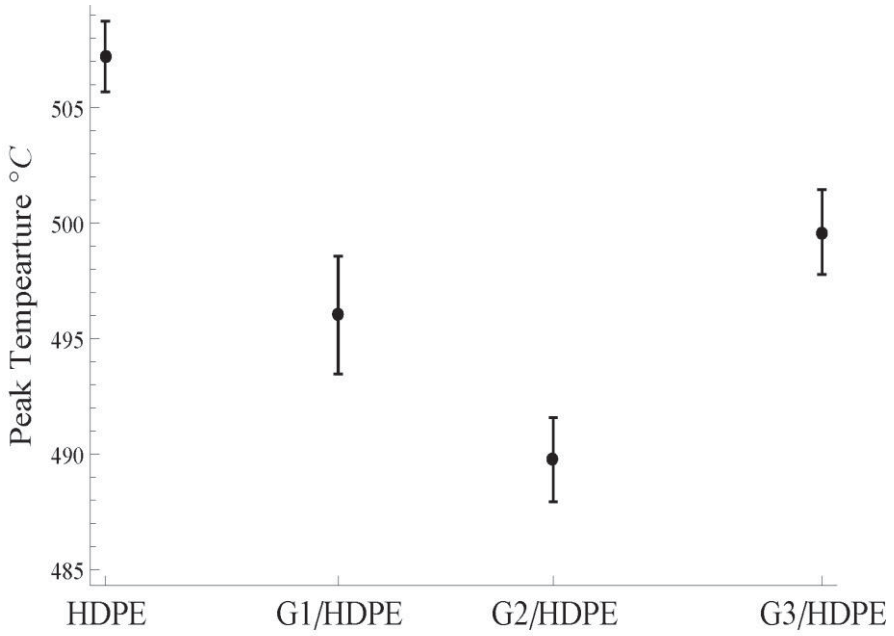

Figure 4-17 Peak decomposition temperatures for HDPE and HDPE/graphene nanocomposites

4.7 Molecular weight and MWD of the nanocomposites

The molecular weights of the synthesized nanocomposites were analyzed with the help of high temperature size exclusion chromatography. The results showed an increase in molecular weight of the nanocomposite, for 10 and 15 mg of graphene, those corresponding to G2/HDPE and G3/HDPE respectively. The highest M_w is obtained with 10 mg of filler. At higher loadings of graphene such as 15 mg the steric hindrance tends to overcome, therefore reducing the M_w. The increase in molecular weight can be due to the steric and electronic effect of graphene [113,114]. It has been found that M_w of metallocene polymerized polymers increases with electron donating effect [115]. The steric effect of graphene and CNTs can be utilized to tune the molecular weight, MWD and catalytic activity of single site catalyst. S. Park et al. used MWCNTs adsorbed with zirconocene to synthesize high molecular polyethylene with high MWD. The increase in

molecular weight was attributed to electronic and steric effect of MWCNTs [116]. Similarly, M. Stürzel et al. prepared ultra-high molecular weight PE by using functionalized graphene as a support for single site chromium catalyst [31]. Furthermore, an increase in PDI is also observed along with increase in molecular weight. This high molecular weight polymers are difficult to process due to high melt viscosity. Therefore, high molecular weight distribution (MWD) is usually desired to overcome this challenge [117,118].

The summarized results are shown in Table 4-. The results obtained from GPC supports the hypothesis derived from DSC, GPC and DMA that there should be an increase in the molecular weight of the graphene filled nanocomposites. So, from these results we can infer that narrow distribution of CRYSTAF profiles for the graphene filled nanocomposites were due to high molecular weights of the samples.

Table 4-10 Molecular weights of samples determined by HT GPC

No.	Sample	M_n	M_w	PDI
1	HDPE	8568.75	30044.75	4.13
2	G1/HDPE	9934.50	31513.50	3.17
3	G2/HDPE	15182.00	119862.75	11.55
4	G3/HDPE	9929.50	78140.50	8.17

4.8 Morphological analysis

Scanning Electron Microscope (SEM) was used to study the morphological properties of the synthesized nanocomposites. In order to get clear insights about the surface, the material was broken and fresh surface was examined. Figure 4-18 (a, b, c and d) show the SEM images of HDPE and HDPE/graphene nanocomposites. From this figure, it can be seen that with the addition of graphene the morphology changes to a fiberous like structure. This is the reason of increase in stiffness and elastic response of the material. However, the fiber like morphology is more evident for G1/HDPE (Figure 4-18a) and less clear for G2/HDPE and G3/HDPE at low resolution. The SEM images of G1/HDPE, G2/HDPE and G3/HDPE at high resolutions are shown in Figure 4-19. At higher resolutions we can observe the fiber like structure in G2/HDPE but not in G3/HDPE. This may be due to the agglomeration of graphene at higher concentrations.

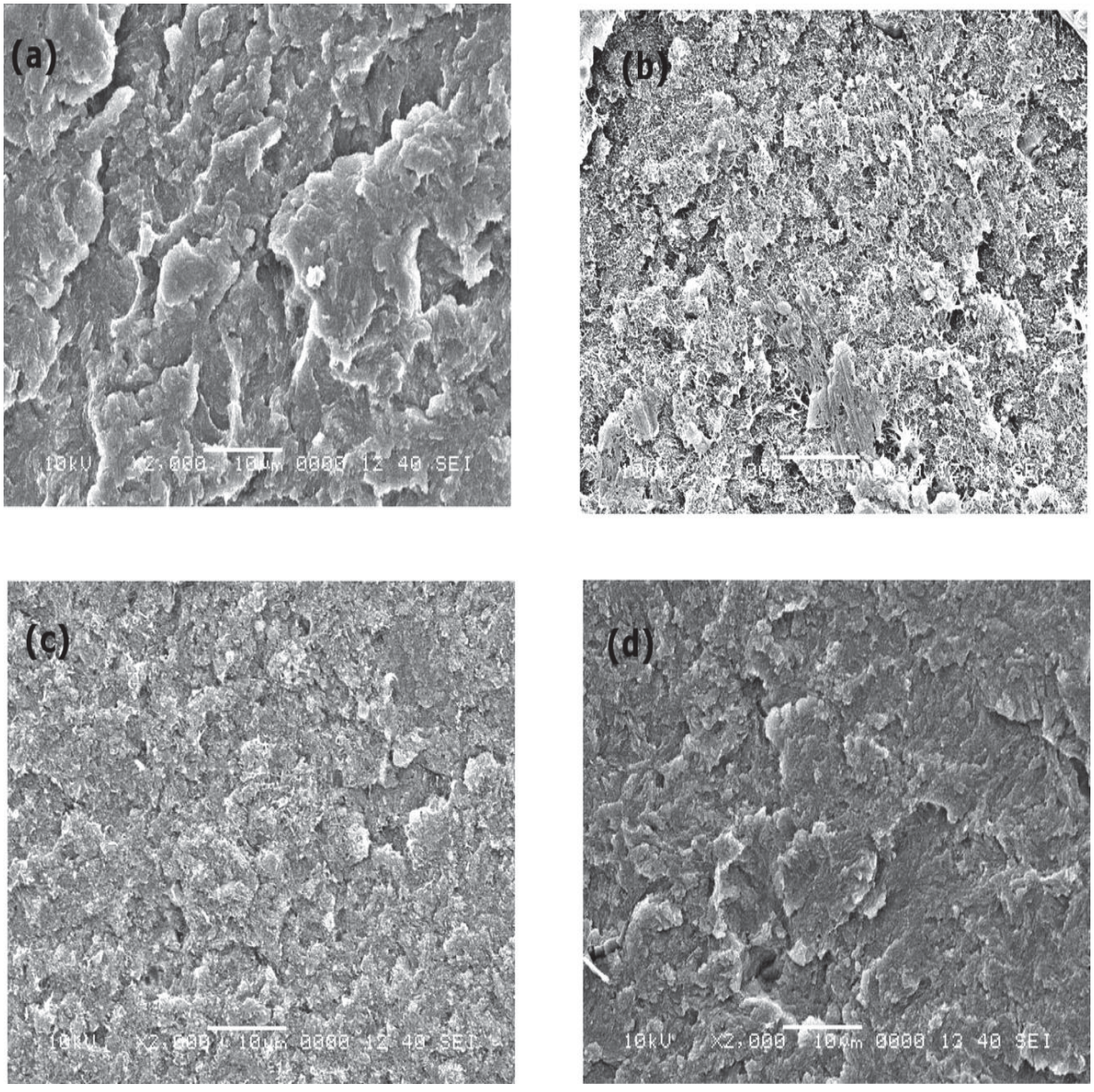

Figure 4-18 SEM images of cross section at 2000x for a) HDPE, b) G1/HDPE, c) G2/HDPE and d) G3/HDPE

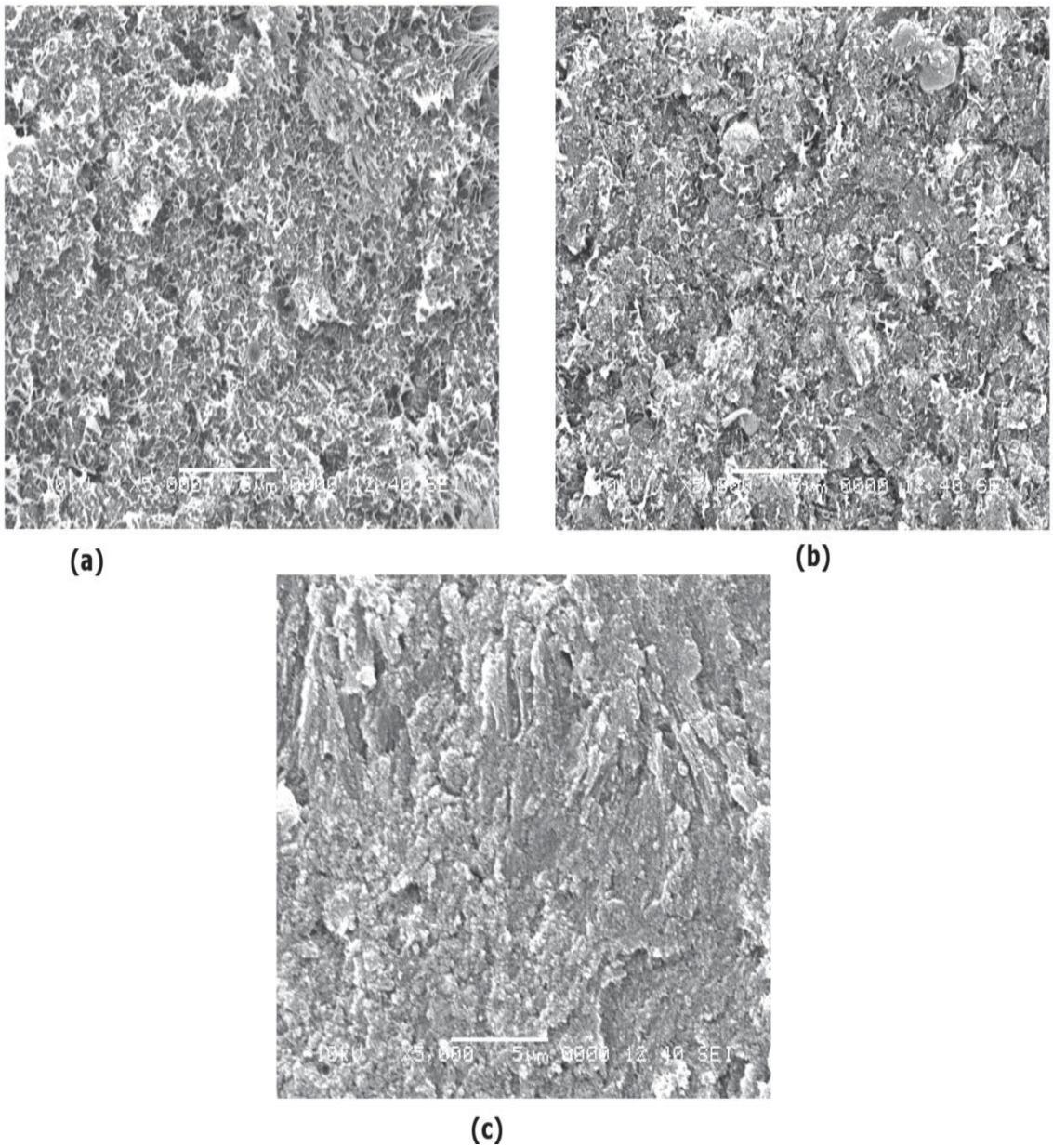

Figure 4- 19 SEM images of cross section at 5000x for a) G1/HDPE, b) G2/HDPE and c) G3/HDPE

4.9 Effect of graphene on natural weathering of HDPE

Thin films of the synthesized nanocomposites along with pristine HDPE were exposed outdoors at the exposure site located at KFUPM, Dhahran, Saudi Arabia. The samples were placed on racks placed at 45 ° angle in the basement. Samples were collected and tested for degradation after a time span of 1 month, 2 months and 3 months. The meteorologicaldata for the Dhahran city is shown in Figure 4-20. The extent of degradation was studied with the help of FTIR, DMA and GPC.

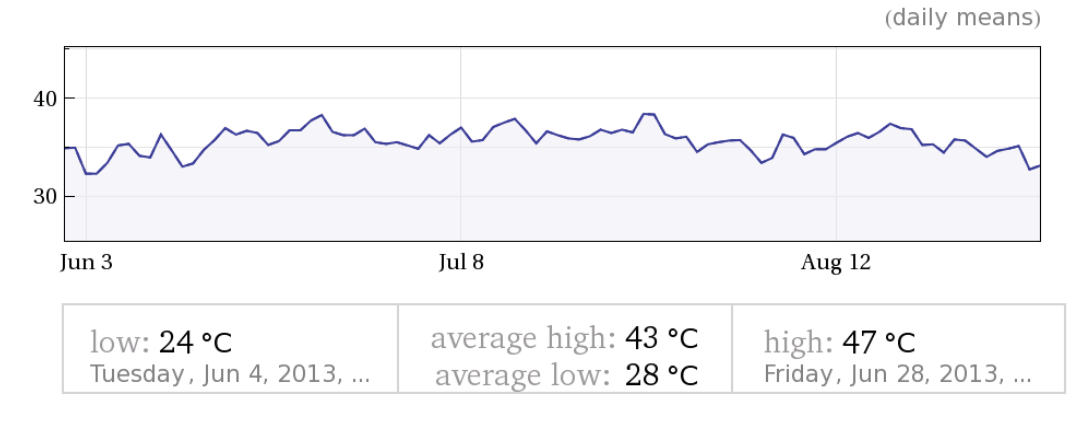

(a)

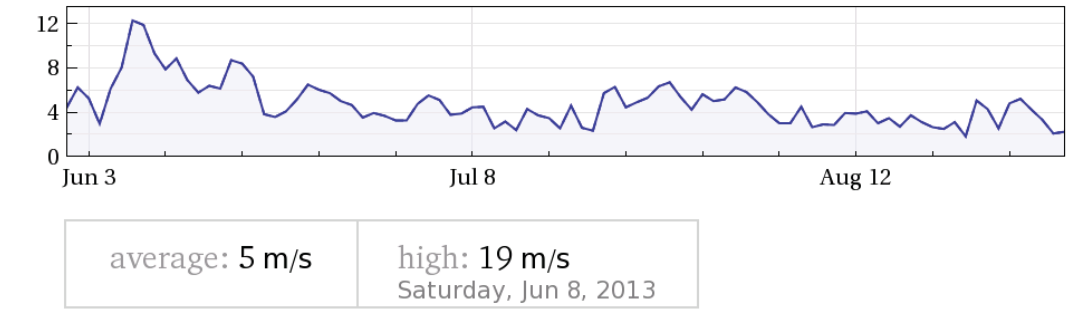

(b)

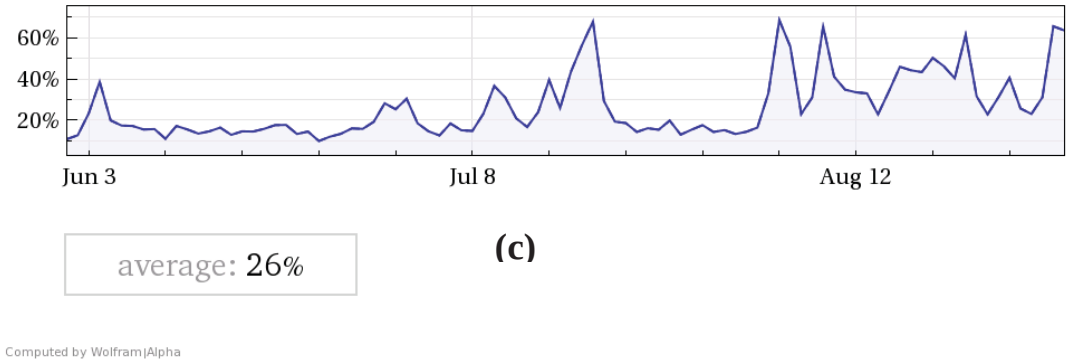

(c)

Figure 4-20 Weather record of Dhahran, Saudi Arabia form Jun to Aug 2013 a) Temperature b) Wind Speed c) Humidity [119]

4.9.1 Change in crystallinity and T_m with the extent of degradation

Figure 4-21 shows the DSC heating curve of neat HDPE and different age weathered HDPE. From the DSC results it is observed that the degree of crystallinity of the pristine HDPE is increased within the first 30 days and then decreased subsequently with the exposure time. The increase in crystallinity indicates the chain scission of HDPE. Density of the chains entanglements is reduced due to degradation *via* Norrish I and II reactions. The resulting shorter chains molecules can crystallize easily due to high chain mobility [120]. As a result of UV degradation,, functional groups like –CO, -OH, -OOH are formed and these groups replace the $–CH_2$ group in the amorphous region. This process is known as secondary crystallization or chemi-crystallization. In chemi-crystallization the crystallinity is increased because the chain mobility is increased [70]. Although the change in the crystallinity is much evident for HDPE, however, the change in crystalline melting temperature is not much pronounced. This consistency in the melting temperature can be attributed to formation of new intermolecular polar bonds of carbonyl groups [71]. The increase in crystallinity of HDPE at initial stages has also been observed in case of rape straw flour (RSF)/HDPE and nano-SiO_2/RSF/HDPE composites [121].

In case of HDPE/graphene nano-composites, the crystallinity is first reduced slightly and then remains constant. Like neat HDPE the crystalline melting temperature is not affected prominently with the extent of exposure. The consistency of crystallinity in the HDPE/graphene nanocomposites may be due to the enhanced stability of the nano-composites. It has been reported that graphene can absorb the UV radiation and prevent degradation of polyurethane/graphene coatings [122].

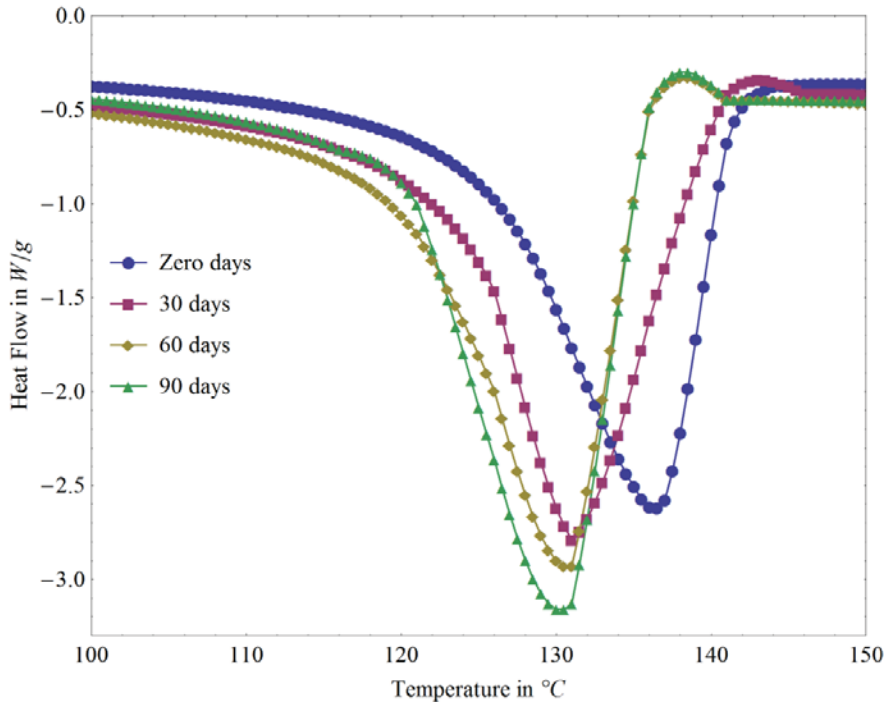

Figure 4-22 Evolution of DSC endotherms for HDPE with exposure time

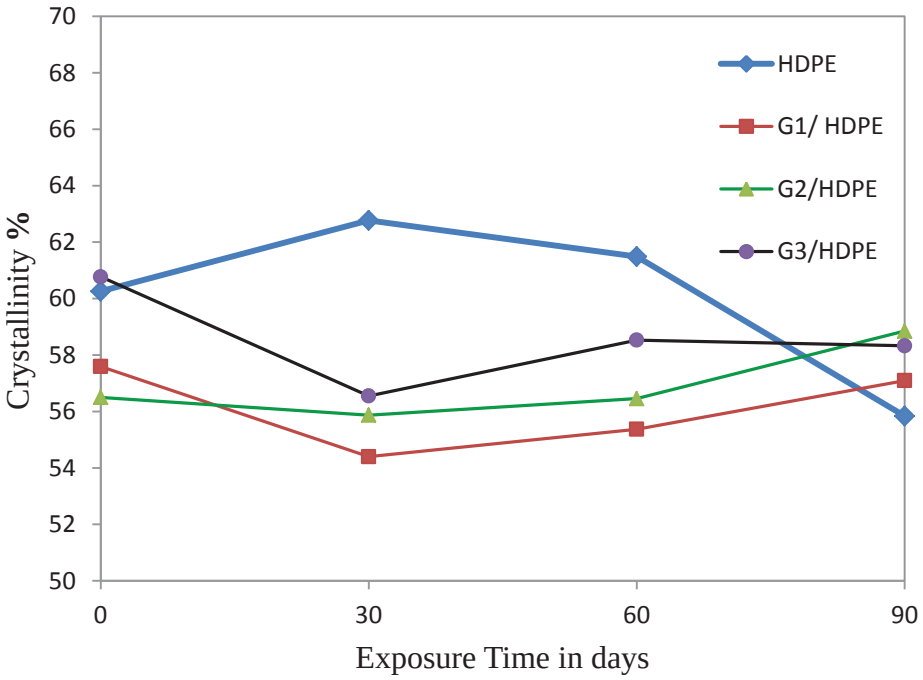

Figure 4-21 Crystallinity as a function of exposure time for HDPE and HDPE/Graphene nano-composites

4.9.2 Fourier transformedinfrared spectroscopy (FTIR)

FTIR is a very powerful technique used to study degradation. During degradation, several changes in the molecular structure of the HDPE takes place and these can be detected by FTIR. Free and associated hydroperoxide and carbonyl groups formed during degradation can be traced. Figure 4-24-a shows the carbonyl region for neat HDPE at different exposure time. It is observed that the intensity of carbonyl peak is increasing with the exposure time due to occurrence of degradation [123]. From Figure 4-24-a the new peaks formed around 1780 to 1700 cm^{-1} corresponds to the carbonyl region, which consist of lactone at 1780 cm^{-1}, ester around 1735 cm^{-1}, the ketone around 1715 cm^{-1} and carboxylic acid groups around 1700 cm^{-1}. These functional groups have also been observed in various studies of HDPE photo-oxidative degradation [124,125].

Unlike neat HDPE, the carbonyl region of all the HDPE/graphene nanocomposites did not change significantly. FromFigure 4-24(b, c and d) it is evident that the carbonyl groups formation is being retarded due to the presence of graphene. Similary it be seen from Figure 4-24, that for HDPE there is a peak appeared near 1780 cm^{-1} corresponding to γ-lactone after 60 and 90 days of exposure [126,127]. However, this peak is absent in HDPE/graphene nanocomposites. From this it can be presumed that there might be some changes in the degradation mechanism.

The extent of degradation can be measured quantitatively by measuring the carbonyl index (CI). CI is given by the relationship below [128].

$$CI = (I_{718}/I_{2915}) \times 100$$

Where, I stands for the peak intensity. The peak at 2915 cm^{-1} was used as reference peak for normalizing as this peak showed minimum changes during the exposure time. The peak at 2915 cm^{-1}corresponds to C-H stretching vibrations of -CH_2 group.

The carbonyl index for HDPE and the nano-composites is shown in Figure 4-23.

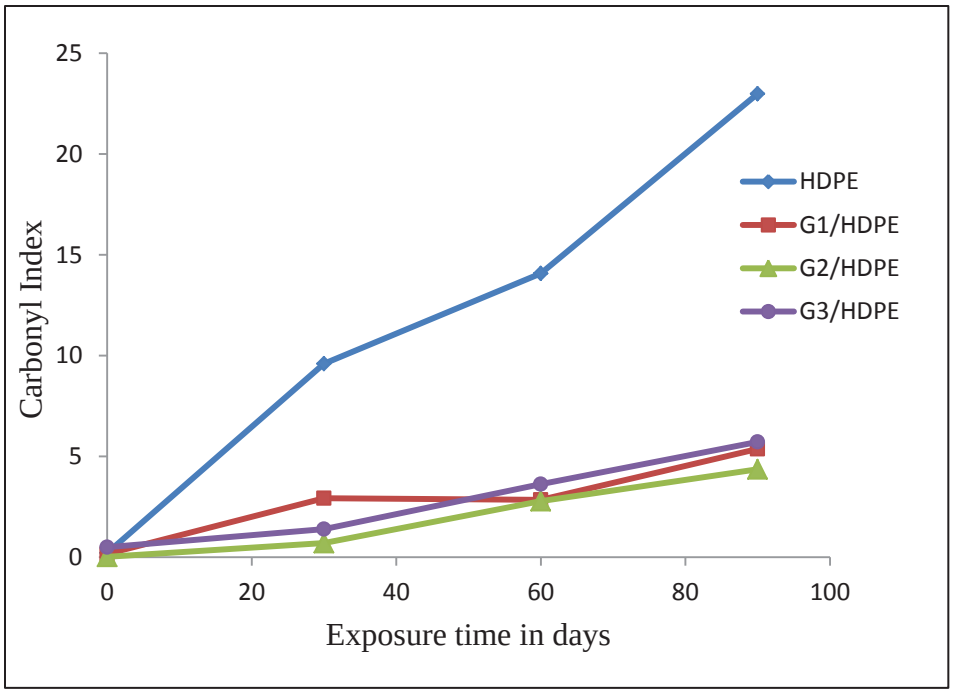

Figure 4-23 Carbonyl Index for HDPE and HDPE/Graphene nano-composites at different exposure time

It is observed that carbonyl index of neat HDPE increases with the exposure time. The increment in CI for HDPE indicates its degradation with time. It has also been reported that the increase in CI is propotional to the chain scissions [129]. On the other hand G1/HDPE, G2/HDPE and G3/HDPE have carbonyl indices less than neat HDPE at all times as presented in Figure 4-23. This shows that graphene is protecting the polymer matrix from degradation by restricting the formation of carbonyl groups.

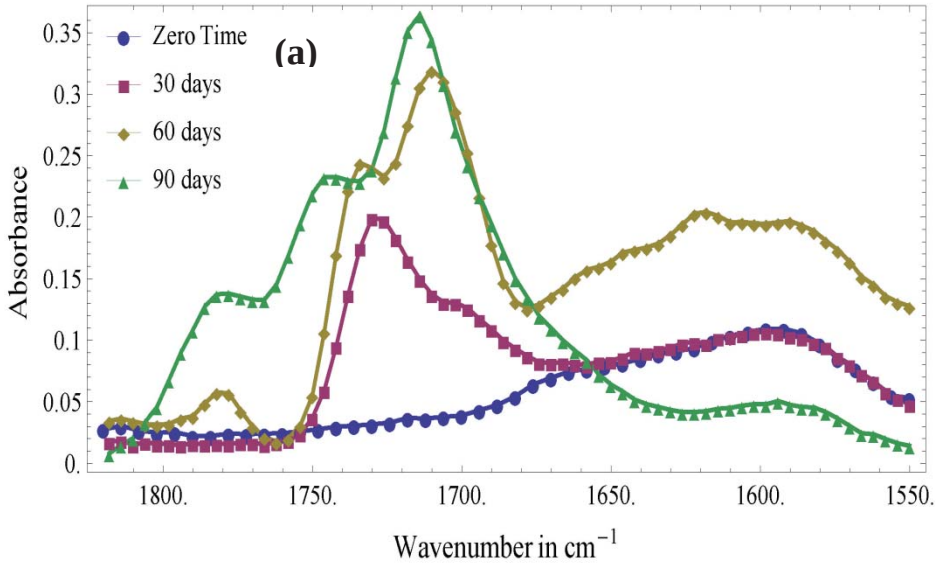
(a)
Zero Time
30 days
60 days
90 days
Absorbance
0.35
0.3
0.25
0.2
0.15
0.1
0.05
0.
1800.
1750.
1700.
1650.
1600.
1550.
Wavenumber in cm^{-1}

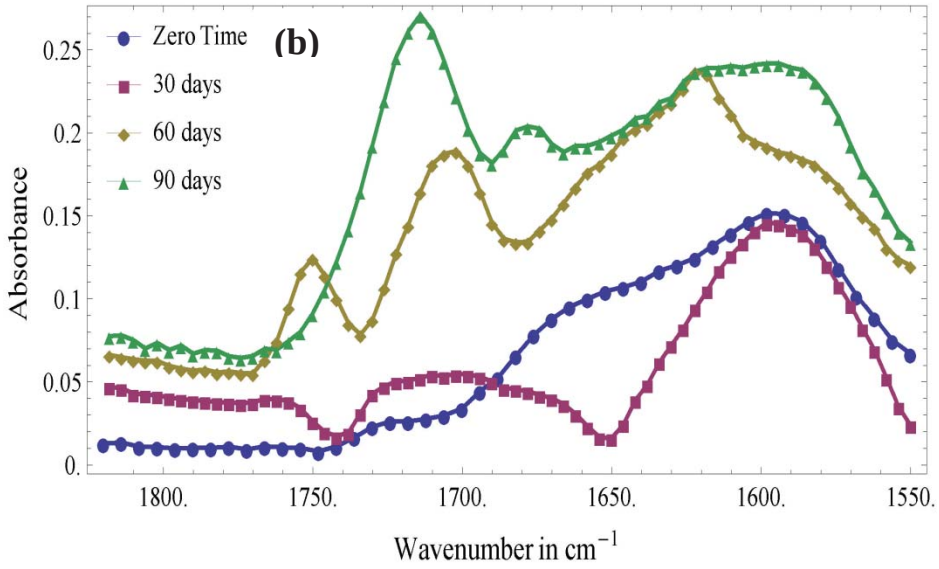
(b)
Zero Time
30 days
60 days
90 days
Absorbance
0.25
0.2
0.15
0.1
0.05
0.
1800.
1750.
1700.
1650.
1600.
1550.
Wavenumber in cm^{-1}

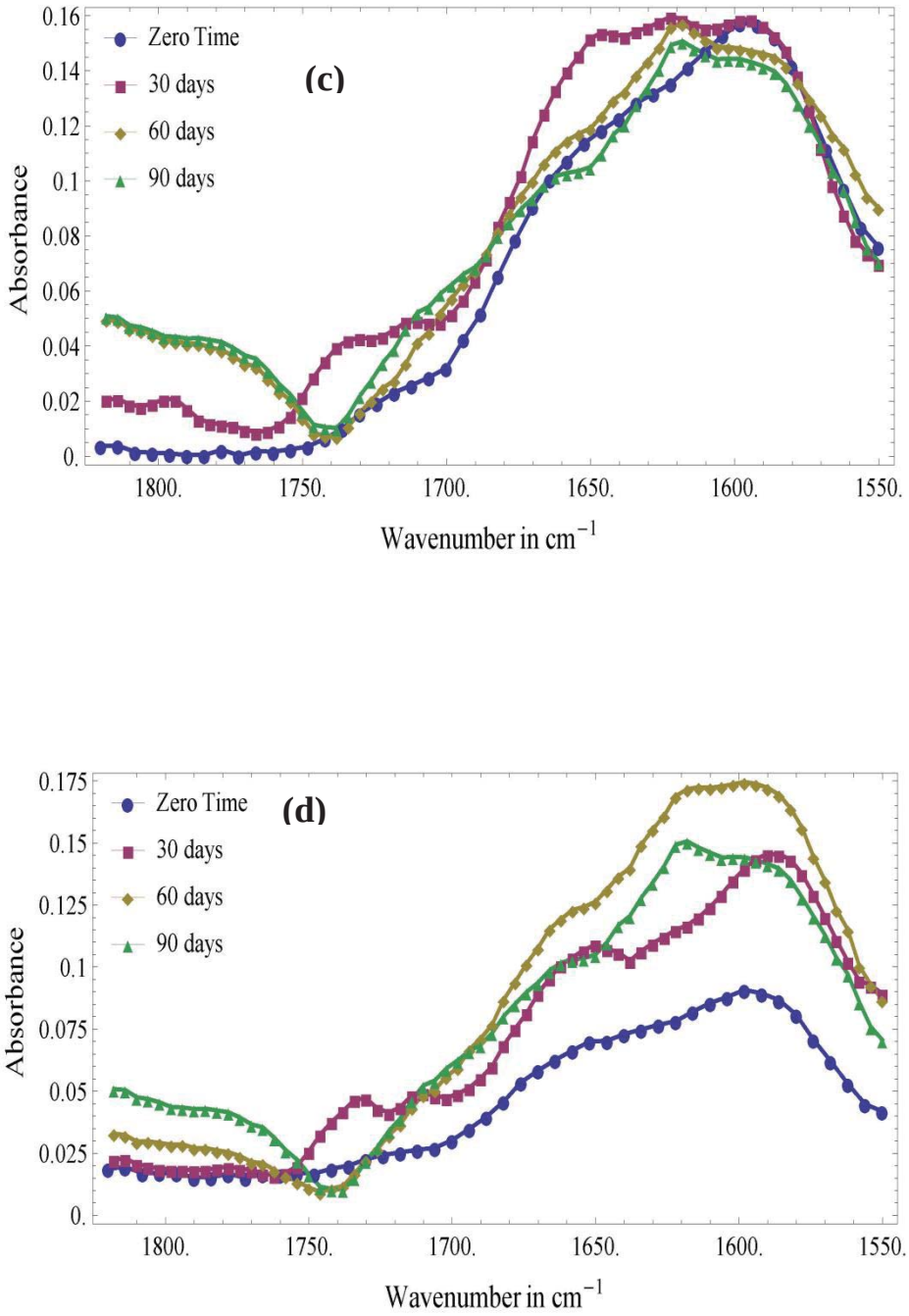

Figure 4-24 Changes in Carbonyl regions for a) HDPE, b) G1/HDPE, c) G2/HDPE and d) G3/HDPE with exposure time

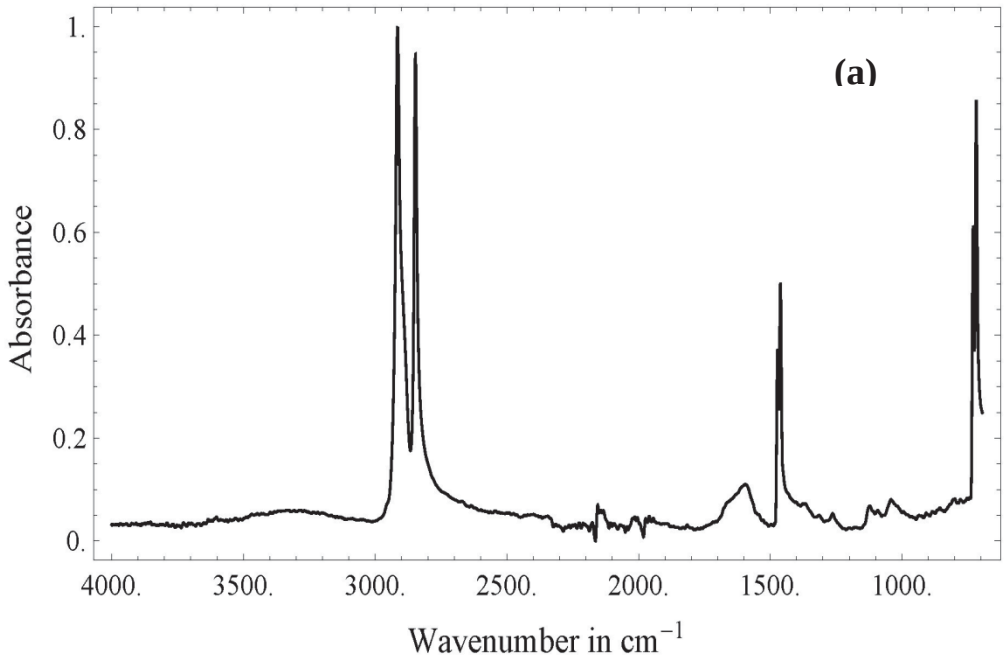
(a)
Absorbance
1.
0.8
0.6
0.4
0.2
0.
4000.
3500.
3000.
2500.
2000.
1500.
1000.
Wavenumber in cm^{-1}

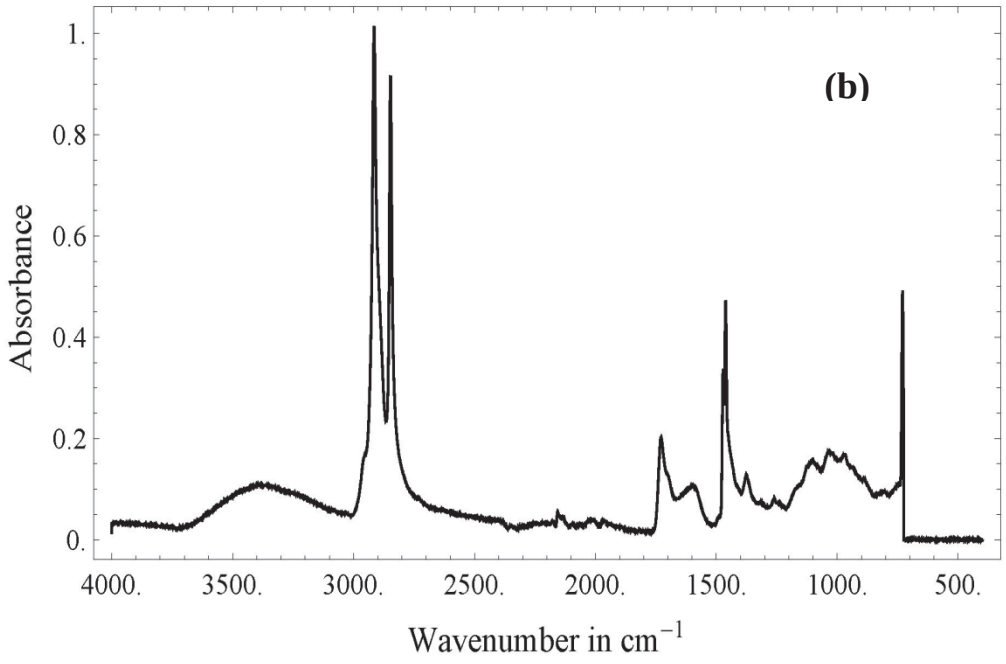
(b)
Absorbance
1.
0.8
0.6
0.4
0.2
0.
4000.
3500.
3000.
2500.
2000.
1500.
1000.
500.
Wavenumber in cm^{-1}

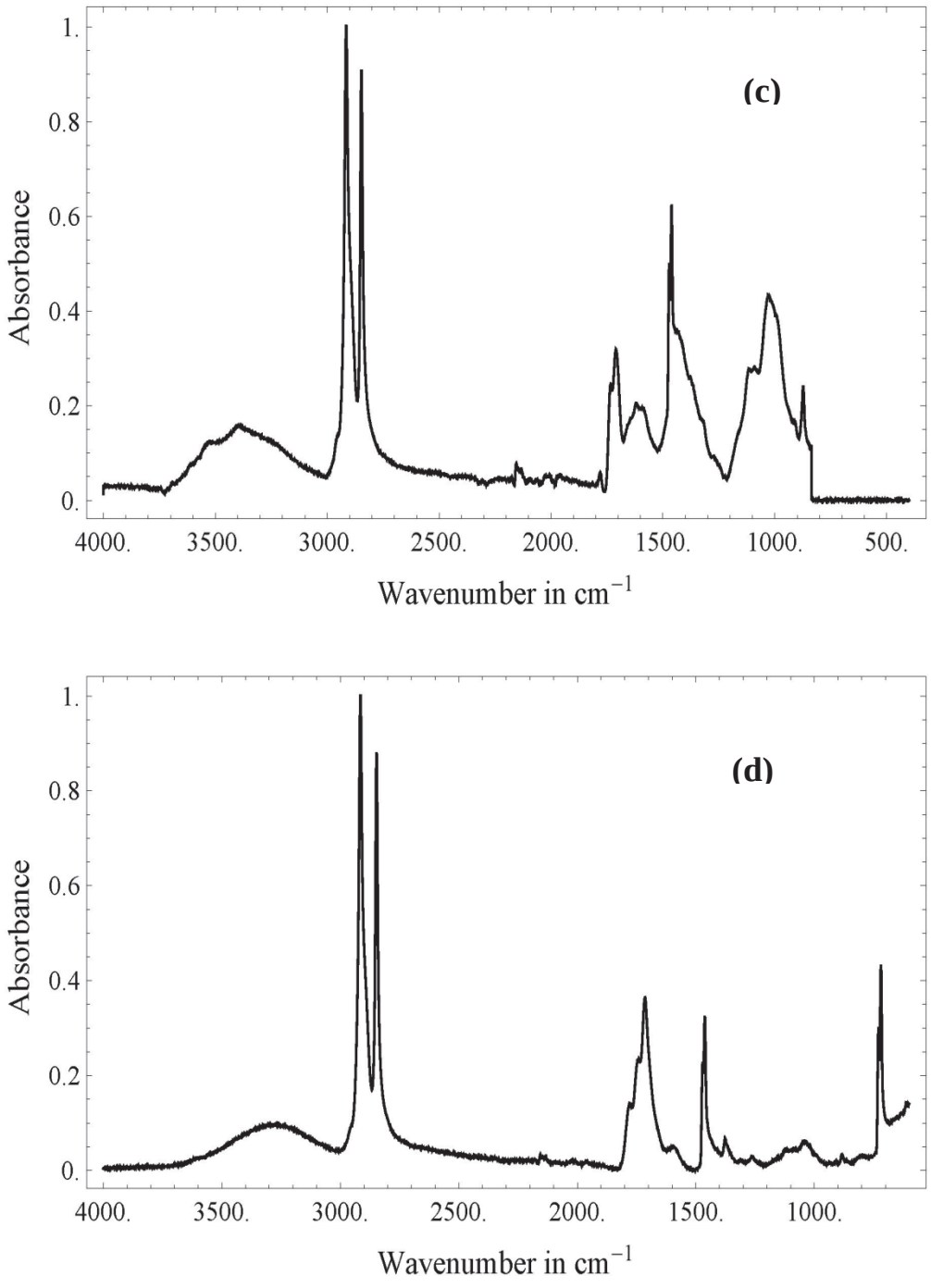

Figure 4-25 FTIR spectra for G3/ HDPE, a) no exposure,b) 30 days, c) 60 days and d) 90 days

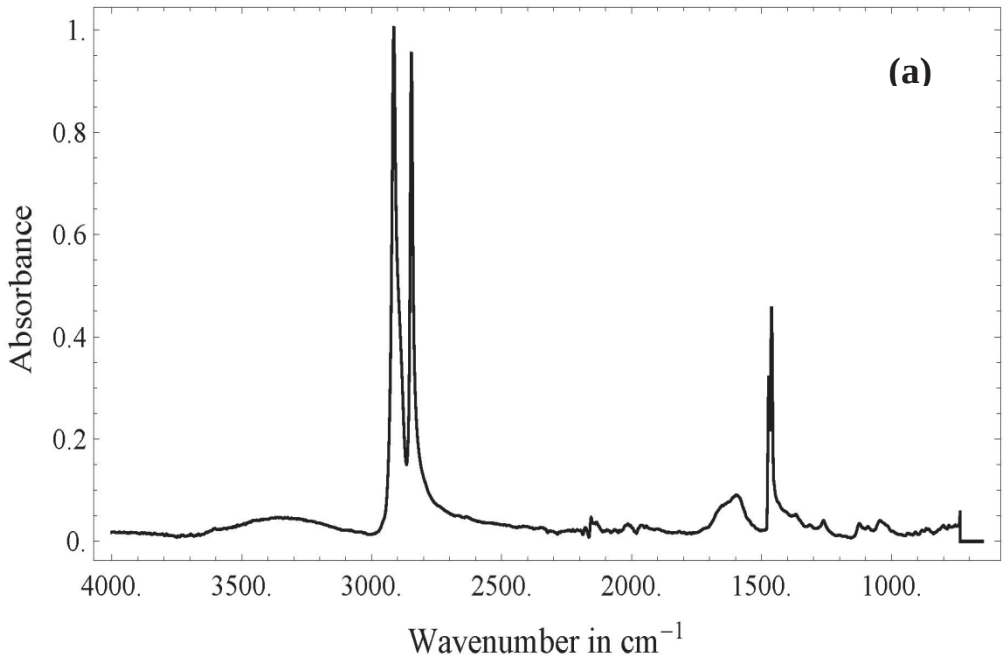
(a)
Absorbance
1.
0.8
0.6
0.4
0.2
0.
4000.
3500.
3000.
2500.
2000.
1500.
1000.
Wavenumber in cm^{-1}

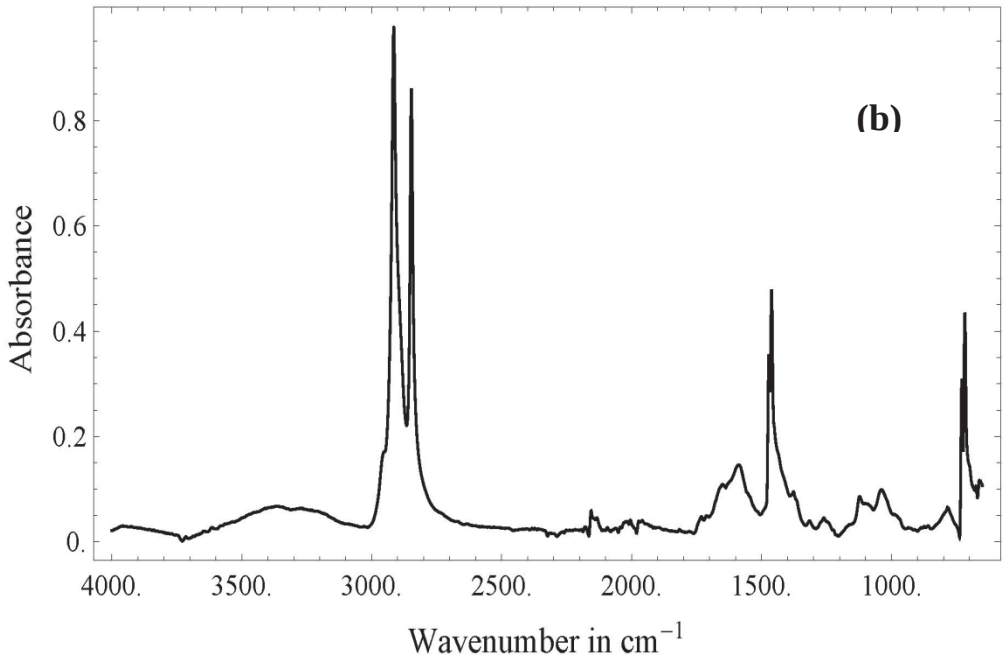
(b)
Absorbance
0.8
0.6
0.4
0.2
0.
4000.
3500.
3000.
2500.
2000.
1500.
1000.
Wavenumber in cm^{-1}

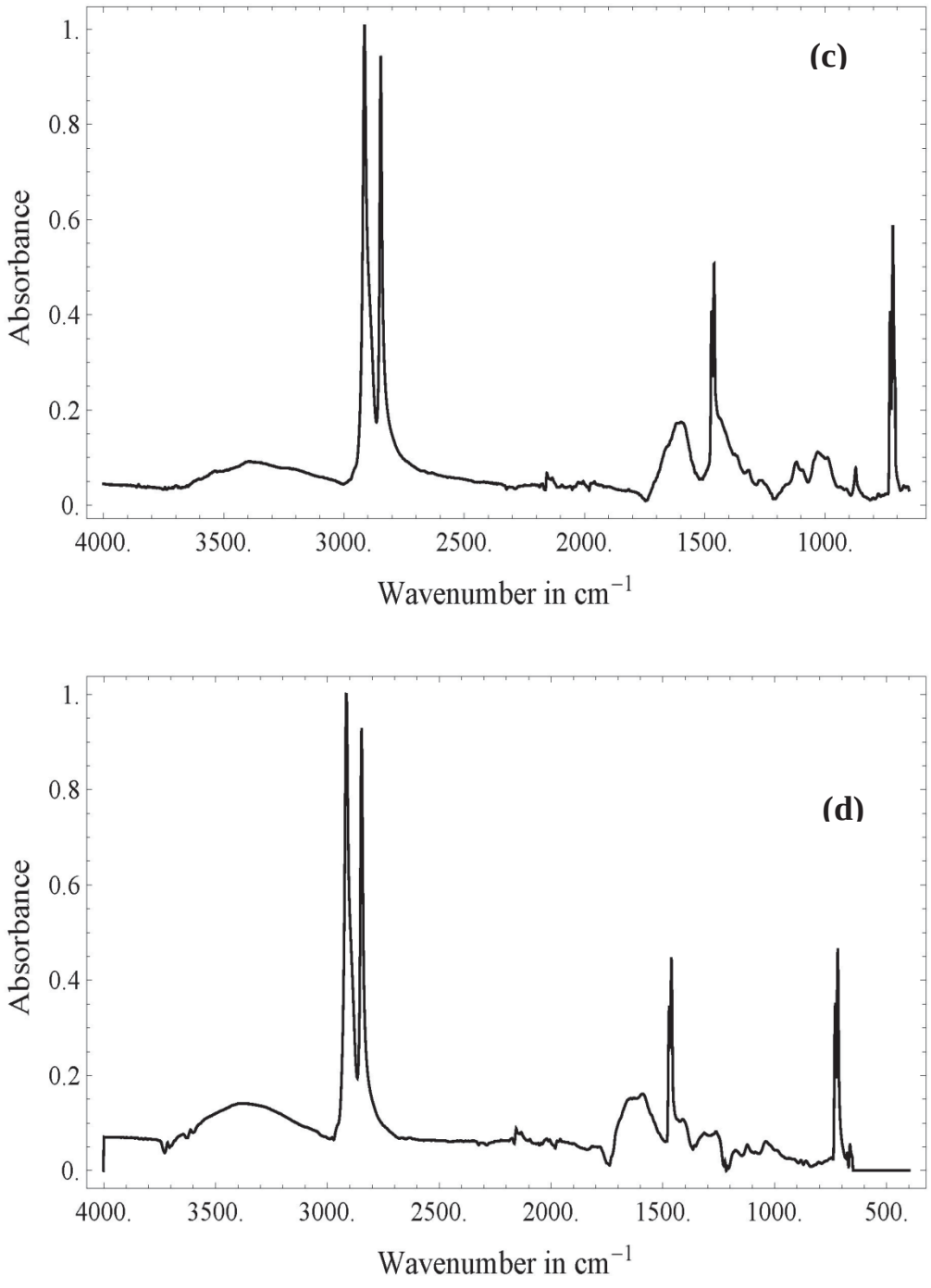

Figure 4-26 FTIR spectra for HDPE a) no exposure,b) 30 days, c) 60 days and d) 90 days

4.9.3 CRYSTAF and molecular weight analysis after degradation

The degraded samples were analyzed for changes in microstructure and molecular weights by CRYSTAF. The CRYSTAF profiles for HDPE and HDPE/graphene nanocomposites are shown in Figure 4-27 (a, b, c, d). For HDPE, as can be seen from Figure 4-27-a, a slight shift in the peak crystallization temperature (T_p) and an increase in broadness of the peak indicate the degradation. This broadness of the peak corresponds to the inter chain heterogeneity [89]. Furthermore, there is a continuous decrease in the height of the peak, which can be related to the decrease in molecular weight. On the other hand, such changes in HDPE/graphene nanocomposites are less pronounced, specifically G2/HDPE and G3/HDPE. From this we can infer that HDPE/graphene has suffered lesser degradation as compared to neat HDPE.

Table 4-9 shows the summarized results for molecular weight analysis of the exposed and the unexposed samples. It can be seen that for all graphene reinforced HDPE nanocomposites, the change in molecular weight is less pronounced specially for the first two months. These observations support the conclusions deduced from FTIR, DSC and CRYSTAF results.

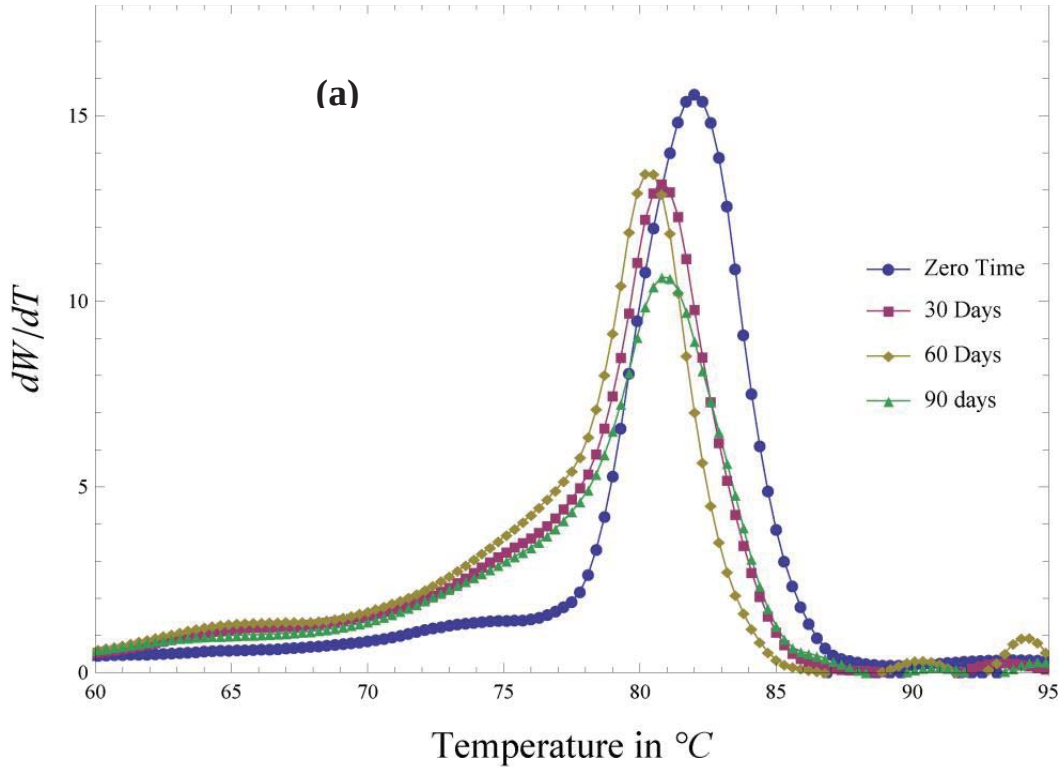
(a)
dW/dT
Temperature in °C
Zero Time
30 Days
60 Days
90 days

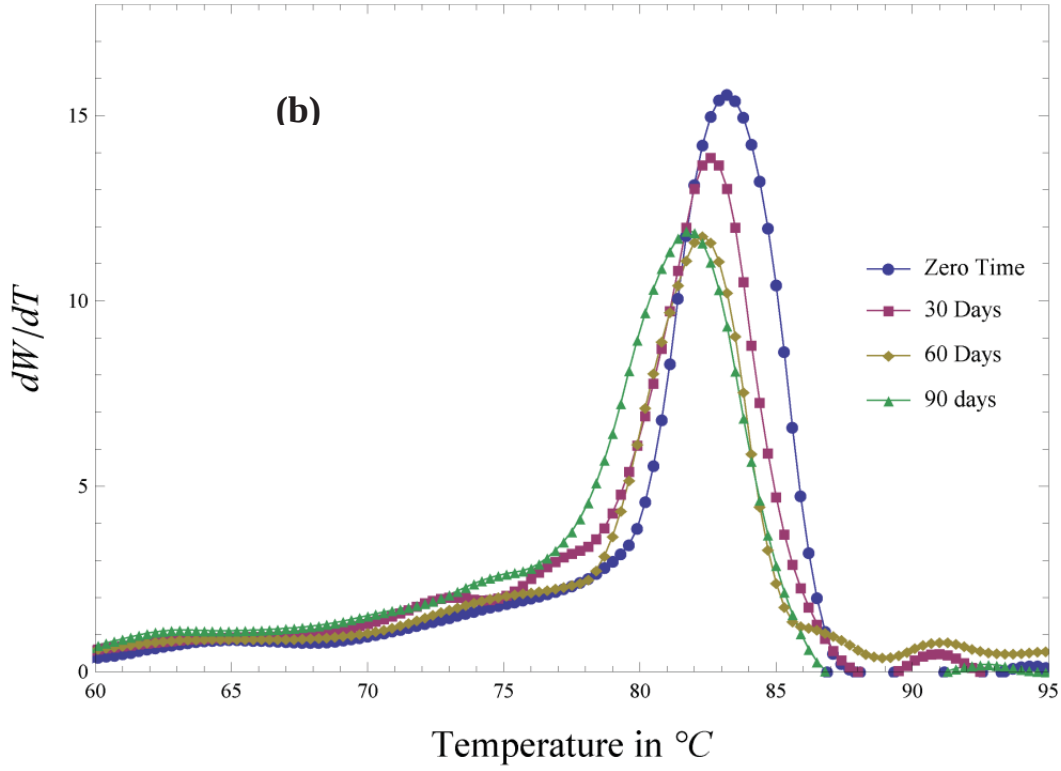
(b)
dW/dT
Temperature in °C
Zero Time
30 Days
60 Days
90 days

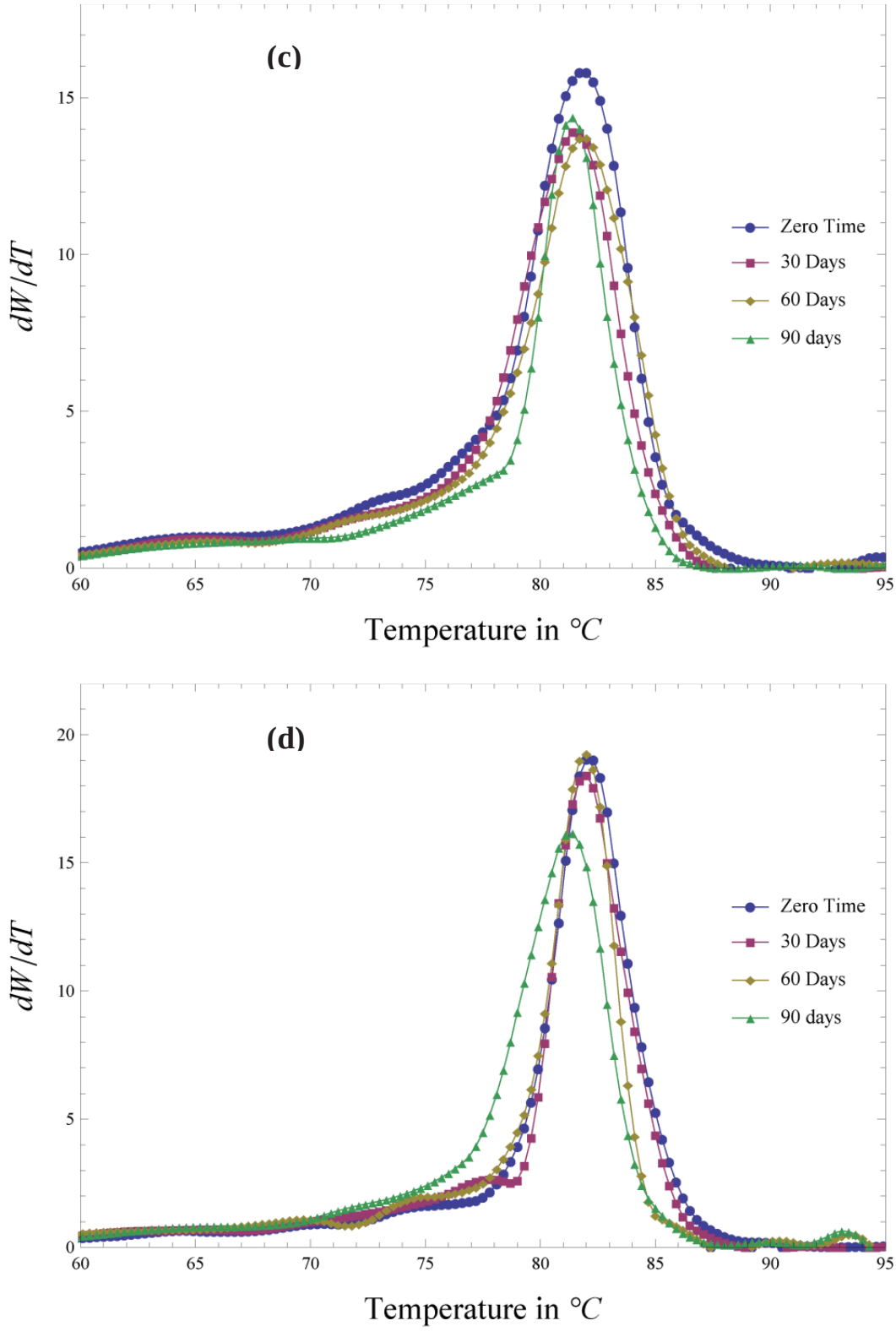

Figure 4-27 CRYSTAF profiles after different exposure of time a) HDPE, b) G1/HDPE, c) G2/HDPE, d) G3/HDPE

Table 4-9 GPC results for HDPE and HDPE/graphene nanocomposites before and after degradation

Sample	0 Time		60 days		90 days	
	M_w	PDI	M_w	PDI	M_w	PDI
HDPE	30044.75	4.13	23265.50	2.80	18911	3.039
G1/HDPE	31513.50	3.17	24970.00	3.09	ND	ND
G2/HDPE	119862.75	11.55	100996.00	10.74	91081	9.378
G3/HDPE	78140.50	8.17	71701.00	5.51	54255	4.17

4.9.4 Dynamic mechanical properties after degradation

The dynamic mechanical properties of HDPE and those of the nanocomposites were analyzed after degradation. It was found that the storage and loss modulus of neat HDPE degraded more quickly as compared to graphene incorporated nanocomposites. Flexibility of polymer chains and structural arrangements affect the properties of polymers. The distinctive mechanical behavior of polymers is due to high molecular weight. The decrease in the molecular weight by chain scission degrades he mechanical strength of polymers. As can be seen from Figure 4-28-a, the storage modulus for HDPE decreased more markedly with the exposure time. This illustrates that the material has suffered degradation. Unlike HDPE for graphene reinforce HDPE nanocomposites specially G2/HDPE and G3/HDPE, the changes in mechanical strength are less pronounced, hence proving the stabilization effect of graphene for HDPE against UV degradation.

The DMA results of HDPE and HDPE/graphene nanocomposites at different exposures of time are shown in Figure 4-28 (a, b, c, d).

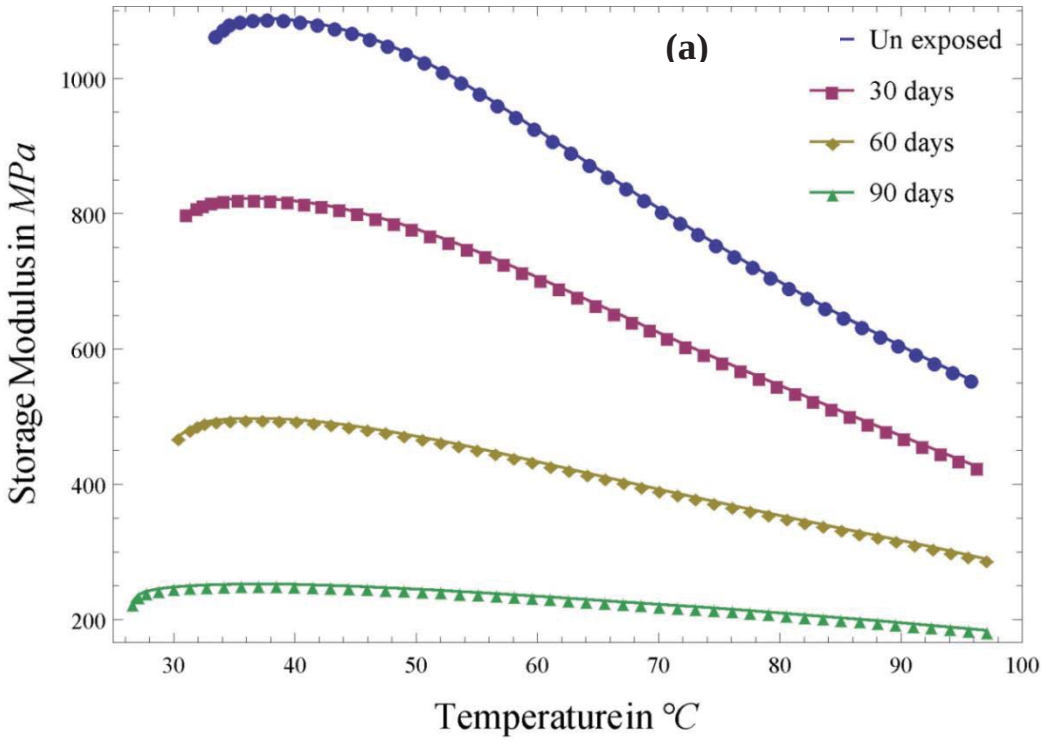

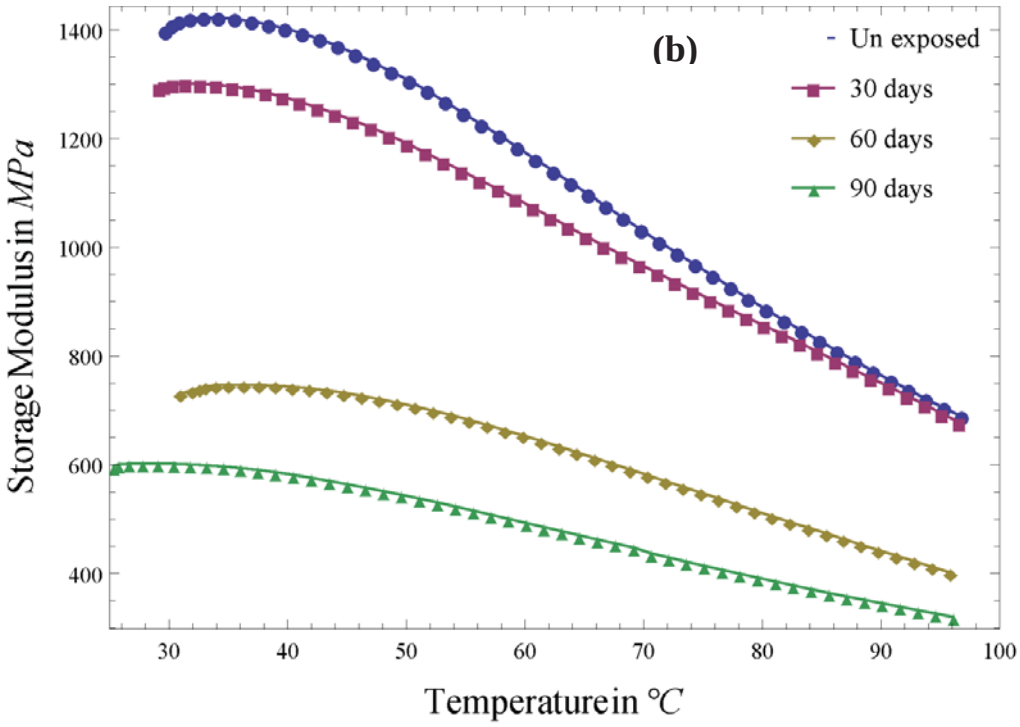

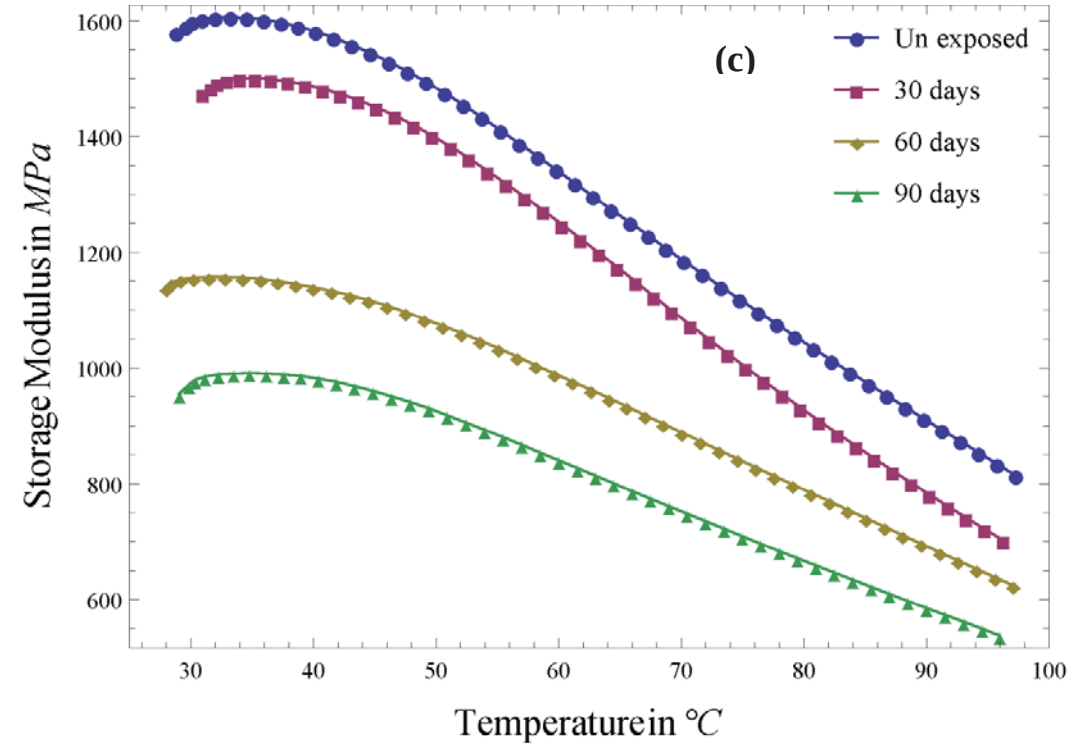

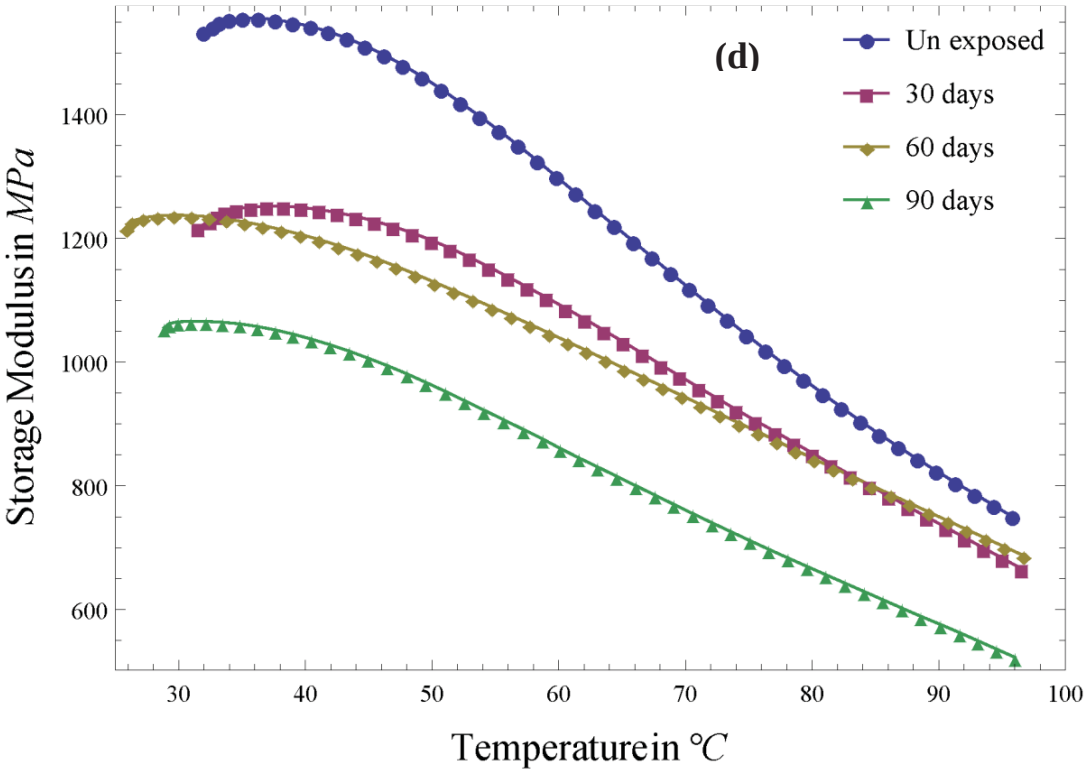

Figure 4-28 Storage modulus at different exposure of time a) HDPE, b) G1/HDPE, c) G2/HDPE and d) G3/HDPE

4.9.6 Morphological analysis after degradation

The samples after exposure were analyzed with SEM. The results are shown in Figure 4-29. For neat HDPE as illustsrated in Figure 4-29, we can see that after 3 months of exposure, there are cracks appeared on the surface, which shows that it has suffered severe degradation. Such cracks are formed as a result of the physical stress due to periodic changes in temperature and humidity. The degradation at surface reduces the strength of material, hence increasing the formation of cracks [77]. Such micro cracks can be seen clearly in Figure 4-29-a. However, for HDPE/graphene nanocomposites, the roughness of the surface is less as compared to neat HDPE. The wide and long micro cracks are absent. Although, some localized spots of degradation are visible. This can be due uneven dispersion of graphene in the polymer matrix. The results of SEM support all previous deductions about the improvement against photo-oxidation due to the addition of graphene.

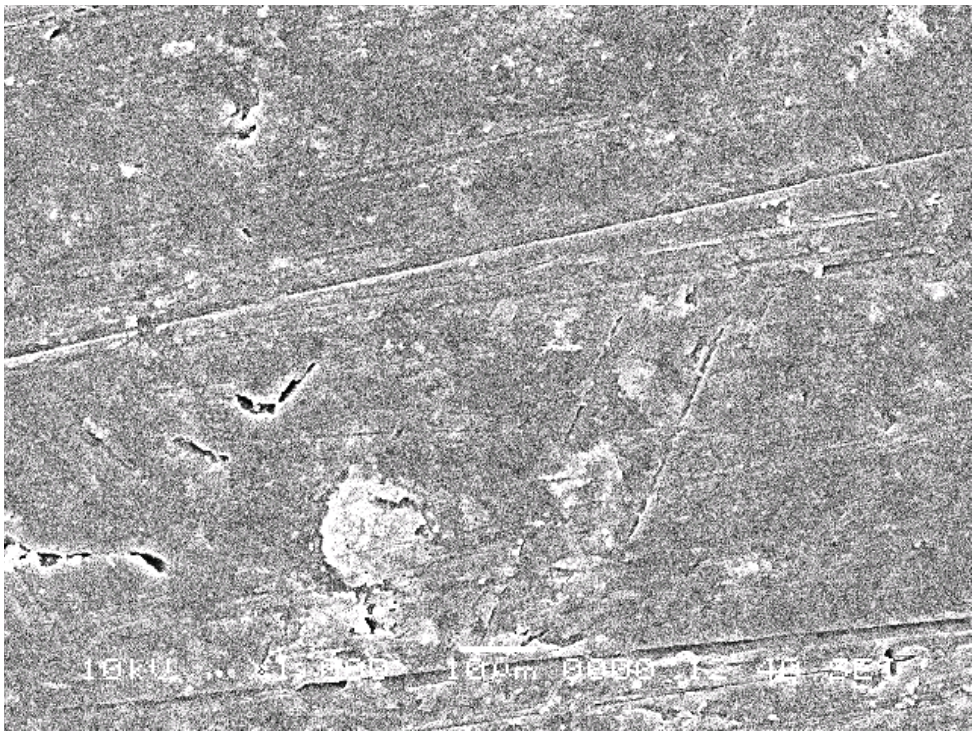

(a)

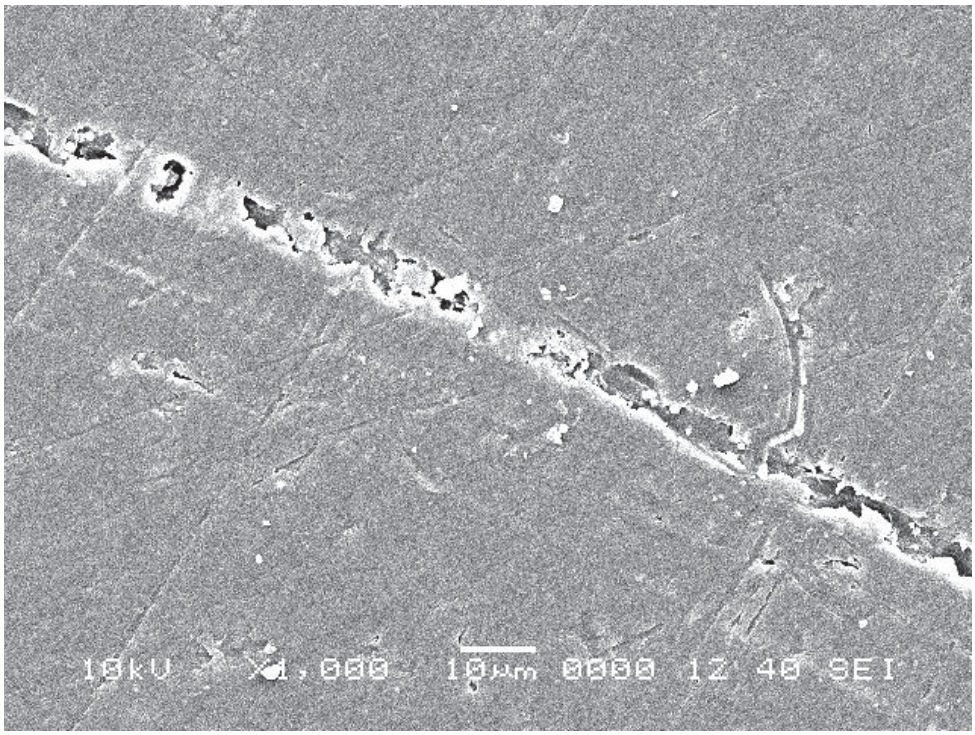

(b)

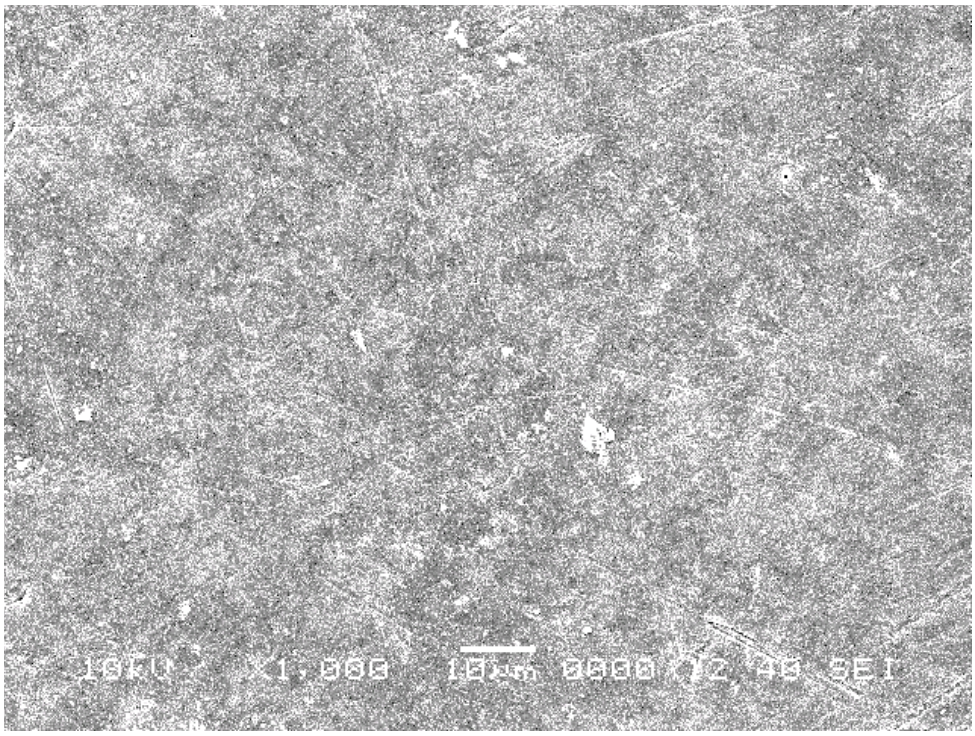

(c)

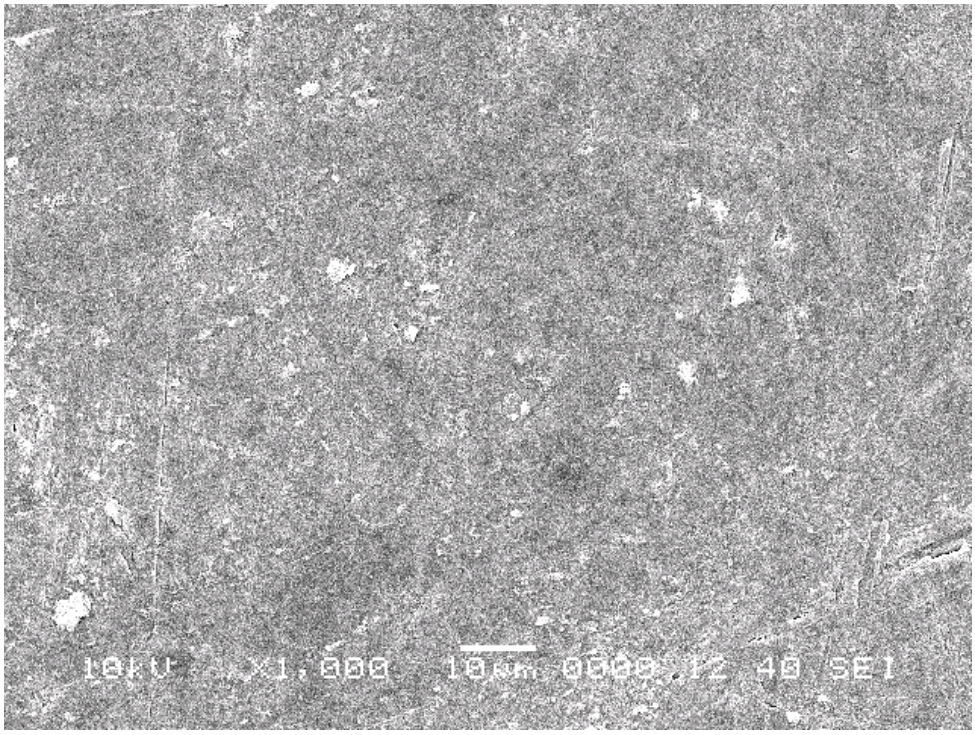

(d)

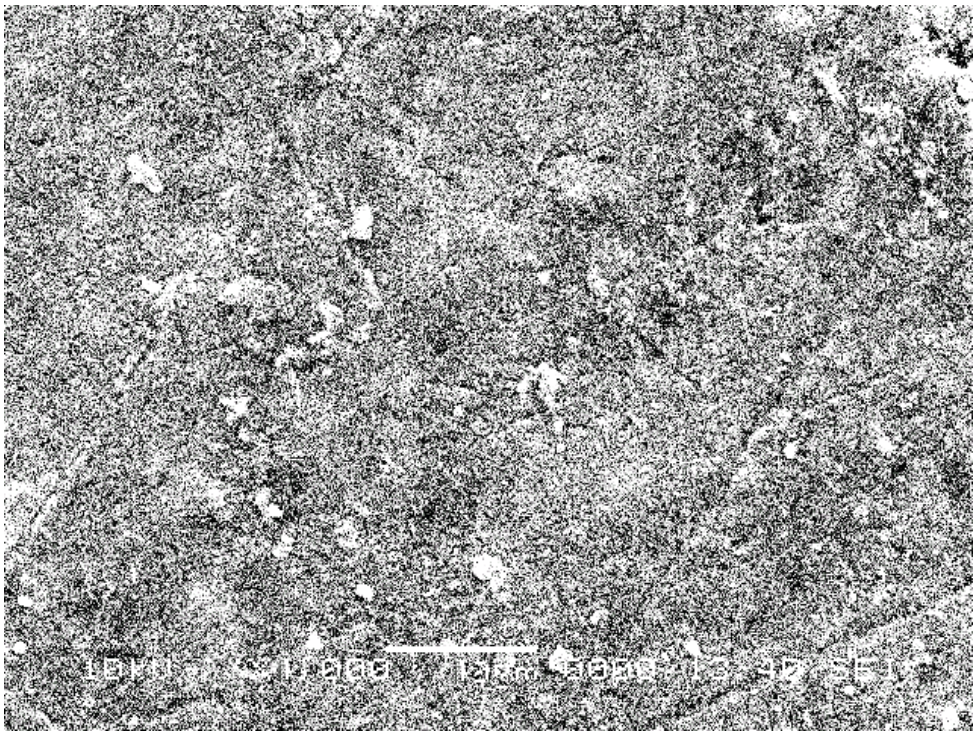

(e)

Figure 4-29 SEM images at 1000x for a) HDPE, b) HDPE, c) G1/HDPE, d) G2/HDPE and e) G3/HDPE

CONCLUSIONS

HDPE/graphene nanocomposites were prepared by *in-situ* polymerization of ethylene. Zirconocene was used as catalyst and MAO co-catalyst. A slight reduction in the activity of catalyst was noticed due to the presence of grapehen.

DSC studies revealed that crystallinity of the nanocomposites is slightly reduced as compared to neat HDPE, however, no pronounced change in T_m was observed. An increase in M_w was found by adding graphene nano-filer. M_w was the highest for 10 mg of filler with 6 mg of catalyst and 5 ml of MAO.

The non-isothermal crystallization of the nanocompositeswas studied by using DSC). The suitability of various models was examined for the crystallization behavior. The Jeizorny and Ozawa model failed to sufficiently describe the crystallization kinetics due to an inappropriate assumption of neglecting the secondary stage crystallization. However Mo-model successfully described the non-isothermal crystallization process. It was observed that incorporation of graphene in HDPE increases the crystallization onset temperature. However, at later stages of crystallization, the nanofiller restricts the movement of chain transfers, thereby increasing the degree of super cooling required for a unit degree of crystallinity and the $t_{1/2}$.

E_A was calculated by using the nonlinear iso-conversional method, which gives the dependence of E_A on temperature at progressive transformation. The results showed that incorporation of graphene into HDPE significantly lowers the E_A of crystallization, hence proving the nucleation. The nucleation activity calculated by Dobvera method also

proved the nucleation of graphene. It was found that nucleation activity, φ for all the nanocomposites was less than 1.

It was found that incorporation of graphene leads to the improved storage modulus of the material and reduced mechanical damping factor (Tan δ). SEM morphology showed that bythe addition of graphene, fiber like network is formed in the polymer matrix, however, this network vanishes at higher loadings of graphene. It was also found that graphene imparts good flame retardant capabilities to the nanocomposites. Microcalorimetry tests revealed that peak heat release rate and peak decomposition temperature is reduced.

The degradation stability of the nano-composites was studied by exposing to the natural environment at Dhahran Saudi Arabia. DSC analysis showed that the crystallinity of neat HDPE increased at the early stage exposure. Unlike HDPE, the change in crystallinity for HDPE/graphene nanocomposites were not pronounced. The carbonyl indices for the nanocomposites were much lower than that of neat HDPE indicating less degradation. Similarly, by analysis of dynamic mechanical properties, it was found that the extent of degradation is far less in graphene reinforced HDPE nanocomposites. Henceforth graphene can be used as a stabilizer against UV degradation of HDPE.

RECOMMENDATIONS

The following recommendations are put forward for future work.

1. Use of graphene as a ligand for the synthesis of metallocene based catalyst, to get better insights of the steric and electronic effect of graphene on metallocene.

2. Extension of this work to the functionalized graphene, for better dispersion of graphene in the polymer matrix through covalent bonding.

3. Study the degradation in artificial weathrometer, in which the effect of different conditions upon degradation can be evaluated in details sucha as ,the intensity of UV light and humidity etc.

REFERENCES

[1] M. Moniruzzaman, K.I. Winey, Macromolecules 39 (2006) 5194.

[2] M. Okamoto, S.S. Ray, in:, N. H.S. (Ed.), Encycl. Nanosci. Nanotechnol., Volume 8, American Scientific Publishers, 2004, p. 58883.

[3] H. Kim, A.A. Abdala, C.W. Macosko, Macromolecules 43 (2010) 6515.

[4] O.C. Compton, S.T. Nguyen, Small 6 (2010) 711.

[5] J.R. Potts, S.H. Lee, T.M. Alam, J. An, M.D. Stoller, R.D. Piner, R.S. Ruoff, Carbon N. Y. 49 (2011) 2615.

[6] A.K. Geim, Science 324 (2009) 1530.

[7] G. Eda, M. Chhowalla, Nano Lett. 9 (2009) 814.

[8] K.S. Novoselov, A.K. Geim, S. V Morozov, D. Jiang, Y. Zhang, S. V Dubonos, I. V Grigorieva, A.A. Firsov, Science 306 (2004) 666.

[9] S. Stankovich, D.A. Dikin, G.H.B. Dommett, K.M. Kohlhaas, E.J. Zimney, E.A. Stach, R.D. Piner, S.T. Nguyen, R.S. Ruoff, Nature 442 (2006) 282.

[10] T. Ramanathan, A.A. Abdala, S. Stankovich, D.A. Dikin, M. Herrera-Alonso, R.D. Piner, D.H. Adamson, H.C. Schniepp, X. Chen, R.S. Ruoff, S.T. Nguyen, I.A. Aksay, R.K. Prud'Homme, L.C. Brinson, Nat. Nanotechnol. 3 (2008) 327.

[11] E.T. Mickelson, C.B. Huffman, A.G. Rinzler, R.E. Smalley, R.H. Hauge, J.L. Margrave, Chem. Phys. Lett. 296 (1998) 188.

[12] J. Chen, M. A.Hamon, H. Hu, Y. Chen, A. M.Rao, P. C.Eklund, R. C.Haddon, Science (80-.). 282 (1998) 95.

[13] J.L. Bahr, J. Yang, D. V Kosynkin, M.J. Bronikowski, R.E. Smalley, J.M. Tour, J. Am. Chem. Soc. 123 (2001) 6536.

[14] S. Stankovich, R.D. Piner, X. Chen, N. Wu, S.T. Nguyen, R.S. Ruoff, J. Mater. Chem. 16 (2006) 155.

[15] C. Lv, Q. Xue, D. Xia, M. Ma, J. Xie, H. Chen, J. Phys. Chem. C 114 (2010) 6588.

[16] H. Kim, Y. Miura, C.W. Macosko, Chem. Mater. 22 (2010) 3441.

[17] Functional Graphene-Polymer Nanocomposites for Gas Barrier Applications - Patents.com, n.d.

[18] H. Kim, C.W. Macosko, Polymer (Guildf). 50 (2009) 3797.

[19] H. Kim, C.W. Macosko, Macromolecules 41 (2008) 3317.

[20] J.R. Potts, D.R. Dreyer, C.W. Bielawski, R.S. Ruoff, Polymer (Guildf). 52 (2011) 5.

[21] Y. Xu, W. Hong, H. Bai, C. Li, G. Shi, Carbon N. Y. 47 (2009) 3538.

[22] A. Satti, P. Larpent, Y. Gun'ko, Carbon N. Y. 48 (2010) 3376.

[23] K.W. Putz, O.C. Compton, M.J. Palmeri, S.T. Nguyen, L.C. Brinson, Adv. Funct. Mater. 20 (2010) 3322.

[24] Y. Cao, J. Feng, P. Wu, Carbon N. Y. 48 (2010) 3834.

[25] T. Wei, G. Luo, Z. Fan, C. Zheng, J. Yan, C. Yao, W. Li, C. Zhang, Carbon N. Y. 47 (2009) 2296.

[26] H.B. Lee, A. Raghu, K.S. Yoon, H.M. Jeong, J. Macromol. Sci. Part B 49 (2010) 802.

[27] M.B. Bryning, D.E. Milkie, M.F. Islam, J.M. Kikkawa, a. G. Yodh, Appl. Phys. Lett. 87 (2005) 161909.

[28] F. de C. Fim, J.M. Guterres, N.R.S. Basso, G.B. Galland, J. Polym. Sci. Part A Polym. Chem. 48 (2010) 692.

[29] J. JANG, M. KIM, H. JEONG, C. SHIN, Compos. Sci. Technol. 69 (2009) 186.

[30] Z. Gu, L. Zhang, C. Li, J. Macromol. Sci. Part B 48 (2009) 1093.

[31] M. Stürzel, F. Kempe, Y. Thomann, S. Mark, M. Enders, R. Mülhaupt, Macromolecules 45 (2012) 6878.

[32] M. Avrami, J. Chem. Phys. 7 (1939) 1103.

[33] T. Ozawa, Polymer (Guildf). 12 (1971) 150.

[34] T. Liu, Z. Mo, H. Zhang, J. Appl. Polym. Sci. 67 (1998) 815.

[35] J. Kim, S. Kwak, S.M. Hong, J.R. Lee, A. Takahara, Y. Seo, Macromolecules 43 (2010) 10545.

[36] A. Khawam, D.R. Flanagan, J. Phys. Chem. B 110 (2006) 17315.

[37] S. Vyazovkin, Macromol. Rapid Commun. 23 (2002) 771.

[38] S. Vyazovkin, N. Sbirrazzuoli, Macromol. Rapid Commun. 27 (2006) 1515.

[39] a. Bērziņš, A. Actiņš, Latv. J. Chem. 51 (2012) 209.

[40] H.L. Friedman, J. Polym. Sci. Part C Polym. Symp. 6 (2007) 183.

[41] T. Ozawa, Bull. Chem. Soc. Jpn. 38 (1965) 1881.

[42] H.E. Kissinger, Anal. Chem. 29 (1957) 1702.

[43] T. Akahira, T. Sunose, Res. Rep. Chiba Inst Technol 16 (1971) 22.

[44] J.L. Bolland, G. Gee, Trans. Faraday Soc. 42 (1946) 244.

[45] S. Moss, H. Zweifel, Polym. Degrad. Stab. 25 (1989) 217.

[46] A. Singh, Radiat. Phys. Chem. 56 (1999) 375.

[47] W.L. Hawkins, Polymer Degradation and Stabilization, Springer Berlin Heidelberg, Berlin, Heidelberg, 1984.

[48] N.S. Allen, Polym. Degrad. Stab. 2 (1980) 155.

[49] J. Lemaire, R. Arnaud, J.-L. Gardette, Polym. Degrad. Stab. 33 (1991) 277.

[50] L.A. Wall, S. Straus, J. Polym. Sci. 44 (1960) 313.

[51] R. Raff, K.. Doak, Crystalline Olefin Polymers Vol.20 Part 2, Interscience, 1965.

[52] Y.A. Shlyapnikov, S.G. Kiryushkin, A.P. Mar'in, Antioxidative Stabilization Of Polymers, CRC Press, 1996.

[53] M.. Rabello, J.. White, Polymer (Guildf). 38 (1997) 6389.

[54] M.. Rabello, J.. White, Polymer (Guildf). 38 (1997) 6379.

[55] R. Gensler, C.J.. Plummer, H.-H. Kausch, E. Kramer, J.-R. Pauquet, H. Zweifel, Polym. Degrad. Stab. 67 (2000) 195.

[56] W.G. Oakes, R.B. Richards, J. Chem. Soc. (1949) 2929.

[57] L.W. Jelinski, J.J. Dumais, J.P. Luongo, A.L. Cholli, Macromolecules 17 (1984) 1650.

[58] K. Murata, Y. Hirano, Y. Sakata, M.A. Uddin, J. Anal. Appl. Pyrolysis 65 (2002) 71.

[59] T. Ueno, E. Nakashima, K. Takeda, Polym. Degrad. Stab. 95 (2010) 1862.

[60] T. Ueno, E. Nakashima, K. Takeda, Polym. Degrad. Stab. 95 (2010) 1862.

[61] A.M. Trozzolo, F.H. Winslow, Macromolecules 1 (1968) 98.

[62] J.F. Rabek, Photodegradation of Polymers: Physical Characteristics and Applications, Ist editio, Springer Berlin Heidelberg, 2011.

[63] G. Akay, T. Tinçer, H.E. Ergöz, Eur. Polym. J. 16 (1980) 601.

[64] S.H. Hamid, M.B. Amin, A.G. Maadhah, Handbook of Polymer Degradation, 3rd ed., M. Dekker, 1992.

[65] M. Mlinac, J. Rolich, M. Bravar, J. Polym. Sci. Polym. Symp. 57 (2007) 161.

[66] F. Severini, R. Gallo, S. Ipsale, N. Del Fanti, Polym. Degrad. Stab. 14 (1986) 341.

[67] F. Severini, R. Gallo, S. Ipsale, N. Del Fanti, Polym. Degrad. Stab. 17 (1987) 57.

[68] A.J. Chirinos-Padrón, P.H. Hernández, E. Chávez, N.S. Allen, C. Vasiliou, M. DePoortere, Eur. Polym. J. 23 (1987) 935.

[69] A. Ram, T. Meir, J. Miltz, Int. J. Polym. Mater. 8 (1980) 323.

[70] J.P. Luongo, J. Polym. Sci. Part B Polym. Lett. 1 (1963) 141.

[71] A. Mathur, V. Kumar, G. Mathur, … Eur. Symp. Therm. … (1981).

[72] A.D. Jenkins, Polymer Science: A Materials Science Handbook, Volume 1, North-Holland Pub. Co., 1972.

[73] A. Davis, D. Sims, Weathering of Polymers (Google eBook), Springer, 1983.

[74] P. Gijsman, G. Meijers, G. Vitarelli, Polym. Degrad. Stab. 65 (1999) 433.

[75] M.U. Amin, G. Scott, L.M.K. Tillekeratne, Eur. Polym. J. 11 (1975) 85.

[76] E.G. Bobalek, J.N. Henderson, T.T. Serafini, J.R. Shelton, J. Appl. Polym. Sci. 2 (1959) 210.

[77] A. Blaga, R.S. Yamasaki, J. Mater. Sci. 11 (1976) 1513.

[78] M. Raab, L. Kotulák, J. Kolařík, J. Pospíšil, J. Appl. Polym. Sci. 27 (1982) 2457.

[79] M. Iring, E. Földes, K. Barabás, T. Kelen, F. Tüd˝os, L. Ódor, Polym. Degrad. Stab. 14 (1986) 319.

[80] A. Holmström, A. Andersson, E.M. Sörvik, Eur. Polym. J. 13 (1977) 483.

[81] R. Davidson, Eur. Polym. J. 17 (1981) 163.

[82] S.K. Esthappan, S.K. Kuttappan, R. Joseph, Mater. Des. 37 (2012) 537.

[83] R. Yang, P.A. Christensen, T.A. Egerton, J.R. White, Polym. Degrad. Stab. 95 (2010) 1533.

[84] S. Barus, M. Zanetti, P. Bracco, S. Musso, A. Chiodoni, A. Tagliaferro, Polym. Degrad. Stab. 95 (2010) 756.

[85] I. Grigoriadou, K.M. Paraskevopoulos, K. Chrissafis, E. Pavlidou, T.-G. Stamkopoulos, D. Bikiaris, Polym. Degrad. Stab. 96 (2011) 151.

[86] M. Atiqullah, M.M. Hossain, M.S. Kamal, M.A. Al-Harthi, M.J. Khan, A. Hossaen, I. Hussain, AIChE J. 59 (2013) 200.

[87] R. Guimarães, F.C. Stedile, J.H.. dos Santos, J. Mol. Catal. A Chem. 206 (2003) 353.

[88] L.. Simon, R.. de Souza, J.B.. Soares, R.. Mauler, Polymer (Guildf). 42 (2001) 4885.

[89] S. Anantawaraskul, J.B.. Soares, P.M. Wood-Adams, B. Monrabal, Polymer (Guildf). 44 (2003) 2393.

[90] M. Tajvidi, R. Falk, in:, Sevent Int. Conf. Woodfiber-Plastic Compos., Wisconsin, USA, 2003, pp. 187–195.

[91] L. Nielsen, Trans. Soc. Rheol. (1969).

[92] F.D.C. Fim, N.R.S. Basso, A.P. Graebin, D.S. Azambuja, G.B. Galland, J. Appl. Polym. Sci. 128 (2013) 2630.

[93] K. Sewda, S.N. Maiti, Polym. Bull. 70 (2013) 2657.

[94] R.P. Chartoff, B. Maxwell, Polym. Eng. Sci. 8 (1968) 126.

[95] S.G. Hatzikiriakos, Polym. Eng. Sci. 40 (2000) 2279.

[96] D. Yan, W.-J. Wang, S. Zhu, Polymer (Guildf). 40 (1999) 1737.

[97] Y.-H. Shi, Q. Dou, J. Therm. Anal. Calorim. 112 (2012) 901.

[98] X. Shi, J. Wang, B. Jiang, Y. Yang, J. Appl. Polym. Sci. 128 (2013) 3609.

[99] C.I. Ferreira, C. Dal Castel, M.A.S. Oviedo, R.S. Mauler, Thermochim. Acta 553 (2013) 40.

[100] A. Jeziorny, Polymer (Guildf). 19 (1978) 1142.

[101] R. Ou, C. Guo, Y. Xie, Q. Wang, BioResources 6 (2011) 4547.

[102] Q. Jiasheng, H. Pingsheng, J. Mater. Sci. 38 (2003) 2299.

[103] X. Chen, L. Wang, Y. Liu, J. Shi, H. Shi, Polym. Eng. Sci. 49 (2009) 2342.

[104] M. Joshi, B.S. Butola, Polymer (Guildf). 45 (2004) 4953.

[105] A. Chafidz, I. Ali, M.E. Ali Mohsin, R. Elleithy, S. Al-Zahrani, J. Polym. Res. 19 (2012) 9860.

[106] S. Vyazovkin, C.A. Wight, J. Phys. Chem. A 101 (1997) 8279.

[107] S. Vyazovkin, D. Dollimore, J. Chem. Inf. Model. 36 (1996) 42.

[108] G.I. Senum, R.T. Yang, J. Therm. Anal. 11 (1977) 445.

[109] a. Dobreva, M. Alonso, M. Gonzalez, a. Gonzalez, J. a. de Saja, Thermochim. Acta 258 (1995) 197.

[110] S. Ran, C. Chen, Z. Guo, Z. Fang, J. Appl. Polym. Sci. (2014) n/a.

[111] D. Zhuo, R. Wang, L. Wu, Y. Guo, L. Ma, Z. Weng, J. Qi, J. Nanomater. 2013 (2013).

[112] S.-P. Liu, J. Ind. Eng. Chem. (2013).

[113] T.K. Han, H.K. Choia, D.W. Jeungb, Y.S. Ko, Macromol. Chem. Phys. 2447 (1995) 2637.

[114] S. Park, S.W. Yoon, K.-B. Lee, D.J. Kim, Y.H. Jung, Y. Do, H. Paik, I.S. Choi, Macromol. Rapid Commun. 27 (2006) 47.

[115] B. Choi, J. Lee, S. Lee, J.-H. Ko, K.-S. Lee, J. Oh, J. Han, Y.-H. Kim, I.S. Choi, S. Park, Macromol. Rapid Commun. 34 (2013) 533.

[116] S. Park, S.W. Yoon, K.-B. Lee, D.J. Kim, Y.H. Jung, Y. Do, H. Paik, I.S. Choi, Macromol. Rapid Commun. 27 (2006) 47.

[117] T.K. Han, H.K. Choia, D.W. Jeungb, Y.S. Ko, Macromol. Chem. Phys. 196 (1995) 2637.

[118] D. Yan, W.-J. Wang, S. Zhu, Polymer (Guildf). 40 (1999) 1737.

[119] A. Wolfram, 15 Dec (2013).

[120] S.A. Jabarin, E.A. Lofgren, J. Appl. Polym. Sci. 53 (1994) 411.

[121] P. Zou, H. Xiong, S. Tang, Carbohydr. Polym. 73 (2008) 378.

[122] N. Nuraje, S.I. Khan, H. Misak, R. Asmatulu, ISRN Polym. Sci. 2013 (2013) 1.

[123] A. Valadez-Gonzalez, J.M. Cervantes-Uc, L. Veleva, Polym. Degrad. Stab. 63 (1999) 253.

[124] A. Tidjani, R. Arnaud, J. Polym. Sci. Part A Polym. Chem. 31 (1993) 603.

[125] J. Lacoste, D.J. Carlsson, J. Polym. Sci. Part A Polym. Chem. 30 (1992) 493.

[126] S.H. Hamid, W.H. Prichard, Polym. Plast. Technol. Eng. 27 (1988) 303.

[127] D.I. Bower, The Vibrational Spectroscopy of Polymers, Cambridge University Press, 1992.

[128] N.M. Stark, L.M. Matuana, Polym. Degrad. Stab. 86 (2004) 1.

[129] G. Wypych, HANDBOOK MATERIAL, 2nd ed., ChemTec Publishing, Ontario, Canada, 1995.

VITAE

Name	Farrukh Shehzad
Nationality	Pakistani
Date of Birth	25th March, 1989
Email	farrukh.che@gmail.com
Address	VPO Gar Munara, Tehsil and District Swabi, Khyber Pakhtunkhwa, Pakistan
Academic Background	BSc Chemical Engineering, University of Engineering and Technology, Peshawar, Pakistan
Publications	**F.Shehzad**, S.P. Thomas, M.A. Al-Harthi, Non-isothermal crystallization kinetics of high density polyethylene/graphene nanocomposites prepared by in-situ polymerization, **Thermochimica Acta**, **589**, 10 August 2014, Pages 226-234
Seminars & Presentations	1. Graduate seminar on High density polyethylene/graphene nanocomposites, 5th May 2013. 2. Heterogeneous modeling of a fixed bed water gas shift reactor, KFUPM 7th Graduate Research Day on 3rd Feb, 2013. 3. Poster Presentation of Improving Overall Heat Transfer Coefficient of Rising Film Evaporator for Sugar Industry, UET Peshawar, Pakistan Dec, 2011.